

ABSTRACT

LEININGER, DUSTIN ALLEN. Algebraic Topology Gets On My Nerves: TDA with Some Deep Learning and Chromatic Homology with Some PDEs. (Under the direction of Dr. Andrew Cooper and Dr. Tye Lidman).

This thesis is comprised of two projects. Chapter 1 contains an introduction to each. The main results of the first project can be found in Chapter 4. The main results of the second project can be found in Section 8.3 and Chapter 9.

The first project is contained in chapters 2 through 4. It concerns the relatively new class of summary statistic in the field of topological data analysis called persistence curves. We investigate the response of four persistence curves to the presence of three noise types. We do this by computing the persistence curves for a data set of images as the images are injected with increasing levels of the three noise types. We then build a machine learning model to classify the images based on their persistence curves with and without noise. We then propose and apply three methods for reducing the effects of the noise.

The second project is contained in chapters 5 through 9. It concerns applying the technology of chromatic homology to smooth manifolds. Chromatic homology is a categorification of the chromatic polynomial for finite simple graphs which, when evaluated with coefficients in the deRham complex of a smooth manifold, gives rise to a bicomplex whose associated spectral sequences converge to the homology of the configuration space of the manifold over the graph. According to the Hodge Theorem, deRham cohomology is intimately related to solutions to partial differential equations. We investigate whether smooth maps between smooth manifolds, or graph morphisms between graphs, induce maps between their associated bicomplexes. Next, we perform a novel computation which provides evidence that the intermediate pages of the spectral sequences contain similar information about solutions to partial differential equations.

Algebraic Topology Gets On My Nerves: TDA with Some Deep Learning
and Chromatic Homology with Some PDEs

by
Dustin Allen Leininger

A dissertation submitted to the Graduate Faculty of
North Carolina State University
in partial fulfillment of the
requirements for the Degree of
Doctor of Philosophy

Mathematics

Raleigh, North Carolina
2020

APPROVED BY:

Dr. Bojko Bakalov

Dr. Radmila Sazdanovic

Dr. Andrew Cooper
Co-chair of Advisory Committee

Dr. Tye Lidman
Co-chair of Advisory Committee

BIOGRAPHY

Born on February 24th 1992 in a small town buried deep in the Appalachian Mountains of western North Carolina to young parents Tanya Maxwell and Steve Leininger, Dustin spent his youth divided between reading and exploring the forests and rivers. However, his demure nature was more than compensated for by his younger sister Stevy, three years his junior, who embraced the world with a fierce passion for life and no small amount of endearing deviance. Dustin's family continued to grow after his father remarried to Jessica O'Brian, his second sister Harley was born in the year 2001 and his mother remarried to Steve Williams some years later.

Most of Dustin's friends came to him through playing on the school football team (from the third to the ninth grade), and through playing the tenor saxophone in the school band (from sixth grade to eleventh). Although he often excelled in his studies at Avery County High School, it was while attending the North Carolina Governor's School in the summer of 2009 that he first began to nurture his curiosity into a passion for learning. This experience breathed fresh air onto dim embers initially ignited and fostered by the dedicated educators in his life. He went on to become Student Body President his senior year.

From there Dustin came down from the mountains to the city of Raleigh to attend North Carolina State University. His academic interests were diverse and he obtain bachelor's of science degrees in physics and mathematics with minors in english and philosophy. Although, this eventually led to a hindering indecisiveness when choosing a graduate career. He ultimately returned to North Carolina State University and entered into the graduate program in mathematics which allowed him to remain in contact with the many close friends he made during his undergraduate studies. This is where we find Dustin Leininger today, glued to his desk chair furiously typing away in the final weeks of his graduate career; working, hoping, and planning for whatever comes next.

ACKNOWLEDGEMENTS

Thanks to my advisors Dr. Andrew Cooper and Dr. Tye Lidman as well my committee which is comprised of Dr. Bojko Bakalov, Dr. Donald Martin, and Dr. Radmila Sazdanović.

Thanks also to my parents Tanya Williams and Steve Leininger as well as my sisters Stevy and Harley Leininger for their unwavering love and support.

Thanks to the numerous friends I have made over the course of my studies for their support, guidance, understanding, and good times.

Finally, thanks to the exceptional high school educators whom I was fortunate to have and who inspired and encouraged me to be more; Mr. Hank Hardin and Mrs. Dawn Aldridge Poore.

TABLE OF CONTENTS

List of Tables	vi
List of Figures	vii
Chapter 1 Introduction	1
1.1 1 st Project: TDA and Machine Learning	1
1.1.1 Motivation	1
1.1.2 Algebraic Topology and Data	2
1.1.3 Objective	3
1.2 2 nd Project: Chromatic Homology and PDEs	3
1.2.1 The deRham Complex and Laplace's Equation	3
1.2.2 The Chromatic Complex	4
Chapter 2 Background	6
2.1 Algebraic Topology	6
2.1.1 The Simplex Category and Geometric Realizations	7
2.1.2 The Algebra of Homology	21
2.1.3 Functors	25
2.2 Topological Data Analysis	26
2.2.1 Open Covers from Data	26
2.2.2 Persistent Homology	30
2.2.3 Persistence Curves	36
Chapter 3 Methods	40
3.1 The Data Set	41
3.2 Persistence Homology	42
3.3 Persistence Curves	45
3.4 Noise Injections	47
3.5 Deep Learning	49
Chapter 4 Results and Analysis	52
4.1 TCPs and Noise	52
4.1.1 Extended Topological Color Profiles	55
4.1.2 The Effects of Noise	61
4.2 Filtering Out the Noise	64
4.2.1 Area Normalization	66
4.2.2 Lifespan Truncation	67
4.2.3 Re-Centering	74
4.2.4 Training on Images Directly	75
4.2.5 Conclusions Concerning the Proposed Filtration Methods	77

Chapter 5	Algebraic Preliminaries	78
5.1	Differential Graded Algebras	78
5.2	Spectral Sequences	82
5.3	Filtrations of DGAs	85
5.4	Bicomplexes and Their Filtrations	87
Chapter 6	Graph Colorings and Bicomplexes	95
6.1	Preliminary on Graphs	95
6.2	The Chromatic Complex	97
6.3	The Chromatic Bicomplex	105
6.4	de Rham Cohomology in Particular	111
Chapter 7	Manifolds and Simplices	116
7.1	Simplicial Manifolds	116
7.2	The Simplicial Bicomplex	118
Chapter 8	Simplicial and Chromatic Relations	124
8.1	A Morphism of Bicomplexes	124
8.2	An Example Vertical Filtration Computation	128
8.3	Functoriality in the Bicomplexes	132
8.3.1	Functoriality in the Manifold	132
8.3.2	Functoriality in the Graph	136
Chapter 9	Chromatic Homology and PDEs?	139
9.1	An Example Computation	139
9.2	The Problem Child	147
9.2.1	The First Case in the First Column	149
9.2.2	The Second Case in the First Column	150
9.2.3	Conclusion	154
References		155

LIST OF TABLES

Table 3.1	Formulas for computing the persistence curves used in this study. . .	46
Table 9.1	16 cases to consider for determining if $[\alpha \otimes \beta] = [\omega \otimes \nu] \in E_2^{20}$. For each of the four choices of assumptions about $\int \beta$ and $\int \nu$, there are four choices for $\int \alpha$ and $\int \omega$	148

LIST OF FIGURES

Figure 3.1	aluminium	42
Figure 3.2	brown bread	42
Figure 3.3	corduroy	42
Figure 3.4	cork	42
Figure 3.5	cotton	42
Figure 3.6	cracker	42
Figure 3.7	lettuce	42
Figure 3.8	linen	42
Figure 3.9	white bread	42
Figure 3.10	wood	42
Figure 3.11	wool	42
Figure 3.12	The six persistence diagrams for the linen texture example 3.8.	43
Figure 3.13	A 255x255 pixel gray-scale image artificially generated using the function $f(x, y)$ and its representation as a surface in \mathbb{R}^3	44
Figure 3.14	The three color channels of the linen example 3.8 alongside their respective PDs and Betti Curves at threshold 128.	47
Figure 3.15	Gauss 1.1	48
Figure 3.16	Gauss 4	48
Figure 3.17	Gauss 8	48
Figure 3.18	Gauss 12	48
Figure 3.19	Gauss 16	48
Figure 3.20	Speckle 1.1	48
Figure 3.21	Speckle 4	48
Figure 3.22	Speckle 8	48
Figure 3.23	Speckle 12	48
Figure 3.24	Speckle 16	48
Figure 3.25	S&P 1.1	48
Figure 3.26	S&P 4	48
Figure 3.27	S&P 8	48
Figure 3.28	S&P 12	48
Figure 3.29	S&P 16	48
Figure 3.30	Diagram of the MLP architecture.	50
Figure 4.1	The Betti-TCP of the linen example of Figure 3.8. The first three peaks are the β_0 -number at each threshold in the red, green and blue color channels respectively. Similarly, the second three peaks are the β_1 -number at each threshold in each of the three color channels respectively.	53

Figure 4.2	The Life-TCP of the linen example of Figure 3.8. The first three peaks are the total lifespans of every generator in zeroth homology alive at each threshold in the red, green and blue color channels respectively. Similarly, the second three peaks are the total lifespans of every generator in first homology alive at each threshold in each of the three color channels respectively.	53
Figure 4.3	The Midlife-TCP of the linen example of Figure 3.8. The first three peaks are the total mid-lives of every generator in zeroth homology alive at each threshold in the red, green and blue color channels respectively. Similarly, the second three peaks are the total mid-lives of every generator in first homology alive at each threshold in each of the three color channels respectively.	54
Figure 4.4	The Multiplicativelife-TCP of the linen example of Figure 3.8. The first three peaks are the total multiplicative-lives of every generator in zeroth homology alive at each threshold in the red, green and blue color channels respectively. Similarly, the second three peaks are the total multiplicative-lives of every generator in first homology alive at each threshold in each of the three color channels respectively.	54
Figure 4.5	The Betti ETCP and the Betti aETCP for the linen example 3.8	56
Figure 4.6	Training accuracy and loss for the Betti ETCP and the Betti aETCP. Final training accuracies for the ETCP data and the aETCP data were 97.83% and 98.00% respectively.	57
Figure 4.7	Training accuracy and loss for the Life ETCP and the Life aETCP. Final training accuracies for the ETCP data and the aETCP data were 98.59% and 97.80% respectively.	58
Figure 4.8	Training accuracy and loss for the Midlife ETCP and the Midlife aETCP. Final training accuracies for the ETCP data and the aETCP data were 98.35% and 97.73% respectively.	59
Figure 4.9	Training accuracy and loss for the Multiplicative ETCP and the Multiplicative aETCP. Final training accuracies for the ETCP data and the aETCP data were 98.48% and 97.87% respectively.	60
Figure 4.10	The Betti ETCPs for the linen example 3.8 with Gaussian noise injected with SNRdB = (1.1, 4, 8, 12, 16, ∞). Where SNRdB= ∞ denotes the ETCP without any noise injection.	62
Figure 4.11	The four peaks in a given plot are four histograms of the generators according to lifespan for the linen example 3.8 in the red color channel, the first two peaks being β_0 and β_1 generators of the original image; the third and fourth peaks corresponding to the β_0 and β_1 generators of the inverse image.	63

Figure 4.12	The ten pre-trained models were evaluated on the data set of noise injected ETCs without any pre-processing. The accuracy of the ten models were average at each SNRdB and for each noise type. The red dot is the accuracy of the model on the noiseless ETCs without pre-processing.	65
Figure 4.13	The ten pre-trained models were evaluated on the data set of ETCs injected with noise and normalized by area. The accuracies of the ten models were average at each SNRdB and for each noise type. The red dot is the accuracy of the model on the noiseless ETCs with area normalization.	66
Figure 4.14	The ten pre-trained models were evaluated on the data set of ETCs injected with noise and normalized by removing the 1% longest lived and shortest lived generators. The accuracies of the ten models were average at each SNRdB and for each noise type. The red dot is the accuracy of the model on the noiseless ETCs with 1% truncation. .	67
Figure 4.15	The ten pre-trained models were evaluated on the data set of ETCs injected with noise and normalized by removing the 2% longest lived and shortest lived generators. The accuracies of the ten models were average at each SNRdB and for each noise type. The red dot is the accuracy of the model on the noiseless ETCs with 2% truncation. .	68
Figure 4.16	The ten pre-trained models were evaluated on the data set of ETCs injected with noise and normalized by removing the 3% longest lived and shortest lived generators. The accuracies of the ten models were average at each SNRdB and for each noise type. The red dot is the accuracy of the model on the noiseless ETCs with 3% truncation. .	69
Figure 4.17	The ten pre-trained models were evaluated on the data set of ETCs injected with noise and normalized by removing the 4% longest lived and shortest lived generators. The accuracies of the ten models were average at each SNRdB and for each noise type. The red dot is the accuracy of the model on the noiseless ETCs with 4% truncation. .	70
Figure 4.18	The ten pre-trained models were evaluated on the data set of ETCs injected with noise and normalized by removing the 5% longest lived and shortest lived generators. The accuracies of the ten models were average at each SNRdB and for each noise type. The red dot is the accuracy of the model on the noiseless ETCs with 5% truncation. .	71
Figure 4.19	The ten pre-trained models were evaluated on the data set of ETCs injected with noise and normalized by removing the 8% longest lived and shortest lived generators. The accuracies of the ten models were average at each SNRdB and for each noise type. The red dot is the accuracy of the model on the noiseless ETCs with 8% truncation. .	72

Figure 4.20	The ten pre-trained models were evaluated on the data set of ETCs injected with noise and normalized by removing the 10% longest lived and shortest lived generators. The accuracies of the ten models were average at each SNRdB and for each noise type. The red dot is the accuracy of the model on the noiseless ETCs with 10% truncation.	73
Figure 4.21	The ten pre-trained models were evaluated on the data set of ETCs injected with noise and normalized by subtracting from each ETCs the average over all ETCs. The accuracies of the ten models were average at each SNRdB and for each noise type. The red dot is the accuracy of the model on the noiseless ETCs.	74
Figure 4.22	The ten pre-trained CNN models were evaluated on the data set of images injected with noise. The accuracies of the ten models were average at each SNRdB and for each noise type. The red dot is the accuracy of the model on the noiseless images.	76

CHAPTER

1

INTRODUCTION

1.1 1st Project: TDA and Machine Learning

1.1.1 Motivation

More and more often data scientists are being asked to distill actionable information from data sets of unprecedented size and complexity. The robust fields of statistics and data science provide numerous methods and techniques for modeling large volumes of data. However, in order to begin building a model for a given data set it is often necessary to have some qualitative information about the data. This qualitative information informs many aspects of the initial stages of developing an appropriate model of the data by helping to

answer some basic questions such as, should the data set be sliced into smaller sets which are then analyzed independently? If so, how should it be sliced? Which summary statistics of a given data set are going to be most informative?

Most often what is meant by 'qualitative information' is intrinsic structure. With respect to the question of slicing a data set, it would be helpful to know if the data itself is already naturally clustered into smaller sets. While methods have been developed to detect the intrinsic structure of data sets they often rely on embedding the data into a metric space. For example, k-nearest neighbor attempts to resolve a given data set into constituent clusters but requires a metric to define what counts as a 'nearest neighbor'. What is needed in this case is a qualitative description of the data that is truly intrinsic to the data, i.e. independent of the choice of embedding and possibly other choices of representation.

1.1.2 Algebraic Topology and Data

Algebraic topology is a field of mathematics that dates back to the early 20th century and is primarily concerned with the development and computation of topological (more precisely, homotopy) invariants of manifolds. Namely, it seeks to associate to a given manifold a collection of quantities which remain constant under continuous transformations. In this way, the homotopy invariants capture and describe the intrinsic structure of the given manifold. For example, Betti numbers count the number of voids within a given manifold in various dimensions (more on this later).

While algebraic topology has predominantly been a theoretical subject, beginning in the early 2000's algorithms were developed and implemented to apply the tools of algebraic topology to data sets. These methods were expanded, modified, and improved forming a new field of study subsequently referred to as Topological Data Analysis (TDA). The goal of TDA is to leverage the power of homotopy invariants to describe the shape of a given

data set (independent of embedding) thereby providing insight into its intrinsic structure. Subsequently, it has grown from a tool primarily used to qualitatively describe data sets into one which can provide robust summary statistics of data sets in its own right.

1.1.3 Objective

The aim of this project is to investigate a class of topological summary statistics and attempt to provide a characterization of them in terms of accuracy as representations of data sets and in terms of their sensitivity to noise. This was done by computing the topological summary statistics from a data set of images with increasing levels of various image noise types. An analysis of the resulting topological statistics was conducted and some pre-processing methods were proposed to combat the presence of noise and enhance the efficacy of the statistics overall. As an application, simple deep learning models were constructed and trained to classify the labeled images based on their topological summaries.

1.2 2nd Project: Chromatic Homology and PDEs

1.2.1 The deRham Complex and Laplace's Equation

Let M be a smooth orientable manifold and $(\Omega^*(M), d)$ denote it's deRham complex. Then a Riemannian metric, $g(\cdot, \cdot)$, on M induces a co-differential $\delta : \Omega^{k+1}(M) \rightarrow \Omega^k(M)$ which can be used to define a generalized Laplace operator on M know as the Beltrami-Laplace operator $\Delta : \Omega^k(M) \rightarrow \Omega^k(M)$ where $\Delta = (d + \delta)^2$.

Furthermore, the Hodge Theorem states that the deRham complex of M has the following orthogonal decomposition

$$\Omega^k(M, \mathbb{R}) = \Delta(\Omega^k(M, \mathbb{R})) \oplus H_{dR}^k(M, \mathbb{R})$$

$$\Omega^k(M, \mathbb{R}) = d(\Omega^{k-1}(M, \mathbb{R})) \oplus \delta(\Omega^{k+1}(M, \mathbb{R})) \oplus H_{dR}^k(M, \mathbb{R})$$

from which it follows that the deRham cohomology $H^*(M)$ is in fact the space of solutions to the generalized Laplace equation $\Delta\alpha = 0$ and thus the dimension of $H^*(M)$ is the number of independent solutions.

Given that the deRham cohomology effectively counts the number of solutions to Laplace's equation, it becomes a question as to whether variations and/or augmentations of the deRham complex count solutions to other PDEs.

Furthermore, the deRham theorem provides an isomorphism between the deRham cohomology and singular homology of M , $I : H_{dR}^*(M, \mathbb{R}) \rightarrow H_*^{Sing}(M, \mathbb{R})$. Therefore, the deRham cohomology of M , while arising from the smooth structure on M , is in fact independent of it. Note that this implies that computing cohomology with respect to the deRham differential eliminates information about the smooth structure of M .

1.2.2 The Chromatic Complex

Let G be a finite simple graph. The chromatic polynomial, $P_G(\lambda)$ is a function which returns the number of ways to color the vertices of G with λ -many colors such that no adjacent pair has have the same color. The chromatic complex $CHR^*(G, A)$ is a homology theory (with coefficients in an algebra A) which categorifies the chromatic polynomial.

It has been shown that letting $A = \Omega^*(M)$ in the chromatic complex elevates it to a bicomplex, $CHR^{**}(G, \Omega(M))$. Furthermore, the vertical and horizontal filtrations of the chromatic bicomplex give rise to spectral sequences which converge to the singular homology of the configuration space of M over G (denoted M_G , see definition 7.2.1).

In the vertical filtration, cohomology is first computed with respect to the deRham differential while in the horizontal filtration it is first computed with respect to the chromatic differential. Therefore, the spectral sequence associated to the horizontal filtration preserves

more smooth information for longer than that of the vertical filtration.

Therefore, the second project of this thesis is an investigation into the chromatic bi-complex with the aim of determining whether or not the intermediate pages of the spectral sequence arising from the horizontal filtration carry information about solutions to PDEs on the underlying manifold M .

CHAPTER

2

BACKGROUND

2.1 Algebraic Topology

In statistics, a data set is traditionally thought of as being a discrete sample from an underlying space (or distribution) of all such data. This primary aim of much of statistics and probability theory is to recover properties of this underlying space based on the given data set. The principal aim of TDA is to describe the shape of the underlying space from which the given data set is sampled. The primary tool of TDA is *persistent homology* which is based on algorithmically computing singular homology.

In algebraic topology, in order to compute the singular homology of a manifold it is

necessary to first equip it with a combinatorial structure. This combinatorial structure can then be enhanced by the addition of graded algebras which ultimately allow for the computation of singular homology.

Therefore, an account of how TDA computes the singular homology of an underlying space (from which a given data set is drawn) must begin with an explanation of how one equips a space with a combinatorial structure. Then it will be necessary to describe how the combinatorial structure of an underlying space may be estimated from a finite data set. This is the project of the next two sub-sections.

2.1.1 The Simplex Category and Geometric Realizations

Most modern literature in algebraic topology utilizes singular complexes, originally developed by Eilenberg (1944), when it pertains to singular homology. While often being practically expedient for theoretical purposes, it relies on infinitely generated modules over various rings (depending on the application) and is therefore outside of the scope of modern computers. However, an antecedent of singular complexes, known as simplicial complexes, are finitely generated and compute the same invariants as singular homology. These are therefore what are commonly used to compute singular homology in TDA. From here on the term *homology* will refer to simplicial homology.

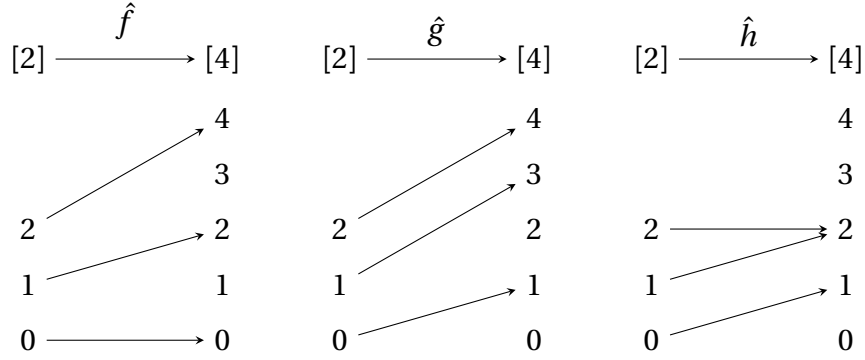
While simplicial complexes are a rich subject of study in their natural habitat of combinatorics, here they are presented in the categorical context which is more amenable to the topologists perspective. Those readers familiar with simplicial complexes and homology may feel free to skip to the next subsection.

Definition 2.1.1. The *CoSimplex Category* Δ^{co} is given by the following Objects and Morphisms.

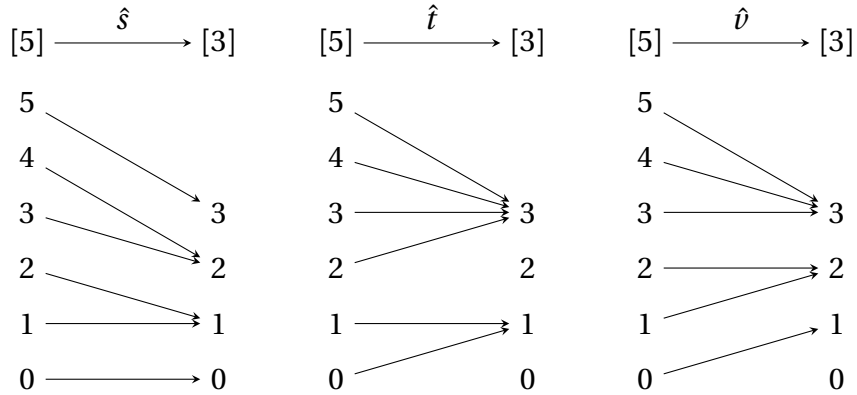
$$Obj(\Delta^{co}) = \{\text{non-empty, finite ordinals: } [n] = \{0, \dots, n\}\}$$

$$Hom_{\Delta^{co}}([m], [n]) = \left\{ \begin{array}{l} \text{order preserving functions } f : [m] \rightarrow [n] \\ \text{e.g. if } i \leq j \in [m] \text{ then } f(i) \leq f(j) \in [n] \end{array} \right\}$$

Example 2.1.1. Some elements of $Hom_{\Delta^{co}}([2], [4])$.



Example 2.1.2. Some elements of $Hom_{\Delta^{co}}([5], [3])$.



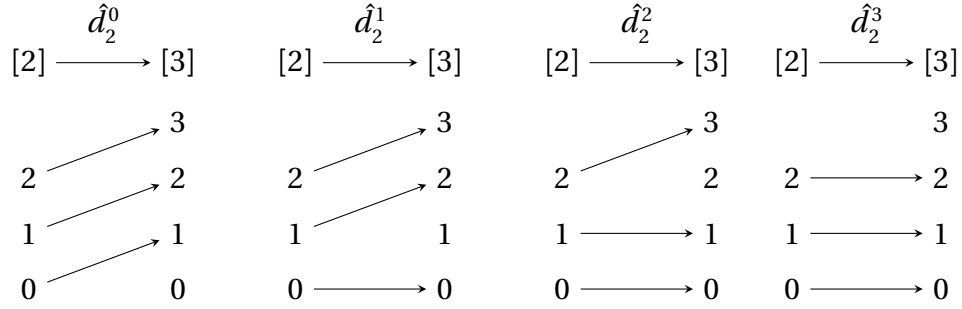
Definition 2.1.2. For each object $[n] \in Obj(\Delta^{co})$, there exists a collection of morphisms called *Coface Maps* $\{\hat{d}_n^i\}_{i=0}^{n+1} \subset Hom_{\Delta^{co}}([n], [n+1])$ given by

$$\hat{d}_n^i = \left\{ \begin{array}{ll} k & , \quad k < i \\ k+1 & , \quad k > i \end{array} \right\}$$

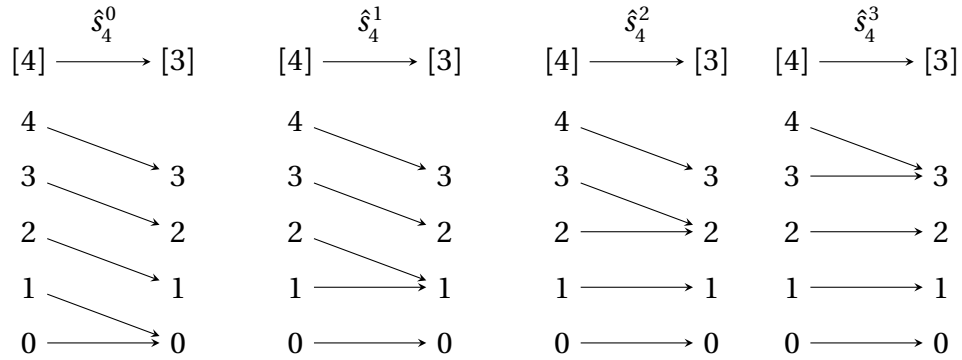
Similarly, for each object $[n+1] \in \text{Obj}(\Delta^{co})$, there exists a collection of morphisms called *Codegeneracy Maps* $\{\hat{s}_{n+1}^i\}_{i=0}^n \subset \text{Hom}_{\Delta^{co}}([n+1], [n])$ given by

$$\hat{s}_n^i = \begin{cases} k & , \quad k < i \\ k-1 & , \quad k > i \end{cases}$$

Example 2.1.3. All the co-faces maps in $\text{Hom}_{\Delta^{co}}([2], [3])$.



Example 2.1.4. All the codegeneracy maps in $\text{Hom}_{\Delta^{co}}([4], [3])$.



Lemma 2.1.1. For each $[n], [m] \in \text{Obj}(\Delta^{co})$, every morphism in $\text{Hom}_{\Delta^{co}}([m], [n])$ can be written as a composition of coface and codegeneracy maps. In other words, the coface and codegeneracy maps generate all morphisms via composition.

Lemma 2.1.2. *The coface and codegeneracy maps obey the following relations*

$$\left\{ \begin{array}{ll} d_{n+1}^j \circ d_n^i = d_{n+1}^i \circ d_n^{j-1} & , \quad i < j \\ s_{n-1}^j \circ s_n^i = s_{n-1}^i \circ s_n^{j+1} & , \quad i \leq j \\ s_{n+1}^j \circ d_n^j = s_{n+1}^j \circ d_n^{j+1} = Id_{n-1} & , \quad \forall i, j \\ s_{n+1}^j \circ d_n^i = d_{n-1}^i \circ s_n^{j-1} & , \quad i < j \\ s_{n+1}^j \circ d_n^i = d_{n-1}^{i-1} \circ s_n^j & , \quad i > j+1 \end{array} \right\}$$

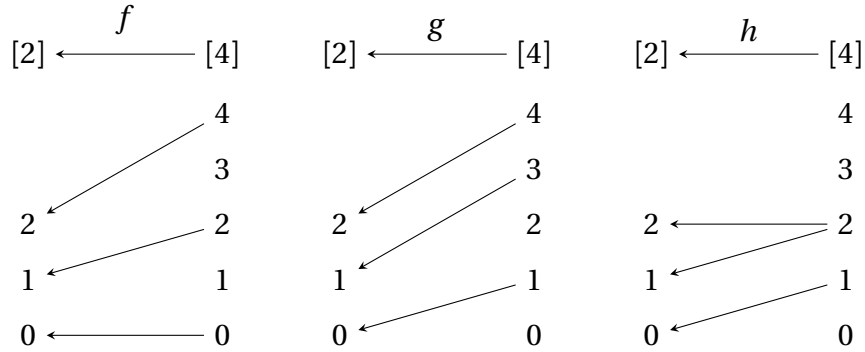
Definition 2.1.3. The *Simplex Category* Δ is the categorical opposite of Δ^{co} . That is to say, it is given by

$$Obj(\Delta) = Obj(\Delta^{co})$$

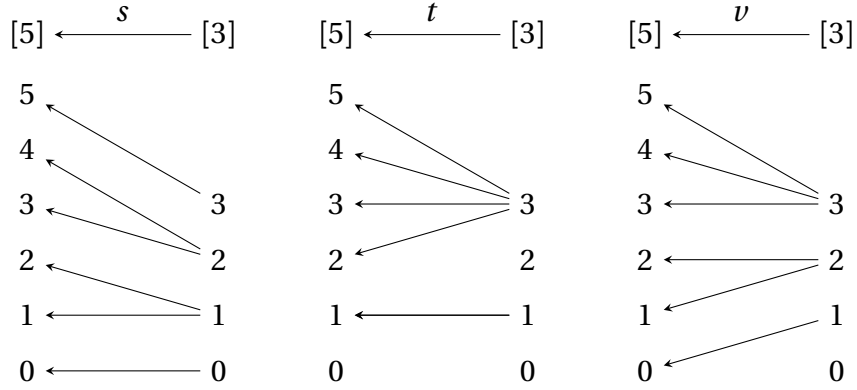
$$Hom_{\Delta}([n], [m]) = Hom_{\Delta^{co}}([m], [n])$$

$Hom_{\Delta}([n], [m])$ is $Hom_{\Delta^{co}}([m], [n])$ where all the arrows have been reversed.

Example 2.1.5. *Some elements of $Hom_{\Delta}([4], [2])$. Compare to Ex 2.1.1.*



Example 2.1.6. Some elements of $Hom_{\Delta}([3],[5])$. Compare to Ex 2.1.2.



From now on, we will write the morphisms in the simplex category such that arrows point from left to right. The face and degeneracy maps are similarly defined. Explicitly, they are given by the following.

Definition 2.1.4. For each object $[n+1] \in Ob j(\Delta)$, there exists a collection of morphisms called *Face Maps* $\{d_{n+1}^i\}_{i=0}^{n+1} \subset Hom_{\Delta}([n+1],[n])$ given by

$$d_n^i = \begin{cases} k & , \quad k < i \\ \text{omit} & , \quad k = i \\ k+1 & , \quad k > i \end{cases}$$

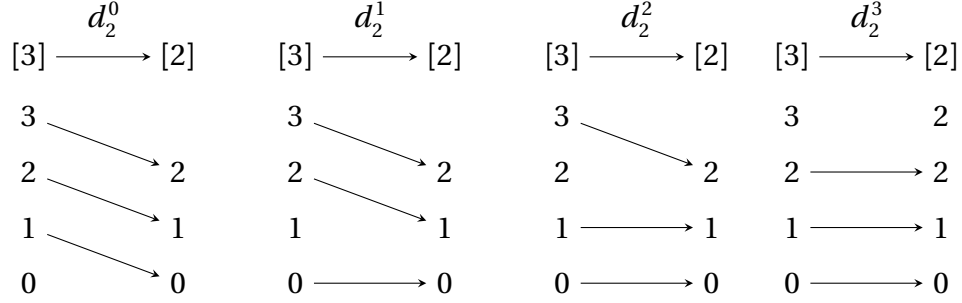
Similarly, for each object $[n] \in Ob j(\Delta)$, there exists a collection of morphisms called *Degeneracy Maps* $\{s_n^i\}_{i=0}^n \subset Hom_{\Delta^{co}}([n],[n+1])$ given by

$$s_n^i = \begin{cases} k & , \quad k < i \\ \text{duplicate} & , \quad k = i \\ k-1 & , \quad k > i \end{cases}$$

See the following two examples where some face and degeneracy maps are written out explicitly.

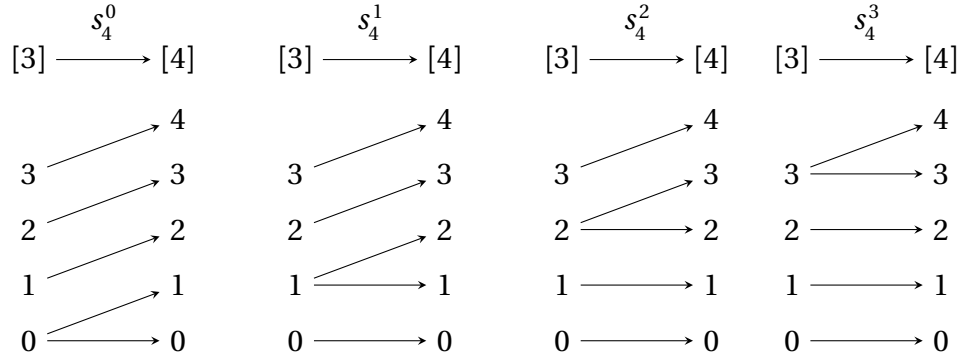
Example 2.1.7. All the faces maps in $\text{Hom}_\Delta([3], [2])$.

Compare to Ex 2.1.3.



Example 2.1.8. All the degeneracy maps in $\text{Hom}_\Delta([3], [4])$.

Compare to Ex 2.1.4.



As in the cosimplex category, the face and degeneracy maps generate all of the morphisms in the simplex category.

Lemma 2.1.3. The face and degeneracy maps obey the following relations

$$\left\{ \begin{array}{ll} d_{n-1}^i \circ d_n^j = d_{n-1}^{j-1} \circ d_n^i & , \quad i < j \\ s_{n+1}^i \circ s_n^j = s_{n+1}^{j+1} \circ s_n^i & , \quad i \leq j \\ d_{n+1}^j \circ s_n^j = d_{n+1}^{j+1} \circ s_n^j = Id_n & , \quad \text{for all } j \\ d_{n+1}^i \circ s_n^j = s_{n-1}^{j-1} \circ d_n^i & , \quad i < j \\ d_{n+1}^i \circ s_n^j = s_{n-1}^j \circ d_n^{i-1} & , \quad i > j+1 \end{array} \right.$$

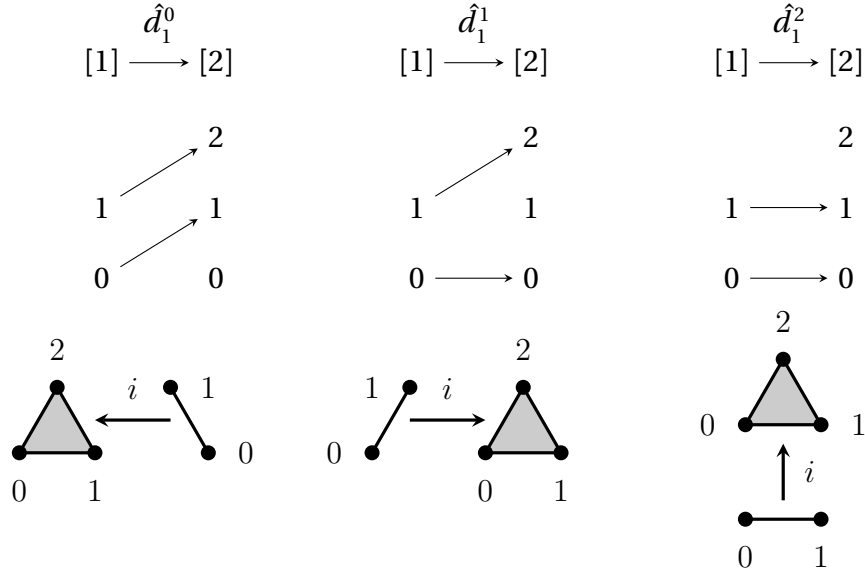
Definition 2.1.5. The standard N -Simplex $\|\Delta^n\| \subset \mathbb{R}^{n+1}$ is the set of points $t = (t_0, \dots, t_n)$ such that $0 \leq t_i \leq 1$ for all $i \in \{0, \dots, n\}$ and $\sum_{i=0}^n t_i = 1$.

Example 2.1.9. The following are the standard n -simplices for small n . The vertices have been labeled according to standard conventions which will be explained shortly.

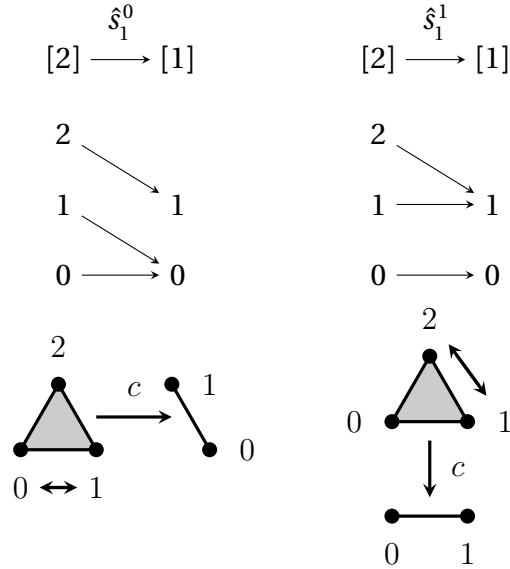
$$\begin{aligned}
 \|\Delta^0\| &= \begin{array}{c} \bullet \\ 0 \end{array} \\
 \|\Delta^1\| &= \begin{array}{c} \bullet \text{---} \bullet \\ 0 \quad 1 \end{array} \\
 \|\Delta^2\| &= \begin{array}{c} 2 \\ \bullet \\ \triangle \\ \bullet \text{---} \bullet \\ 0 \quad 1 \end{array} \\
 \|\Delta^3\| &= \text{solid tetrahedron with vertices } \{0, 1, 2, 3\}
 \end{aligned}$$

In order to provide some geometric intuition to the essentially combinatorial simplex category, it may be equivalently described as follows. To each object $[n] \in Ob \mathbf{j}\Delta$ associate the standard n -simplex $\|\Delta^n\|$. As for $Hom_{\Delta}(-, -)$, it is generated by face and degeneracy maps. Therefore it suffices to provide appropriate analogues for the standard simplices to establish an identification. Coface maps correspond to inclusions of codimension-1 simplices and codegeneracy maps correspond to collapse maps to codimension-1 simplices. Thus face maps correspond to projects onto codimension-1 simplices and degeneracy maps correspond to expansions into codimension-1 simplices.

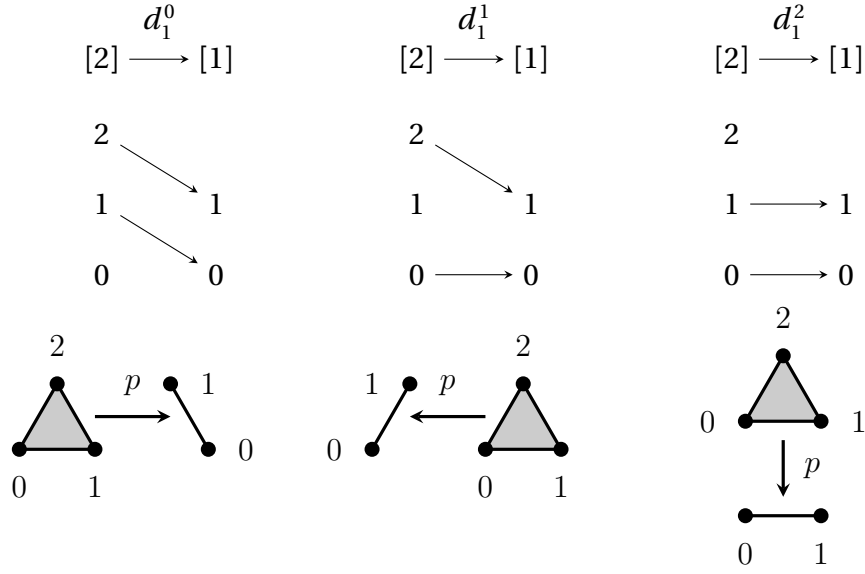
Example 2.1.10. *Coface maps $\{\hat{d}_1^i\}_{i=0}^2 \subset Hom_{\Delta^{co}}([1],[2])$ are represented by the following inclusions*



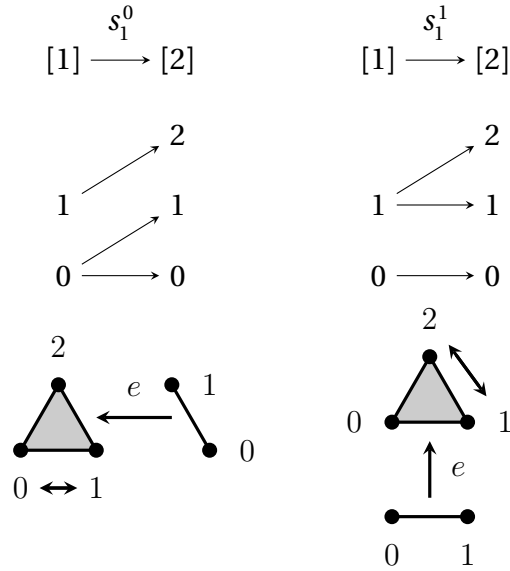
Example 2.1.11. *Codegeneracy maps $\{\hat{s}_1^i\}_{i=0}^1 \subset Hom_{\Delta^{co}}([2],[1])$ are represented by collapsing two vertices in the 2-simplex to obtain the 1-simplex.*



Example 2.1.12. Face maps $\{d_1^i\}_{i=0}^2 \subset \text{Hom}_\Delta([2], [1])$ are represented by the following projections



Example 2.1.13. Degeneracy maps $\{s_1^i\}_{i=0}^1 \subset \text{Hom}_\Delta([1], [2])$ are represented by duplicating one vertex in order to expand the 1-simplex into a 2-simplex



Definition 2.1.6. Let \mathcal{C} be a category with objects $Obj(\mathcal{C})$ and morphisms $Hom_{\mathcal{C}}(A, B)$ for $A, B \in Obj(\mathcal{C})$. A *Simplicial Object* in \mathcal{C} is the image of a covariant functor $F : \Delta \rightarrow \mathcal{C}$. Equivalently, it is the image of a contravariant functor $G : \Delta^{co} \rightarrow \mathcal{C}$.

Specifically, it is a sequence of objects $\mathbf{X} = \{X_n\}_{n=0}^{\infty}$ equipped with morphisms

$$\partial_{n-1}^i : X_n \rightarrow X_{n-1} \quad \text{and} \quad \delta_{n+1}^i : X_n \rightarrow X_{n+1}$$

for each $0 \leq i \leq n$ which obey the face and degeneracy map relations

$$\left\{ \begin{array}{ll} \partial_{n-1}^i \circ \partial_n^j = \partial_{n-1}^{j-1} \circ \partial_n^i & , \quad i < j \\ \delta_{n+1}^i \circ \delta_n^j = \delta_{n+1}^{j+1} \circ \delta_n^i & , \quad i \leq j \\ \partial_{n+1}^j \circ \delta_n^j = \partial_{n+1}^{j+1} \circ \delta_n^j = Id_n & , \quad \text{for all } j \\ \partial_{n+1}^i \circ \delta_n^j = \delta_{n-1}^{j-1} \circ \partial_n^i & , \quad i < j \\ \partial_{n+1}^i \circ \delta_n^j = \delta_{n-1}^j \circ \partial_n^{i-1} & , \quad i > j+1 \end{array} \right\}$$

Definition 2.1.7. The *Geometric Realization* $\|\mathbf{X}\|$ of a simplicial object $\mathbf{X} = \{X_n\}_{n=0}^{\infty}$ is given by the quotient of the disjoint union $\bigsqcup_n (\|\Delta^n\| \times X_n)$ by the relations

$$(d_n^i(t), x) \sim (t, \delta_{n+1}^i(x)) \quad \text{for } t \in \|\Delta^{n+1}\| \text{ and } x \in X_n$$

$$(s_n^i(t), x) \sim (t, \partial_{n+1}^i(x)) \quad \text{for } t \in \|\Delta^{n-1}\| \text{ and } x \in X_n$$

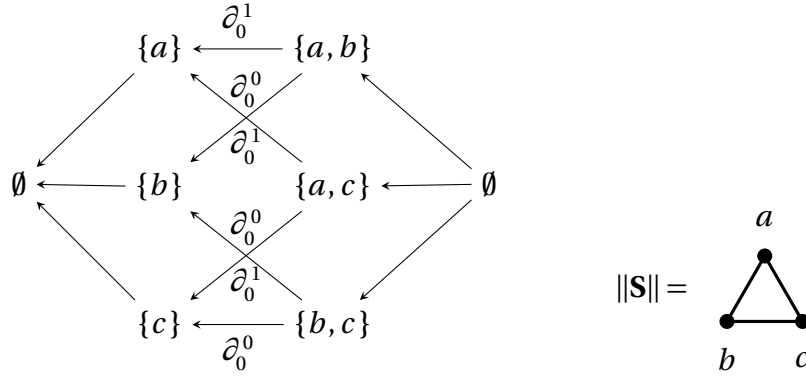
Example 2.1.14. Let **Set** denote the category of finite sets and set maps and define a simplicial set $F : \Delta \rightarrow \mathbf{Set}$, $\mathbf{S} = \{S_n\}_{n=0}^\infty$ as follows

$$F([0]) = \{\{a\}, \{b\}, \{c\}\} \equiv S_0$$

$$F([1]) = \{\{a, b\}, \{b, c\}, \{a, c\}\} \equiv S_1$$

$$F([n]) = \emptyset \equiv S_n \quad , \text{ else}$$

Then the face maps $d_0^0, d_0^1 : [1] \rightarrow [0]$ induce the following maps



For the geometric realization, each element of S_0 gets assigned a vertex $\|\Delta^0\|$ and each element of S_1 gets assigned an edge $\|\Delta^1\|$. The relations define how to glue the vertices to the edges.

In other literature simplicial sets (more precisely, their geometric realizations) are called simplicial complexes. Note that since each face map induces $n + 1$ maps for each element of X_n , the diagram of a simplicial object will always be a cubic lattice.

Note that Ex 2.1.14 is not complete since it does not include the degenerate simplices and degeneracy maps. That is, S_1 should also contain the degenerate simplices $\{a, a\}$, $\{b, b\}$, and $\{c, c\}$. They are required as the images of the degeneracy map $s_0^0 : [0] \rightarrow [1]$ which simply duplicates the vertex. In the same way, all of the sets S_n are non-empty since they at least contain the images of the induced degeneracy maps. For instance, the degeneracy maps s_1^0

and s_1^1 require that S_2 be given as follows

$$F([2]) = \left\{ \begin{array}{l} \{a, a, a\}, \{b, b, b\}, \{c, c, c\}, \{a, a, b\}, \\ \{a, b, b\}, \{a, a, c\}, \{a, c, c\}, \{b, b, c\}, \{b, c, c\} \end{array} \right\} \equiv S_2$$

Namely, the degeneracy map s_1^0 duplicates the first element in an element of S_1 to obtain an element of S_2 , e.g. $s_1^0(\{a, b\}) = \{a, a, b\} \in S_2$.

However it is not uncommon to neglect degenerate simplices and degeneracy maps since they do not contribute to the geometric realization. Namely, in the geometric realization the degenerate 2-simplex $\{a, a, a\} \in S_2$ is collapsed to the degenerate 1-simplex $\{a, a\} \in S_1$ which is itself collapsed to the vertex $\{a\} \in S_0$.

Finally, it is possible to bring this discussion full circle by noting that each standard simplex $\|\Delta^n\|$ can be obtained as the geometric realization of a simplicial set. Namely, let S be a set with cardinality $|S| = n + 1$ and $\mathcal{P}(S)$ be its power set. Define $S_i = \{s \in \mathcal{P}(S) \mid |s| = i + 1\}$ and note that $\bigcup_{i=0}^{n-1} S_i = \mathcal{P}(S)$. Then the sequence $\{S_i\}_{i=0}^{n-1}$ is a simplicial set whose geometric realization is the standard n -simplex, $\|\Delta^n\|$.

For instance, if the addition $F([2]) = \{\{a, b, c\}\} \equiv S_2$ had been made to example Ex 2.1.14, then the union of the sequence of sets would have been $\bigcup_{i=0}^2 S_i = \mathcal{P}(S)$ where $S = \{a, b, c\}$ and the geometric realization would have been the full 2-simplex, $\|\Delta^2\|$.

Definition 2.1.8. A *Simplicial Space* is a sequence of topological spaces

$\mathbf{X} = \{X_n\}_{n=0}^\infty$ equipped with continuous maps

$$\partial_{n-1}^i : X_n \rightarrow X_{n-1} \quad \text{and} \quad \delta_{n+1}^i : X_n \rightarrow X_{n+1}$$

for each $0 \leq i \leq n$ which obey the following face and degeneracy map relations

$$\left\{ \begin{array}{ll} \partial_{n-1}^i \circ \partial_n^j = \partial_{n-1}^{j-1} \circ \partial_n^i & , \quad i < j \\ \delta_{n+1}^i \circ \delta_n^j = \delta_{n+1}^{j+1} \circ \delta_n^i & , \quad i \leq j \\ \partial_{n+1}^j \circ \delta_n^j = \partial_{n+1}^{j+1} \circ \delta_n^j = Id_n & , \quad \text{for all } j \\ \partial_{n+1}^i \circ \delta_n^j = \delta_{n-1}^{j-1} \circ \partial_n^i & , \quad i < j \\ \partial_{n+1}^i \circ \delta_n^j = \delta_{n-1}^j \circ \partial_n^{i-1} & , \quad i > j+1 \end{array} \right\}$$

Define a *simplicial manifold* as a simplicial space where the topological spaces are smooth manifolds and where the face and degeneracy maps are smooth maps.

Definition 2.1.9. (The Nerve Construction)

Let M be a manifold and $\{U_i\}_{i \in A}$ be an open cover of M . For $I = (i_1, \dots, i_k)$ a sequence of integers $i_1 \leq \dots \leq i_k$ in A , define $l(I) = k$ as the length of I and $U_I = U_{i_1} \cap \dots \cap U_{i_k}$ when the intersection is non-empty.

Now let $N_n = \bigsqcup_{l(I)=n+1} U_I$, so that $N_0 = \bigsqcup_i U_i$ is the disjoint union of the elements of $\{U_i\}_{i \in A}$, $N_1 = \bigsqcup_{l(I)=2} U_i \cap U_j$ is the disjoint union of all non-empty pair-wise intersections of sequential elements ($i \leq j$) of $\{U_i\}_{i \in A}$, etc.

Then $\mathbf{N} = \{N_n\}_{n=0}^\infty$ is a simplicial manifold with induced face and degeneracy maps given by inclusions and repetitions. The face and degeneracy maps between N_0 and N_1 are given by

$$\partial_0^0 : U_i \cap U_j \rightarrow U_j, \partial_0^1 : U_i \cap U_j \rightarrow U_i, \delta_0^0 : U_i \rightarrow U_i \cap U_i.$$

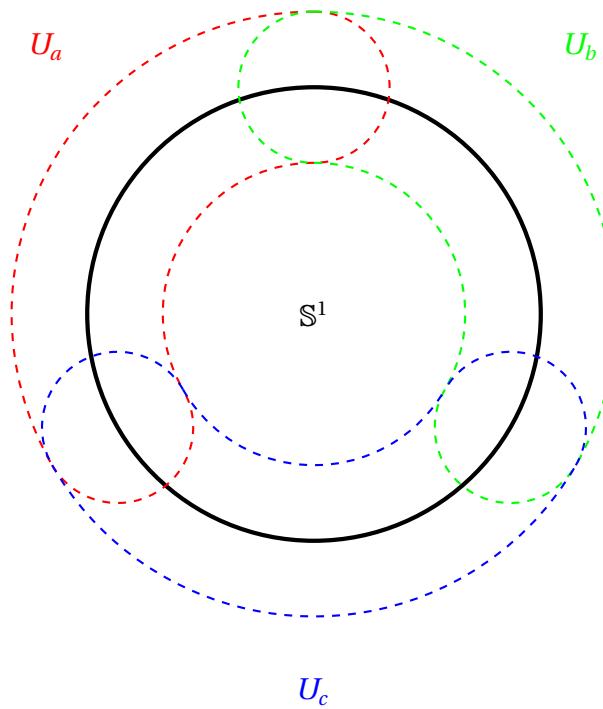
The simplicial manifold \mathbf{N} is called the *Nerve* of the open cover $\{U_i\}_{i \in A}$ of M .

Theorem 2.1.4. (The Nerve Theorem, Borsuk (1948))

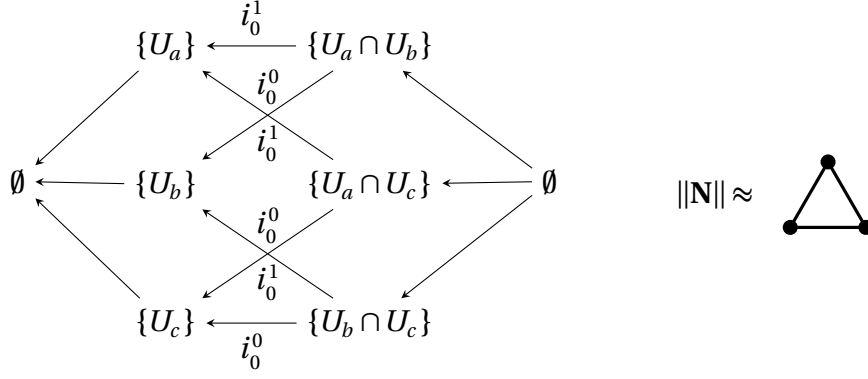
Let M be a manifold and $\{U_i\}_{i \in A}$ be an enumerable open cover of M . If for any non-empty subsets of the open cover $\{U_{i_k}\} \subseteq \{U_i\}_{i \in A}$ it is the case that $\bigcap_k U_{i_k}$ is either empty or contractible, then the geometric realization of the nerve of $\{U_i\}_{i \in A}$, $\|\mathbf{N}\|$, is homotopy equivalent to M .

The nerve construction provides a method for generating a simplicial complex from a manifold given an open cover. The nerve theorem provides sufficient conditions on the open cover to guarantee that the simplicial complex possesses the required information about the manifold to compute the homology, namely the homotopy type. The last thing to consider is how to equip a simplicial complex with the algebraic necessities for computing homology. Before that is attempted, first consider the following example which demonstrates the nerve construction and theorem in a simple enough case.

Example 2.1.15. Consider the manifold S^1 with open cover $\{U_a, U_b, U_c\}$ depicted below:



Following the nerve construction 2.1.9, a simplicial complex is constructed by considering the elements of the open cover and their mutual intersections. In this case each element of the open cover, as well as all pair-wise intersections, are open intervals. Furthermore, all higher order intersections (e.g. triple intersections) are empty. Lastly, the face maps of the complex are induced by inclusion maps and yields the following nerve complex (again ignoring the degenerate simplices).



Because the elements of the open cover and their intersections are contractible, as required by the nerve theorem 2.1.4, the geometric realization of the nerve complex is in fact homotopy equivalent to the circle. In this case, the vertices of the triangle are associated with the three elements of the open cover and the three edges are the three non-empty pair-wise intersections.

2.1.2 The Algebra of Homology

Now that the combinatorial precursor has been covered, it remains to add the algebraic necessities. Again, the presentation is from the categorical perspective.

Definition 2.1.10. Let R be a commutative ring with identity. An R -Algebra is a ring A with identity together with a ring homomorphism $f : R \rightarrow A$ mapping 1_R to 1_A such that the subring $f(R)$ is contained in the center of A .

Definition 2.1.11. A Graded R -algebra is an R -algebra with a direct sum decomposition into sub-modules, $\mathcal{A}^* = \bigoplus_{i \in \mathbb{Z}} A^i$. Elements in a given grading A^k are said to be of degree k .

Definition 2.1.12. Let \mathcal{A}^* and \mathcal{B}^* be graded algebras. A map $\phi : \mathcal{A}^* \rightarrow \mathcal{B}^*$ is a *morphism of graded R -algebras* if and only if it respects module structure of \mathcal{A}^* and \mathcal{B}^* as well as preserves degrees.

Definition 2.1.13. Let \mathcal{A}^* be a graded R -algebra. A *differential* on \mathcal{A}^* is a map $d : \mathcal{A}^* \rightarrow \mathcal{A}^*$ such that d has degree -1, $d \circ d = 0$.

A graded R -algebra equipped with a differential is called a *Differential Graded R -algebra* (DGA, or chain complex) and is denoted (\mathcal{A}^*, d) .

Definition 2.1.14. The category of differential graded algebras, **DGA**, has objects $Obj(\mathbf{DGA}) = \{(\mathcal{A}^*, d) \mid (\mathcal{A}^*, d) \text{ is a DGA}\}$ with morphisms, denoted $Hom_{\mathbf{DGA}}((\mathcal{A}^*, d), (\mathcal{B}^*, \delta))$, given by the collection of all graded R -algebra morphisms $\phi : \mathcal{A}^* \rightarrow \mathcal{B}^*$ such that the following diagram commutes for each grading i .

$$\begin{array}{ccc} A^{i+1} & \xrightarrow{\phi} & B^{i+1} \\ d \downarrow & & \downarrow \delta \\ A^i & \xrightarrow{\phi} & B^i \end{array}$$

Definition 2.1.15. Let (\mathcal{A}^*, d) be a DGA. Then the condition that $d \circ d = 0$ implies that $\text{Im}(d) \subseteq \text{Ker}(d)$. Therefore, the *Homology* of a DGA is a graded R -algebra given by $H_*(\mathcal{A}^*, d) = \bigoplus_{i \in \mathbb{Z}} H_i(\mathcal{A}^*, d)$ where

$$H_i(\mathcal{A}^*, d) = \frac{\text{Ker}(d : A^i \rightarrow A^{i-1})}{\text{Im}(d : A^{i+1} \rightarrow A^i)}.$$

If \mathcal{A}^* is a DGA over a ring R , then $H_*(\mathcal{A}^*, d)$ is said to be the homology of (\mathcal{A}^*, d) with coefficients in R .

Now that algebraic machinery sufficient for computing homology has been described, it remains to give a procedure for ascribing this machinery to a simplicial complex.

Definition 2.1.16. (The Homological Construction)

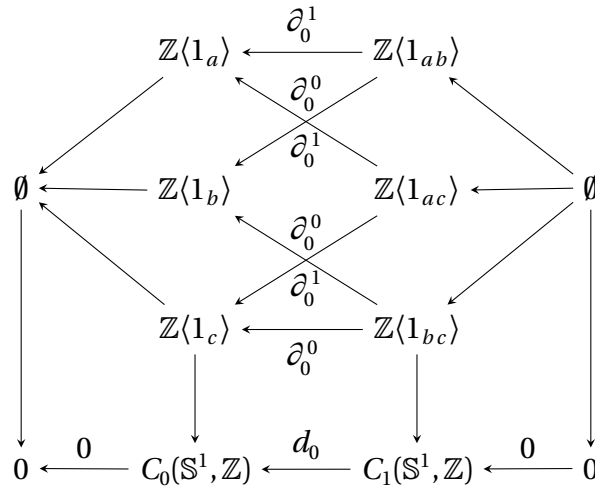
Let $\mathbf{S} = \{S_n\}_{n=0}^\infty$ be a simplicial complex and A be an algebra over a ring R . The DGA associated to \mathbf{S} , denoted $C_*(\mathbf{S})$, is constructed in the following manner.

The n^{th} -grading of $C_*(\mathbf{S})$ is given by $C_n(\mathbf{S}) = \bigoplus_{e \in S_n} A$. In words, each element of S_n has an associated copy of the algebra A and the n^{th} -grading of $C_*(\mathbf{S})$ is given by the direct sum over the elements of S_n .

The differential is induced by the face maps of the simplicial complex as an alternating sum, $d_j = \sum (-1)^i \partial_j^i$.

In topological literature, the resulting DGA is often denoted by $(C_*(\mathbf{S}, R), d)$ and is called a chain complex of \mathbf{S} with coefficients in R .

Example 2.1.16. In example 2.1.15 the simplicial (nerve) complex of \mathbb{S}^1 with open cover $\{U_a, U_b, U_c\}$ was constructed. Here the example is carried through to the DGA where the algebra is the integers, \mathbb{Z} . For clarity, the generator of each \mathbb{Z} summand carries a subscript corresponding to the elements of the open cover and their intersections. Compare the following diagram with that of example 2.1.15.



Therefore, the graded algebra in this case is given by $C_* = C_0 \oplus C_1$, where

$$C_0(\mathbb{S}^1, \mathbb{Z}) = \mathbb{Z}\langle 1_a \rangle \oplus \mathbb{Z}\langle 1_b \rangle \oplus \mathbb{Z}\langle 1_c \rangle$$

$$C_1(\mathbb{S}^1, \mathbb{Z}) = \mathbb{Z}\langle 1_{ab} \rangle \oplus \mathbb{Z}\langle 1_{ac} \rangle \oplus \mathbb{Z}\langle 1_{bc} \rangle$$

The differential is given by a signed sum over the face maps where sign is given by -1 to the power of the superscript of the face map. In this case, the face maps are induced by the inclusions in the simplicial complex and thus simply map generators to generators on the level of the algebras. Specifically, in this case the only non-zero differential map $d_0 : C_1 \rightarrow C_0$ is given by $(w, x, y) \mapsto (x - w, y - x, y - w)$ for $(w, x, y) \in C_1$.

In fact, the differential d_0 can be written as a matrix as follows:

$$d_0 = \begin{pmatrix} -1 & 0 & -1 \\ 1 & -1 & 0 \\ 0 & 1 & 1 \end{pmatrix}.$$

Because d_0 is the only non-zero differential, the homology is given by

$$H_0(\mathbb{S}^1, \mathbb{Z}) = \frac{C_0(\mathbb{S}^1, \mathbb{Z})}{\text{Im}(d_0)} = \mathbb{Z} \quad , \quad H_1(\mathbb{S}^1, \mathbb{Z}) = \text{Ker}(d_0) = \mathbb{Z} \quad , \quad \text{and} \quad H_i(\mathbb{S}^1, \mathbb{Z}) = \emptyset, \text{ else.}$$

The computation of the homology groups $H_*(\mathbb{S}^1, \mathbb{Z})$ could be carried out directly by evaluating the quotients of the algebras. However, given the matrix representation of the differential d_0 , it is enough to compute it's Jordan-normal form to determine the size of it's image and kernel.

$$\hat{d}_0 = \begin{pmatrix} 1 & 0 & 0 \\ 0 & 1 & 0 \\ 0 & 0 & 0 \end{pmatrix}.$$

Lastly, the invariants of primary interest in TDA can be computed.

Definition 2.1.17. Given the homology $H_*(\mathbf{S}, R)$ of a chain complex $C_*(\mathbf{S}, R)$ of a simplicial complex over R , the *Betti Numbers* of \mathbf{S} are given by the ranks of the homology groups. Namely:

$$\beta_i = \text{rank}(H_i(\mathbf{S}, R))$$

where

$$\text{rank}(H_i(\mathbf{S}, R)) = \dim_Q(H_i(\mathbf{S}, R) \otimes_R Q)$$

and Q is the field of fractions over R .

2.1.3 Functors

Now we get to the heart of the machine. The goal of these constructions is to compute invariants of manifolds. However, what guarantees that a simplicial complex derived from a manifold captures any information about the manifold and how do the differential graded algebras extract that information?

The answer is functoriality. In short, functors are maps between categories that preserve the structure of the objects in the domain category. Notice that the morphisms within a given category are maps between objects in that category that preserve the structure of the objects, e.g. the morphisms of the simplex category 2.1.3 preserve the order (and thus relations 2.1.3) and the morphisms of a DGA 2.1.14 preserve the gradings and algebraic operations. Therefore, it is enough for a functor between two categories to commute with the morphisms of those categories to guarantee that the structure of the domain category is captured by the image of the functor in the co-domain category.

Therefore, what is needed to compute the homology of manifolds are functors between a category of manifolds (which has not been explicitly defined here), the simplex category, and the category of DGAs. One such functor is the nerve construction 2.1.9 which describes how to construct a simplicial complex given a manifold and an open cover. Similarly, the homological construction 2.1.16 can be thought of as a functor from a category of simplicial complexes to a category of DGAs. Lastly, computing homology from DGAs can be described as a functor from DGAs to a category of graded rings.

Note that this review of homology, as it pertains to manifolds, is not a complete picture

and many details concerning category theoretic underpinnings have been omitted for brevity. For example, an appropriate category comprised of manifolds with open covers and morphisms between them has not been discussed. However, what has been presented should provide sufficient for what follows.

2.2 Topological Data Analysis

In the previous section, a method for computing the homology of a manifold was reviewed. Namely, given an open cover of the manifold the nerve construction 2.1.9 prescribed how to generate a simplicial complex and the nerve theorem 2.1.4 provided sufficient conditions on the open cover to guarantee that the complex captured the homotopy type of the manifold. Next, the homological construction 2.1.16 demonstrated how to equip the resulting simplicial complex with the algebraic structure required to obtain a DGA which could then be used to compute the homology and Betti numbers of a manifold.

Now, the goal of the present section is to describe how this theoretical machinery can be utilized to analyze data sets. In this case, a given data \mathcal{D} set is thought of as being a finite sample of some underlying space \mathcal{P} . It is the homology of \mathcal{P} which is the aim of TDA. As has been seen in the previous section, this requires an open cover of \mathcal{P} . Therefore, what is needed at this stage is a procedure for approximating an open cover of \mathcal{P} given \mathcal{D}

2.2.1 Open Covers from Data

The earliest methods for constructing open covers from finite data comes from two papers Voronoï (1908b) and Voronoï (1908a) which describe an algorithm for generating covers of \mathbb{R}^n (or more generally a finite dimensional metric space) by what are now commonly referred to as *Voronoi Cells* (not to be confused with the more modern use of the word *cell*

as used in algebraic topology when discussing CW-complexes).

Definition 2.2.1. (Voronoi Cover)

Let V be a metric space with a metric $d(-, -)$ and $\mathbf{S} \subset V$ be a finite set of points in V . For each point $p \in \mathbf{S}$, the cell associated to p is denoted C_p and is given by

$$C_p = \{x \in V \mid d(x, p) \leq d(x, \tilde{p}) \text{ for all } \tilde{p} \neq p \in \mathbf{S}\}$$

The collection of Voronoi cells $\mathbf{C} = \{C_p\}_{p \in \mathbf{S}}$ is called the Voronoi cover of V .

The nerve of a Voronoi cover is referred to in the literature as a Delaunay complex, so called because when V is a Euclidean space the nerve of a Voronoi cover can produce a Delaunay Triangulation (as first described in Delauney (1934)) of the convex hull of \mathbf{S} .

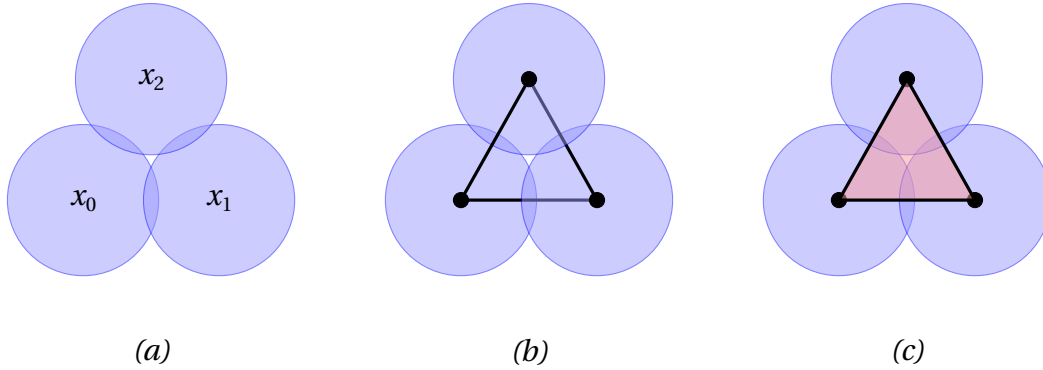
However, if the data set \mathbf{S} is known to be a sample from a metric space $(V, d(-, -))$, then an estimate of an open cover can be provided by taking the open ε -ball around each point in $\mathbf{S} \subset V$. The nerve of this type of cover is referred to as the *Čech Complex* and is denoted $C_*(\mathbf{S}, \varepsilon)$. The following theorem (which can be found in Carlsson (2009)) improves on the nerve theorem 2.1.4 by guaranteeing that there exists an ε such that the Čech complex recovers the homotopy type of the underlying space.

Theorem 2.2.1. *Let $(V, d(-, -))$ be a Riemannian manifold. Then there exists a positive $e \in \mathbb{R}$ such that for each $0 < \varepsilon < e$ there exists a finite subset $\mathbf{S} \subset V$ such that the Čech complex $C_*(\mathbf{S}, \varepsilon)$ has the that homotopy type as V .*

A similar but computationally cheaper approach is given by the *Vietoris-Rips Complex*, denoted $VR_*(\mathbf{S}, \varepsilon)$, in which $k + 1$ data points $\{x_0, \dots, x_{k+1}\} \subset \mathbf{S}$ form a k -simplex if the distance between each pair is less than ε . The primary difference between the Čech and Vietoris-Rips complex is that the parameter ε in the Čech complex refers to the radii of

the open balls while the ε parameter in the Vietoris-Rips complex refers to the distance between the data points themselves.

Example 2.2.1. *A common example of how the Čech complex and the Vietoris-Rips complex can differ given the same data set.*



(a) The ε -balls around three data points x_0 , x_1 and x_2 . (b) the Čech Complex for this arrangement. (c) the Vietoris-Rips complex for this arrangement.

Notice that in example 2.2.1 above the Čech complex is 1-dimensional while the Vietoris-Rips complex is 2-dimensional. This is seen as one of the primary advantages of the Vietoris-Rips complex over the Čech complex. The Čech complex is more likely to generate simplices over a wide range of dimensions while the Vietoris-Rips complex tends to produce simplices in a narrow range of dimensions.

A concern here is that the Vietoris-Rips complex may miss important features which the Čech complex captures with its higher level of resolution. However, given the relationship between parameters ε as used by both constructions, there exists the following relationship (Carlsson 2009)

$$C_*(\mathbf{S}, \varepsilon) \subseteq VR_*(\mathbf{S}, \varepsilon) \subseteq C_*(\mathbf{S}, 2\varepsilon)$$

which guarantees that for a given Čech complex with a fixed ε , there is a choice of ε for the Vietoris-Rips complex which captures the same structure (here \subseteq relation means sub-

complex).

The methods described thus far for generating complexes typically start by taking the entire data set as the vertex set of the complex. However, this may not be necessary and lead to superfluous simplices which substantially increase the complexity of the computation but do not ultimately contribute to homology. Consider example 2.1.15 where a simple simplicial complex was generated using a 3-part open cover of the circle. Because the open cover was small, the simplicial complex was small and the homology of the circles was able to be quickly computed in example 2.1.16. However, one could construct a similar open cover which is much larger. In that case, the simplicial complex and thus the matrix representation of the differential would have been much larger. This would have greatly increased the effort needed to compute the exact same homology.

A more recently developed method for generating complexes from data sets (presented by de Silva and Carlsson (2004)) seeks to mitigate the problem of superfluous simplices. The *Witness Complex* does this by using a subset of the data set $\mathcal{L} \subset \mathbf{S}$ (called the *landmark set*) as the vertex set and the rest of the data set is used to determine how to construct the complex from the landmark set.

Definition 2.2.2. (*Strong Witness Complex*)

Let $(V, d(-, -))$ be a metric space and $\mathcal{L} \subset V$ be a finite subset, called the *landmark set*, and $\varepsilon > 0 \in \mathbb{R}$. For each $v \in V$, let $d_v = \min_{l \in \mathcal{L}} \{d(v, l)\}$. Define the *strong witness complex*, $W^s(V, \mathcal{L}, \varepsilon)$, in the following way. Let \mathcal{L} be the vertex set. A $k + 1$ subset $\{l_0, \dots, l_k\} \subseteq \mathcal{L}$ is a k -simplex if and only if there exists a point $v \in V$ such that for all $0 \leq i \leq k$, $d(v, l_i) \leq d_v + \varepsilon$ (in which case v is called the *witness* to the k -simplex).

Lastly, the first scheme for generating simplicial complexes from discrete data to be implemented on a modern computer does not fall nicely within the open cover paradigm thus far described. However, it deserves remarking upon for its historical importance as

well as for its contemporary uses.

First developed to formalized the notion of "shape" for sets of points in the plane (Edelsbrunner et al. 1983), α -shapes where then generalized to data sets in \mathbb{R}^3 (Edelsbrunner and Mücke 1994). They where then used to develop and implement an algorithm for numerically computing the Betti numbers of simplicial complexes on the 3-sphere (Delfinado and Edelsbrunner 1995) with \mathbb{Z}_2 coefficients which was later improved (Edelsbrunner et al. (2002) and Zomorodian and Carlsson (2005)) to compute the homology of arbitrary simplicial complexes with a broader range of coefficients.

The essential distinction between the methods described thus far and α -shapes is that rather than building a simplicial complex up from a vertex set, an α -shape is constructed by whittling away at the convex hull of the data set. As where the other methods can be thought of as bottom-up, α -complexes are a more top-down approach.

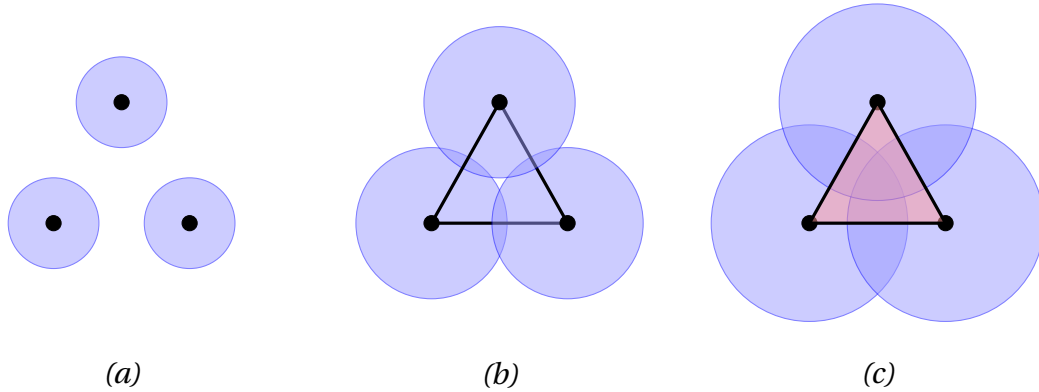
The result is a polytope called the α -shape of the data set. This is then transformed into a simplicial complex (called the α -complex) via a relationship between α -shapes and Delaunay triangulations. A full description of α -shapes and the resulting α -complexes would require a relatively lengthy exposition of Delaunay triangulations and some discrete convex geometry which is beyond the scope of the current narrative. The interested reader is directed to the references for a full description.

2.2.2 Persistent Homology

Note that the methods described in subsection 2.2.1 introduce a new free parameter; ε 's in the case of the Čech, Vietoris-Rips, and Witness complexes, and α in the case of the α -complex. Different choices of these parameters can give rise to simplicial complexes with different homology. The natural question is which value of the parameter is best? The current answer is all of them.

Persistent Homology is among the primary methods used in TDA to extract qualitative information from a data set and was first described by Edelsbrunner et al. (2002) which utilized α -complexes. Persistent homology is the process of iterating through values of the newly introduced free parameter (usually increasing it's value), constructing the complex, and computing homology at each increment of the parameter. The key feature that elevates this method is that the complex associated to a given value of the free parameter is a subcomplex of the complex generated by the next increment of the free parameter.

Example 2.2.2. Consider the Čech complex in which the free parameter ϵ is the radius of an open ball around each point. As the radius of the ϵ -balls increase, the only change is that higher dimensional simplices are added to the complex. This means that each complex generated at a given value of ϵ is a subcomplex of the complex generated for larger values of ϵ .



(a) ϵ is small so all intersections of ϵ -balls are empty, the complex is just a vertex set. (b) for larger ϵ the pairwise intersection of the ϵ -balls is non-empty which produces edges in the complex (c) for even larger ϵ the triple intersection of the ϵ -balls is non-empty which yields a 2-simplex in the complex.

In the literature, a sequence of simplicial complexes $\{S_i\}_{n=0}^k$ is called a *filtration* if each S_i is a sub-complex of S_{i+1} . That is, if there is an inclusion of simplicial complexes, $S_i \hookrightarrow S_{i+1}$.

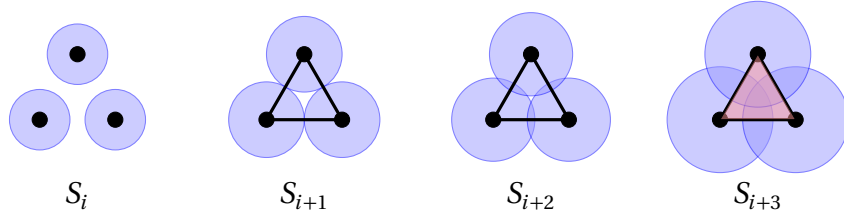
Due to functoriality, an inclusion map between simplicial complexes induces a map on their homology groups, $H_*(S_i) \xrightarrow{i_*} H_*(S_{i+1})$. In the case of TDA, incrementing by the free parameter produces such a filtration, (see example 2.2.2 above).

Utilizing the filtration, and the resulting induced maps on the homologies, it is possible to determine where in a filtration a generator in homology (which represents a topological feature) first appears and when it subsequently disappears. Notice that in example 2.2.2, the first complex has trivial first homology, the second complex has one generator in first homology, and in the third complex that generator has been "filled in" to form the 2-simplex. Therefore, there was a topological feature (represented by a generator of first homology) that appeared in the second complex and *persisted* until the third complex.

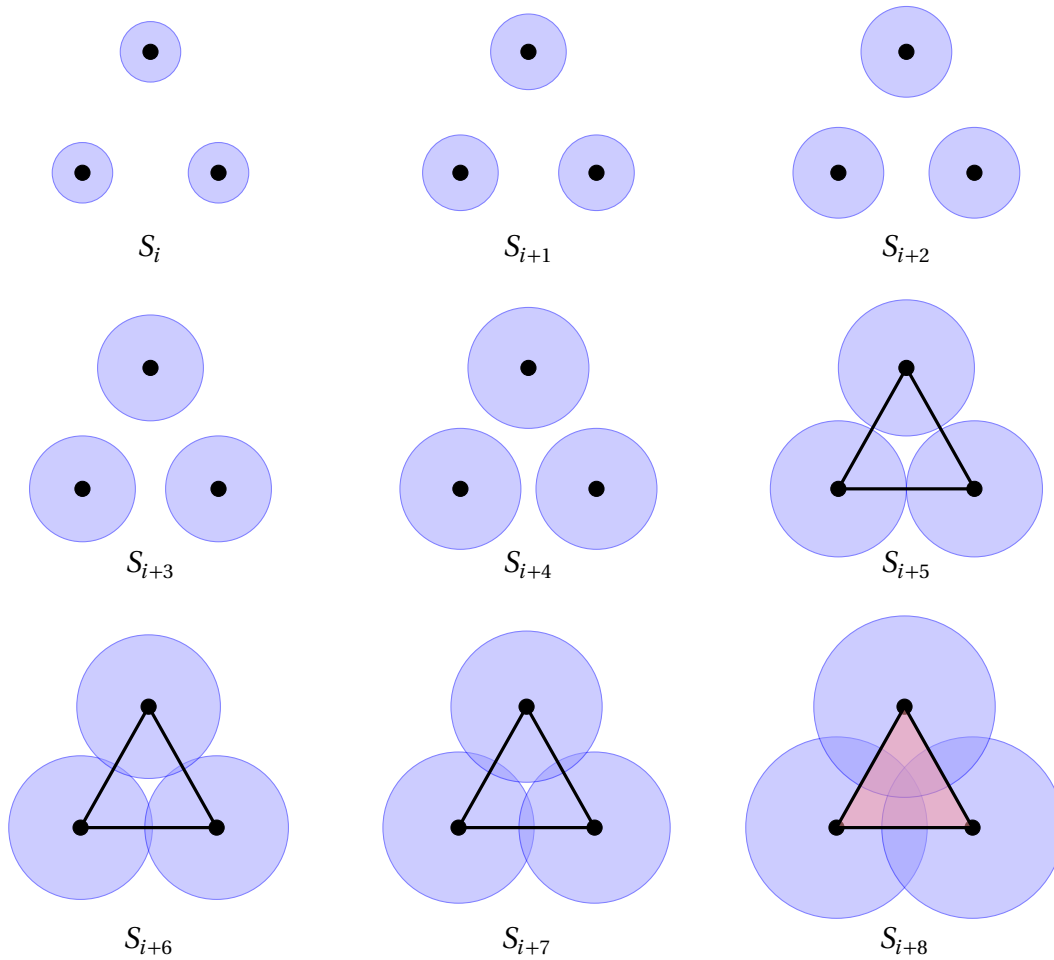
The filtration level at which a topological feature (equivalently, generator in homology) first appears is called its *birth* and the subsequent level of filtration at which it no longer appears is called its *death*. Therefore, once the persistent homology of a data set has been computed, what is left is a (often large) collection of generators in homology with their respective births and deaths. This approach allows the data analyst to examine the topological structure of the data set at various levels of resolution simultaneously as opposed to attempting to select the single "best" value of the free parameter. The new question is, which of these generators are "genuine" features of the data set and which are artifacts of the various choices that have been made?

Edelsbrunner et al. (2002) suggested the following method. The length of time for which a given topological feature persists is called its *lifespan*, $\text{lifespan} = \text{death} - \text{birth}$. Those generators with relatively longer lifespans represent significant topological features of the data set while those with relatively shorter lifespans do not. This perspective is largely motivated by the intuition that it will take more increments of the free parameter for the open balls to fill in a large cavity in the data set than a small one.

Example 2.2.3. *The Čech complex of a configuration of points which are close to one another.*



For comparison, the Čech complex of the same configuration of points but farther apart.

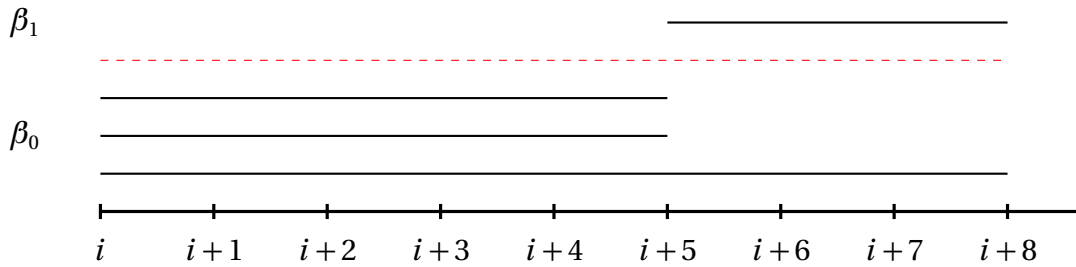


Notice that in the first configuration the homology becomes trivial much faster than in the second configuration. Namely, the three components in the former have a life span of 1 while those in the latter have a life span of 5. Similarly, the generator of first homology has a lifespan of 2 in the first example and a lifespan of 3 in the second.

However, assigning significance to ordering the generators by lifespan is not always reliable and should be used as heuristic rather than a hard rule. Namely, in section 4.1.2 it is shown that noise in a data set tends to flatten the distribution of the lifespans of the generators.

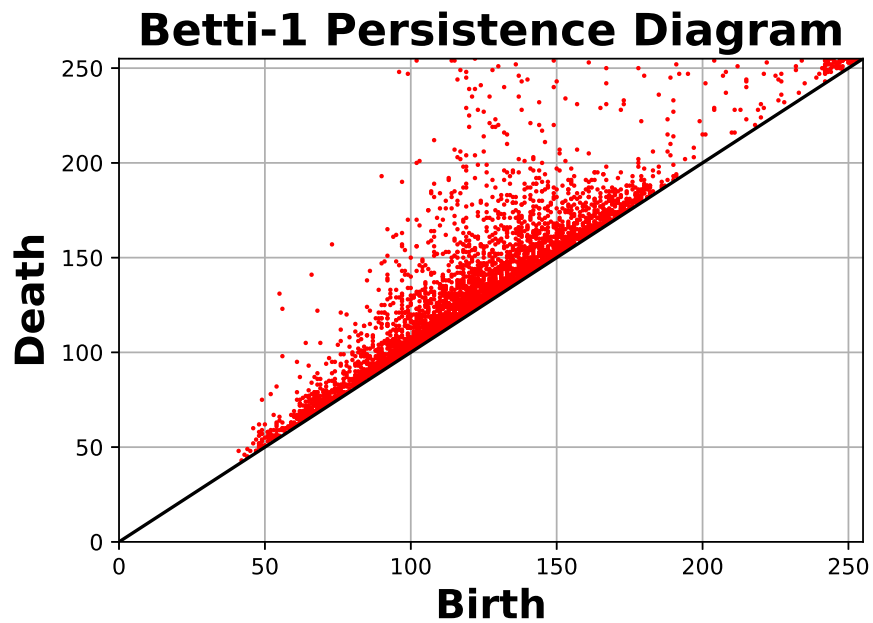
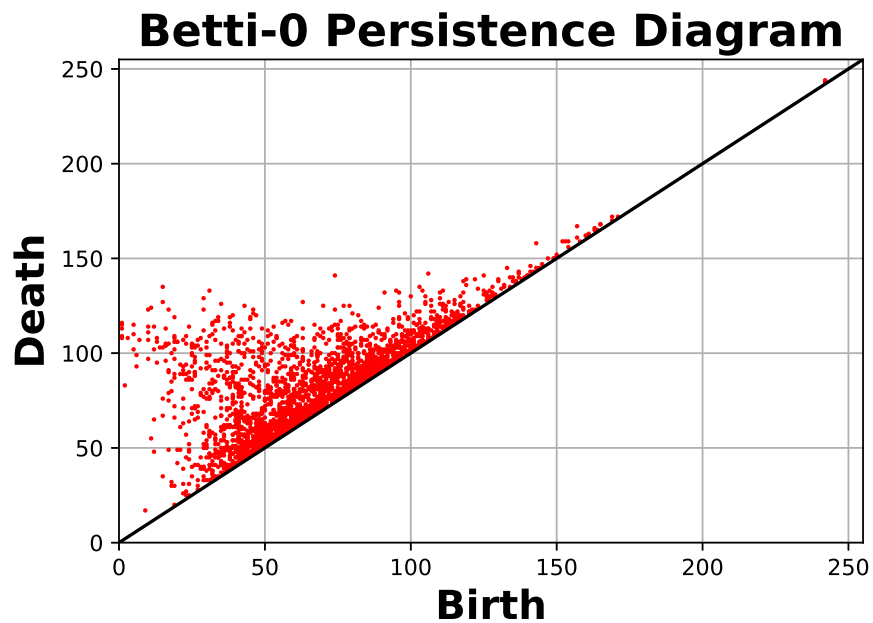
There are two common methods for visualizing the output of persistent homology referred to as *barcodes* and *persistence diagrams* (Edelsbrunner et al. (2002) and Carlsson et al. (2005)). In the barcodes representation, the x-axis is time and each topological feature has an associated interval whose endpoints are its birth and death. These intervals are usually visually separated by Betti number. Persistence diagrams represent the same data with a scatter plot wherein each topological feature corresponds to a point in the plane whose x-coordinate is its birth and its y-coordinate is its death. In this representation, it is often necessary to have a persistence diagram for each Betti number.

Example 2.2.4. *A barcode for the second set of points in example 2.2.3 would look like the following.*



The bottom three lines represent the three connected components which persist from time i until time $i+5$ when they come together to form a single connected component and one loop which persists for the rest of recorded time. That is, from time i to time $i+5$, $\beta_0 \equiv \text{rank}(H_0) = 3$ and $\beta_1 \equiv \text{rank}(H_1) = 0$. At time $i+5$ this changes to become $\beta_0 \equiv \text{rank}(H_0) = 1$ and $\beta_1 \equiv \text{rank}(H_1) = 1$.

Example 2.2.5. Below is an example of two persistence diagrams. Each point represents a generator in zeroth and first homology respectively. The x-coordinate of each point is its corresponding generators birth and y-coordinate its death. More about these diagrams the the data set they were generated from will be discussed later.



Persistence diagrams have been shown to be a complete separable metric space (Mileyko et al. 2011) using the *Wasserstein metric*. Another popular metric on the space of persistence diagrams is called the *bottle-neck distance*. However, while the structure of metric space makes the study of persistence diagrams amenable to standard statistical methods, it has been found to be ill-behaved. Namely, the Wasserstein metric and bottle-neck distance are relatively computationally intensive as compared to more common place metrics. Furthermore, the average of a persistence diagram is not unique as pointed out in Mileyko et al. (2011). These, among other issues, make working with persistence diagrams directly rather difficult. Subsequently, various methods for transforming persistence diagrams into more agreeable representations has become an industry on its own.

2.2.3 Persistence Curves

One attempt to remedy some of these problems is to vectorize the persistence diagrams. That is, transform it into a vector in a Euclidean space. Among the most popular of these methods are so called *Persistence Landscapes* (Bubenik 2015). These are based on *rank functions*.

Definition 2.2.3. (*Rank Functions*)

Given a persistence diagram, define the rank function, $\lambda : \mathbb{R}^2 \rightarrow \mathbb{R}$, by

$$\lambda(b, d) = \begin{cases} \beta^{b,d} & b \leq d \\ 0 & \text{else} \end{cases}$$

where $\beta^{b,d}$ is given by $\text{rank}\left(\text{Im}\left(H_*(S_b) \rightarrow H_*(S_d)\right)\right)$

As in the case of persistence diagrams, all of the non-zero images of λ lie above the diagonal in the first quadrant of \mathbb{R}^2 . Therefore, the *re-scaled rank function* is often used which simply rotates the plane so that the diagonal becomes the x-axis.

Definition 2.2.4. (*Re-scaled Rank Functions*)

Given a persistence diagram, let $m = \frac{d-b}{2}$, $h = \frac{d-b}{2}$, and define $\tilde{\lambda} : \mathbb{R}^2 \rightarrow \mathbb{R}$ as given by

$$\lambda(m, h) = \begin{cases} \beta^{m-h, m+h} & h \geq 0 \\ 0 & \text{else} \end{cases}$$

Using the notation of the re-scaled rank functions, persistence landscapes are given by the following definition.

Definition 2.2.5. (*Persistence Landscapes*)

Given a persistence diagram, the persistence landscape is a function $\lambda : \mathbb{N} \times \mathbb{R}^2 \rightarrow \bar{\mathbb{R}}$ (where $\bar{\mathbb{R}} = [-\infty, \infty]$ is the extended real line). For a given $k \in \mathbb{N}$, it is given by:

$$\lambda(k, t) = \lambda_k(t) = \sup(m \geq 0 \mid \beta^{t-m, t+m} \geq k)$$

As described in Bubenik (2015) and Bubenik (2018), persistence landscapes have many advantages, both computationally and theoretically, over barcodes and persistence diagrams. A thorough comparison is beyond the scope of the present discussion and interested reads are directed to the references.

Following the popularity of persistence landscapes, various other vectorization schemes have been developed. Many of these, including persistence landscapes, fall under the general framework of *Persistence Curves* as defined by Chung and Lawson (2019).

Definition 2.2.6. (*Persistence Curves*)

Let \mathcal{D} be the space of persistence diagrams, \mathcal{F} be the set of all functions $\psi : \mathcal{D} \times \mathbb{R}^3 \rightarrow \mathbb{R}$ such that $\psi(D; b, b, t) = 0$ for all $(b, b) \in D$ and $D \in \mathcal{D}$, and let \mathcal{T} be the set of summary statistics (i.e. $T \in \mathcal{T}$ is a map that takes a multi-set to a scalar). Lastly, let \mathcal{R} represent the space of functions from \mathbb{R} to \mathbb{R} .

Then, define a map $P : \mathcal{D} \times \mathcal{F} \times \mathcal{T} \rightarrow \mathcal{R}$ where:

$$P(D, \psi, T)(t) \rightarrow T(\psi(F_t, t)), t \in \mathbb{R}$$

$P(D, \psi, T)(t)$ is called the *persistence curve* of D with respect to ψ and T .

Example 2.2.6. Let $\max_k(S)$ be the k^{th} largest number of a set S . Then given a persistence diagram D , define

$$l_{(b,d)}(t) = \begin{cases} 0 & t \notin (b, d) \\ t - b & t \in (b, \frac{b+d}{2}] \\ d - t & t \in (\frac{b+d}{2}, d) \end{cases}$$

Then the k^{th} -persistence landscape is given by $\lambda_k(t) = \max_k \{l_{(b,d)}(t) \mid (b, d) \in D\}$. Note that $l_{(b,d)}(t) = \min\{t - b, d - t\}$. To fit persistence landscapes into the framework of persistence curves, let $\psi(b, d, t) = \min\{t - b, d - t\}$ and $T = \max_k$. Then $P(D, \psi, T) \equiv \lambda_k$.

While demonstrating that persistence landscapes fall in the paradigm of persistence curves is significant, it is not the most enlightening/intuitive example. Therefore, consider the following example which recovers the *Betti Curve* which is a function $\beta_k : \mathbb{R} \rightarrow \mathbb{R}$ given by $t \mapsto \text{rank}(H_k(S_t))$.

Example 2.2.7. Let $\mathbf{1} : \mathbb{R}^3 \rightarrow \mathbb{R}$ be given by $\mathbf{1}(x, y, t) \neq 1$ if $x = y$ and 0 otherwise. Let \sum be the usual summation operation. Then in the language of persistence curves, let $\psi \equiv \mathbf{1}$ and $T \equiv \sum$ and define

$$P(D_k, \mathbf{1}, \sum)(t) = \sum (\{\mathbf{1}(D_k; d, b, t) \mid b \leq t, d > t\})$$

Where $\mathbf{1}(D_k; d, b, t)$ indicates that the function $\mathbf{1}(d, b, t)$ is being evaluated on the generators in the persistence diagram of generators in k^{th} homology, D_k . For a fixed time t ,

$\{\mathbf{1}(D_k; d, b, t) \mid b \leq t, d > t\}$ is the collection of values that $\mathbf{1}(D_k; d, b, t)$ takes when evaluated on the subset of generators in D_k whose times of birth and death satisfy $b \leq t$ and $d > t$ (those generators in D_k alive at time t).

Therefore, $\{\mathbf{1}(D_k; d, b, t) \mid b \leq t, d > t\}$ is a collection of 1's the size of which is equal to the number of generators in D_k alive at time t . The summation operation \sum then adds up all of the 1's.

This is just a fancy way of adding up all of the generators in D_k alive at each time t and is therefore equivalent to the Betti Curve, $P(D_k, \mathbf{1}, \sum)(t) = \beta_k(t)$.

In fact, numerous curves can be generated by varying the function $\psi = \mathbf{1}$ in the previous example 2.2.7. It is persistence curves of this type which will be the primary concern going forward.

CHAPTER

3

METHODS

Now that the theoretical ground work has been laid, it is time to describe the project. The previous discussion involved computing the persistent homology and persistence curves (hereafter referred to as PCs) from a given data set. Therefore, a characterization of this class of statistical summaries would require computing them for a relatively large number of data sets. However, in some instances the individual datum within a given data set are complex enough to be considered as data sets in their own right. In this case, persistence curves can be computed for each element of the data set and used for comparison. Here, a data set of images was thought to suffice.

Mathematically, an 8-bit RGB color image is a three dimensional array of integers each element of which lies in the range $[0, 255]$. The space of such images will be denoted

$Ig[m, n, 3]$ where the given image has pixel dimension $m \times n$ and three color channels (red, green, and blue respectively). Thought of in this way, such an image is a structured data set in itself.

In this study, various PCs, in the style of example 2.2.7, were computed for each image in a data set of labeled images. The viability of a given PC was then substantiated by attempting to classify the images, according to their original labels, based on their PCs. This gave a sense of how well a given PC captured characteristic features of a class of images which distinguish it from other classes.

After this was accomplished, an investigation into the robustness of the PCs as statistical summaries was conducted by injecting the images with increasing levels of various noise types and recomputing their PCs. Methods for filtering out the noise at the level of the PCs were then proposed and investigated.

3.1 The Data Set

The KTH-TIPS2b data set was used in this study. It is a collection of 4,752, 200x200 pixel, 8-bit RGB color images of 11 different texture classes. For each of the 11 textures, four samples were used to generate images which were taken under varying illumination, perspective, and scale (hence TIPS) at the School of Computer Science and Communication in Stockholm Sweden. More information about the images in this data set, including how they were collected, can be found in their paper Mallikarjuna et al. (2006). Figures 1-11 below contain a sample image from each texture class.



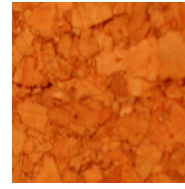
aluminium



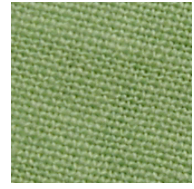
brown bread



corduroy



cork



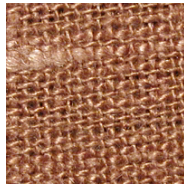
cotton



cracker



lettuce



linen



white bread



wood



wool

Figure 1 - Figure 11

3.2 Persistence Homology

Persistence Diagrams (PDs) were derived from the images using the software Perseus (Mischaikow and Nanda 2013) which is implemented in MATLAB. Each image in the KTH-TIPS2b data set is a 200x200 pixel 8-bit RGB (red-green-blue) image. That means that each image is represented mathematically by a 200x200x3 array with integer values ranging from 0 to 255. Each of these were split into three 200x200 matrices each of which were analyzed independently.

Perseus takes in one of these 200x200 matrices. It then iterates through the integers from 0 to 255 and for each element of the matrix, it either changes its value to 0 or 1 depending on whether the element's value is above or below the integer respectively. This process is

referred to as *thresholding*. It then computes two PDs, one for the Betti-0 invariant and another for the Betti-1 invariant. See Fig.3.12 for examples.

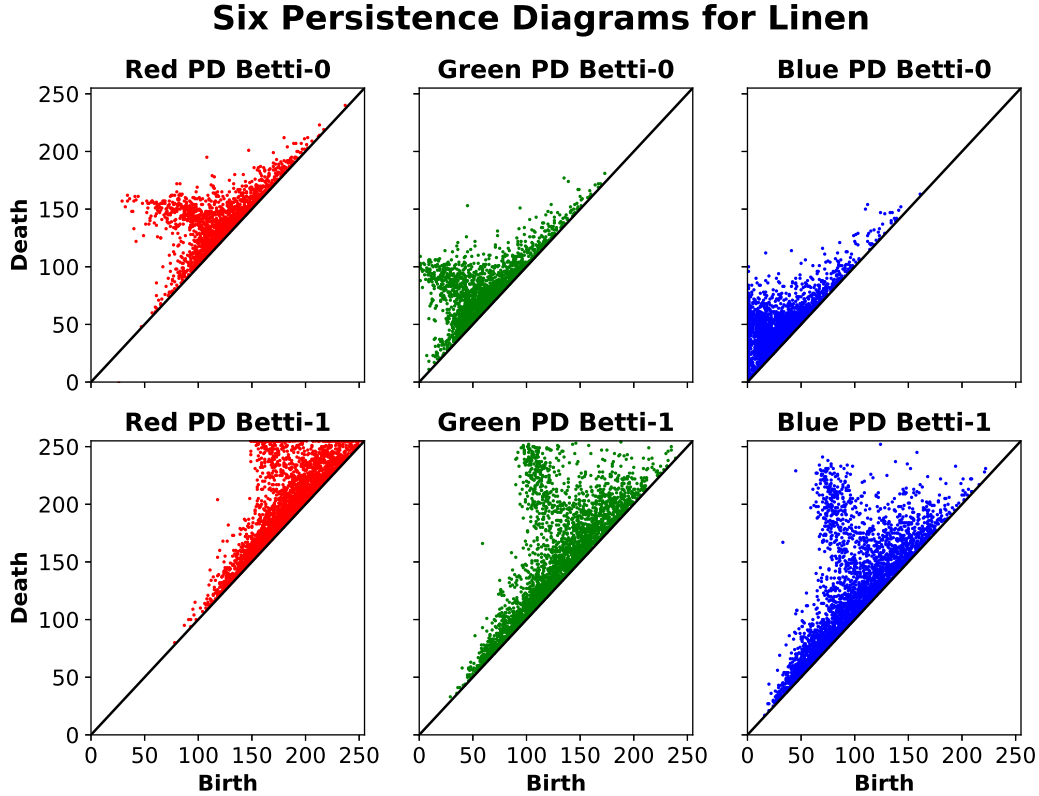


Figure 3.12: The six persistence diagrams for the linen texture example 3.8.

The intuitive way to think about the thresholding process is the following. Each color channel of an image in the data set is a 200×200 matrix of integer values in the range $[0, 255]$. Now think of a given value in the matrix $Im[i, j]$ as the value of a function $Im : \mathbb{R}^2 \rightarrow \mathbb{R}$ which takes $(i, j) \mapsto Im[i, j]$. The graph of this function is a surface bounded in the rectangular prism $[0, 200]^2 \times [0, 255] \subset \mathbb{R}^3$. The thresholding process can then be thought of as taking sublevel sets of the resulting surface at integer values along the z-axis. Each such sublevel surface includes into the next which produces the filtration that underlies the persistent

homology.

See figure 3.13 for an example of an image and its representation as a surface. Furthermore, see example 3.2.1 for how this thresholding process works with this example.

Example: $f(x, y) = 127.5 \cdot \left(\frac{xy}{65025}\right) \cdot \sin\left(\frac{4\pi x}{255}\right) \cdot \sin\left(\frac{4\pi y}{255}\right) + 127.5$

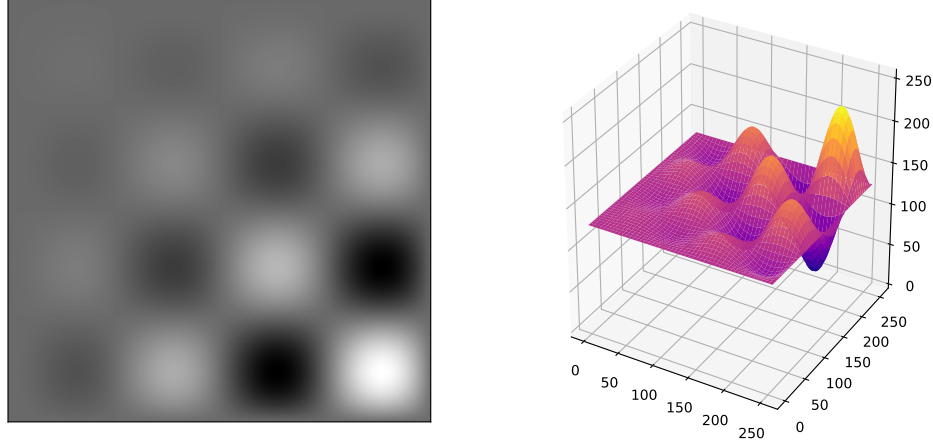
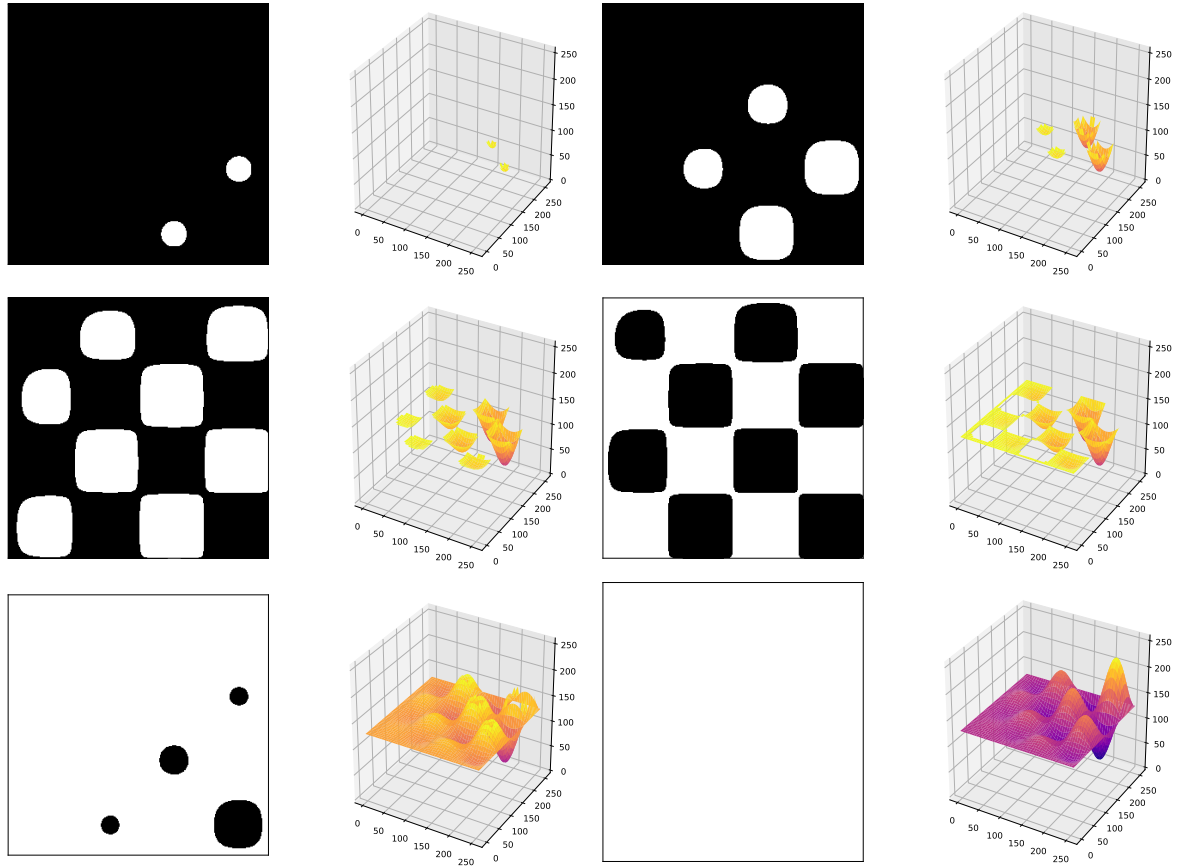


Figure 3.13: A 255x255 pixel gray-scale image artificially generated using the function $f(x, y)$ and its representation as a surface in \mathbb{R}^3 .

Because the image in figure 3.13 is an 8-bit gray-scale image. There is only one color channel and thus only one matrix/surface for which to compute the persistent homology. For the RGB images in the KTH-TIPS2 data set, there are three color channels and therefore three matrices/surfaces for which to compute the persistent homology.

Example 3.2.1. *The resulting images and sublevel surfaces of figure 3.13 at six different threshold values to be read left to right and top to bottom in order of increasing threshold value.*



3.3 Persistence Curves

Each feature (point) in a persistence diagram has three associated values of interest, birth (x-coordinate), death (y-coordinate), and lifespan (death - birth). *Persistence Curves* (PCs) may be derived from aggregating these quantities in various ways over all the features in the diagram (see section 2.2.3 for a formal treatment). For this study, the Betti, Life, Midlife, and Multiplicative Life curves were chosen. Each curve is generated by iterating through the integers from 0 to 255 and at each integer performing a computation on each feature

in a given PD which is alive at that time and summing the results of the computations. The formula for the computation on each feature is what distinguishes the curves and are described in Fig.3.1.

Curve	Formula
Betti	1
Life	(death - birth)
Midlife	$\frac{(\text{death} + \text{birth})}{2}$
Multiplicative Life	$\frac{\text{death}}{\text{birth}}$

Table 3.1: Formulas for computing the persistence curves used in this study.

For example, the Betti Curve simply returns 1 for each feature alive at the given threshold and sums over all of them thus returning the total number features alive at each given time.

For each image in the KTH-TIPS2 data set and each curve type in table 3.1 the analysis produces six curves. Figure 3.14 demonstrates the six Betti curves for the linen example 3.8 mid-computation. These six curves are concatenated to form a 1,530 dimensional vector called the *Topological Color Profile* (abbreviated TCP) of the given image with respect to the given curve. Figures 4.1 - 4.4 depict the four TCPs of the linen example 3.8, one for each curve in table 3.1.

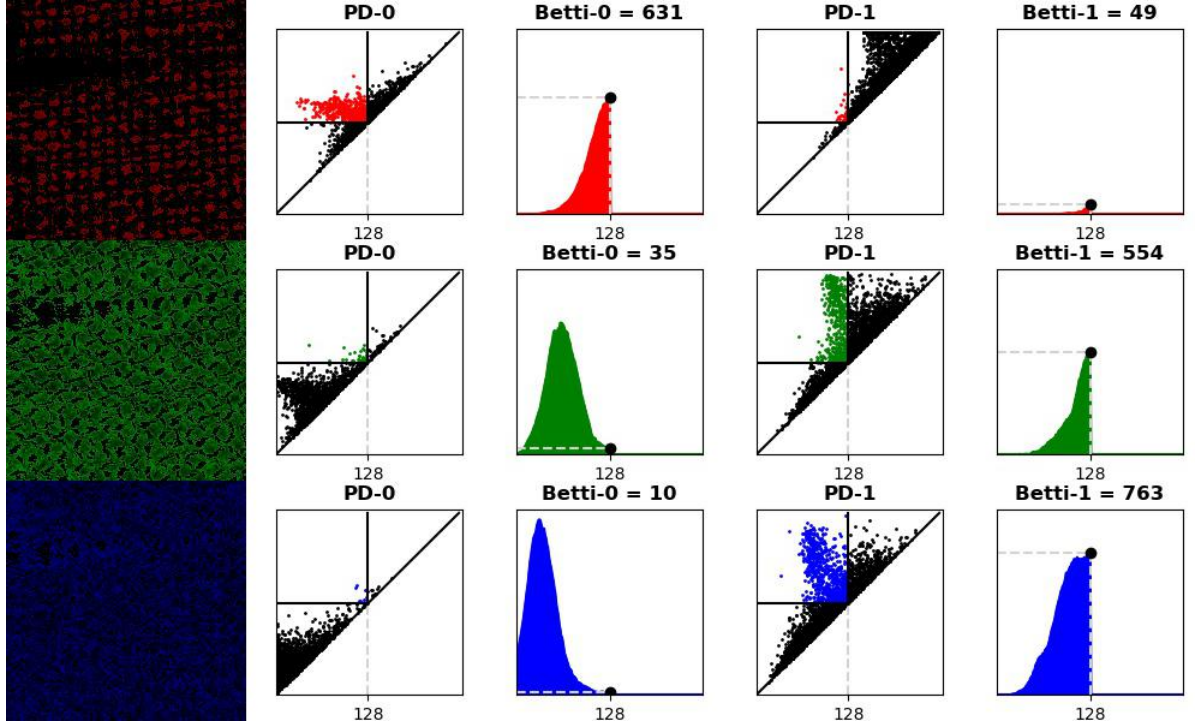


Figure 3.14: The three color channels of the linen example 3.8 alongside their respective PDs and Betti Curves at threshold 128.

3.4 Noise Injections

In order to determine how robust the PCs were to perturbations, the original images were injected with increasing amounts of noise and the TCPs regenerated for the noisy images. For this study the images were injected with Gaussian, speckle, and salt&pepper noise at increasing levels of signal-to-noise-ratio as measured in decibels (SNRdB) by the Eq.3.1 where I is the image before adding noise and J is the image after adding noise.

$$\text{SNRdB} = \log_{10} \left(\frac{\sum J_{ijk}^2}{\sum (J_{ijk} - I_{ijk})^2} \right) \quad (3.1)$$

Gaussian noise adds mean zero noise to each pixel with a variance determined by

the SNRdB value. Speckle noise multiplies mean one noise to each pixel with variance determined by the SNRdB. Finally, salt&pepper noise either maximizes or minimizes a random sample of the pixel values the size of which is determined by the SNRdB. Due to its discontinuous nature, salt&pepper noise was expected to be the most obstructive of the three noise types. The SNRdB values chosen for this study were 1.1 and every two from 2 to 28 totaling 15 SNRdB values. See Figs.18-32 for some examples of noisy images.

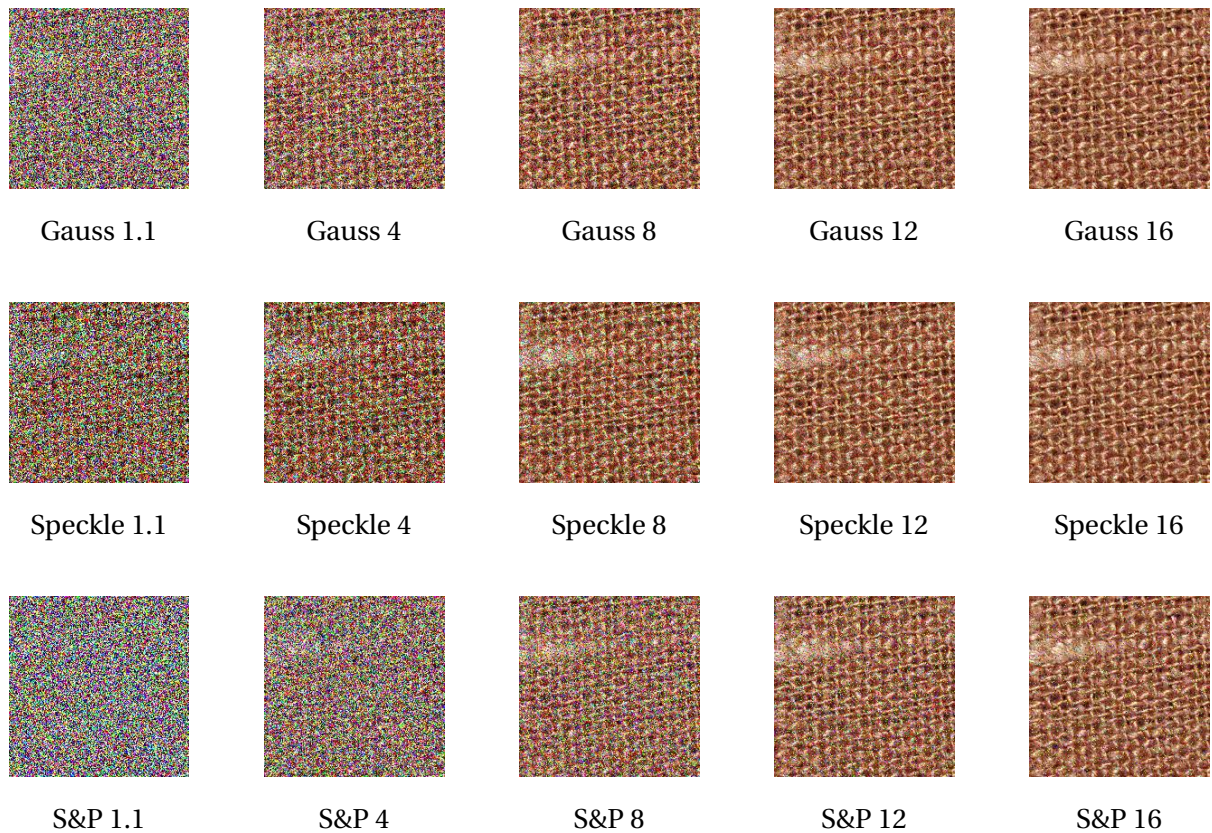


Fig.18 - Fig. 32 The linen example 3.8 injected the three noise types at five of the fifteen levels of SNRdB.

3.5 Deep Learning

A test of the relative viability of a given PC was conducted by attempting to classify the images, according to their original texture classes, based on their TCPs. In order to do this a, machine learning model was built and trained to classify the data set of TCPs. There are various machine learning architectures including SVM, Random Forests, and so called *deep learning* techniques (such as neural and convolutional networks). The subject of machine learning is very much a live and evolving rapidly. What follows is a brief description of the deep learning method used in this study and the interested reader is directed to Goodfellow et al. (2017) for a formal and modern treatment of the topic in general.

The machine learning architecture chosen for this study was a neural network called a *Multi-Layer Perceptron* (MLP). The model takes a TCP as input and returns a prediction as to the class of the TCP's associated image in the form of an eleven dimensional vector, one component for each texture class (also known as a 1-hot encoding). The value of a given component in the output vector is interpreted as the probability that the image associated to the input TCP belongs to the texture classes associated to that component.

An MLP makes these predictions by passing the input vector (TCP) through a sequence of linear transformations with an intermediate non-linear function after each transformation. The final non-linearity normalizes the vector so that it is interpretable as a probability. Each operation (application of linear transformation and non-linear function) reduces the dimension of its input. A vector resulting from one of these operations, if it is not the final output of the model, is referred to as a *hidden layer*. The number of hidden layers, the reduction in dimension after each operation, and the non-linear functions themselves are all hyper-parameters which have to be tuned by hand for a model to be successful.

The MLP used in this study had one hidden layer of dimension 250. That is, the model takes an input TCP of dimension 3,060 (see section 4.1 for why this is doubled from 1,530),

linearly transforms it into a 250 dimensional vector, and passes it to a non-linear function, in this case a *ReLU* (rectified linear). The resulting vector (hidden layer) is then passed to a second linear transformation which reduces its dimension to 11. Finally, it is given to a final non-linear function, in this case a *softmax*, which normalizes the vector so that its components are interpretable as probabilities. See Fig.3.30 for a diagrammatic representation of the architecture.

The components of each linear transformation are parameters of the model. The model is trained by optimizing these parameters with respect to a *loss function* which measures the difference between the models prediction and the correct classification. The loss function and optimization algorithm used in this study were *categorical cross-entropy* and the *Adam Optimizer* (a variant of stochastic gradient descent). This model was implemented in TensorFlow using their Python APIs.

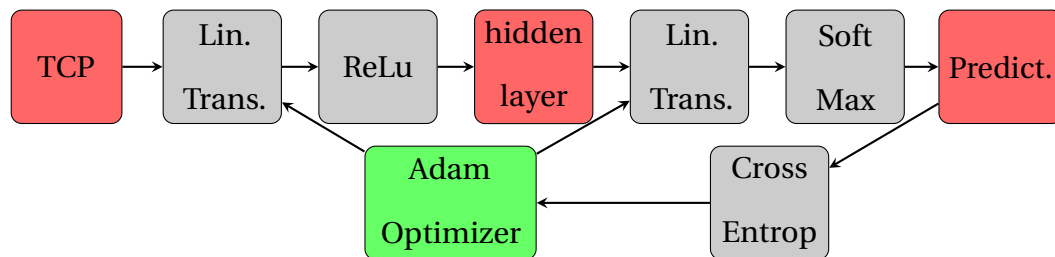


Figure 3.30: Diagram of the MLP architecture.

When training a machine learning model, the data set is split into three parts. The first is called the *training set* and is the data on which the model is optimized. In this study, the, training set accounted for approximately 60% of the images (2,832). The second is called the *validation set* which is used when hand tuning the hype-parameters to determine whether the model is over-fitting to the training set. The final division is the *test set* which is used

to test the model once the hyper-parameters have been settled to again determine if the model is over-fitting to the training/validation set. In this case, the validation and test sets made up approximately 20% of the images (960) each. Furthermore, the splitting of the data set into training, validation, and test sets was uniformly random across each of the four samples of each texture class.

Lastly, in order to increase the models accuracy it is common to optimize over the training set multiple times. Each instance of optimizing the model over the entire training set is called an *epoch*. In this study, ten such models were trained for twelve epochs and their average accuracy and error was recorded at each epoch.

CHAPTER

4

RESULTS AND ANALYSIS

4.1 TCPs and Noise

Recall from section 3.3 that a topological color profile (TCP) associated to a given image in the data set is constructed by concatenating the six persistence curves (PCs) resulting from computing the persistent homology of the image.

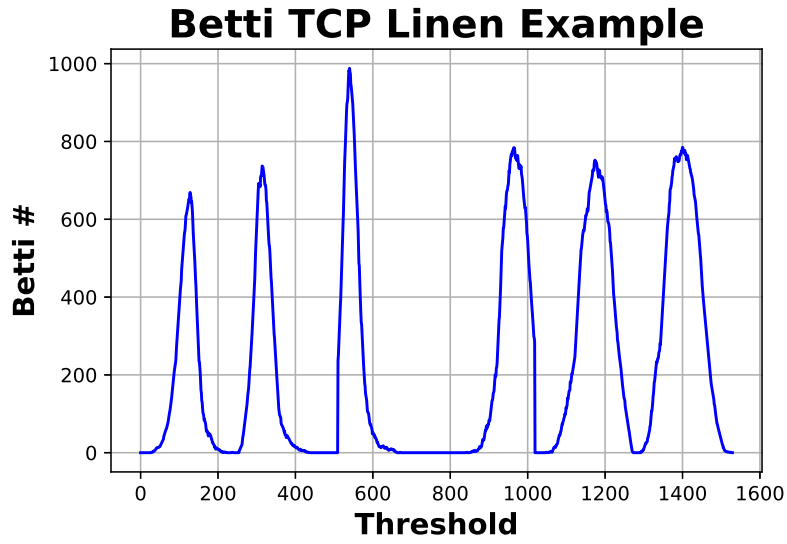


Figure 4.1: The Betti-TCP of the linen example of Figure 3.8. The first three peaks are the β_0 -number at each threshold in the red, green and blue color channels respectively. Similarly, the second three peaks are the β_1 -number at each threshold in each of the three color channels respectively.

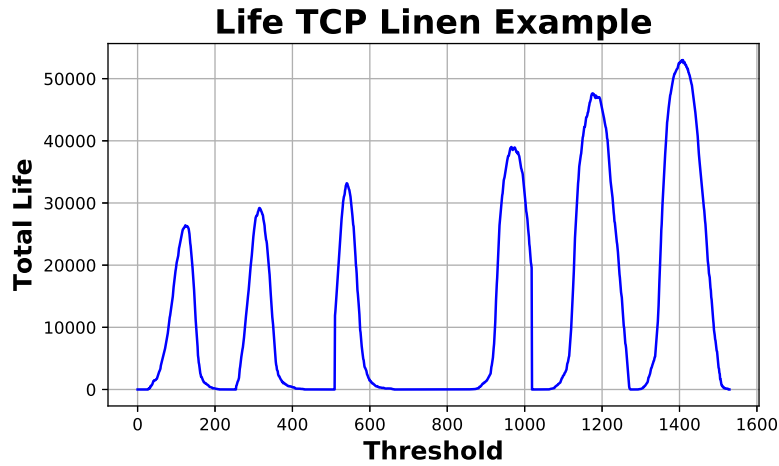


Figure 4.2: The Life-TCP of the linen example of Figure 3.8. The first three peaks are the total lifespans of every generator in zeroth homology alive at each threshold in the red, green and blue color channels respectively. Similarly, the second three peaks are the total lifespans of every generator in first homology alive at each threshold in each of the three color channels respectively.

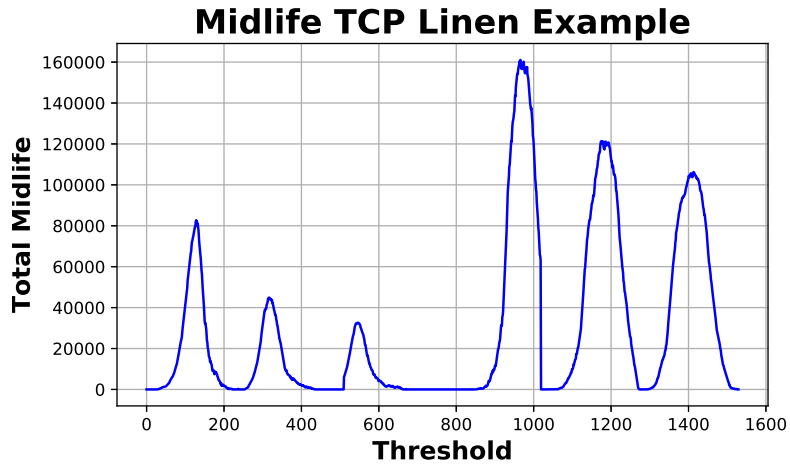


Figure 4.3: The Midlife-TCP of the linen example of Figure 3.8. The first three peaks are the total mid-lives of every generator in zeroth homology alive at each threshold in the red, green and blue color channels respectively. Similarly, the second three peaks are the total mid-lives of every generator in first homology alive at each threshold in each of the three color channels respectively.

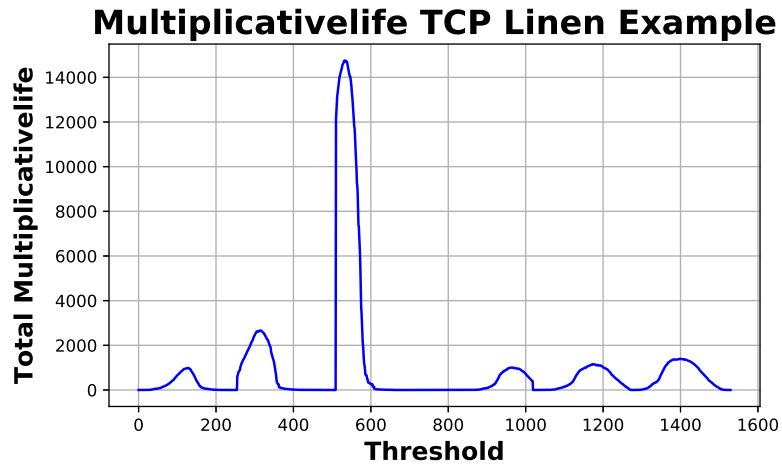


Figure 4.4: The Multiplicativelife-TCP of the linen example of Figure 3.8. The first three peaks are the total multiplicative-lives of every generator in zeroth homology alive at each threshold in the red, green and blue color channels respectively. Similarly, the second three peaks are the total multiplicative-lives of every generator in first homology alive at each threshold in each of the three color channels respectively.

4.1.1 Extended Topological Color Profiles

It is argued in Chung and Lawson (2019) that computing the persistent homology and PCs of a given image misses important information. Namely, generators which intersect the boundary of the image may not be detected by persistent homology alone. Therefore, they suggest computing the persistence curves of the "inverse" image as well. This means, for an 8-bit image Im , computing the persistence curves of Im and $255 - Im$, then concatenating the resulting TCPs into what will be called the extended TCP (ETCP).

Chung and Lawson (2019) present an example of an artificial image for which the additional information captured by the inverse is significant. However, that example is highly atypical compared to natural images where there are far more generators. Alexander Duality (Hatcher 2001) guarantees that generators in the interior of the image will be captured by both the image and its inverse. Therefore, the only additional information to be gained from the inverse image is that related to generators which lie on the boundary.

However, in natural images, the density of generators is generally much higher than that of the example in Chung and Lawson (2019). Since the boundary of an image grows linearly in the dimensions and the area grows quadratically, as the density of generators increases for fixed image dimensions (equivalently, as the size of the image grows with constant generator density) the contribution of those generators that lie on the the boundary of the image diminishes and can therefore be ignored.

To verify this, the deep learning model was trained on ETCPs and artificial ETCPs (aETCP). The aETCPs were generated for a given TCP by reversing the persistence curves for each color channel (for duality reasons) and concatenating them to the original TCP. All that is meant by "reversing" a persistence curve is that the thresholding (and thus the indexing of the vector) are incremented backwards, i.e. $C[i] = C[255 - i]$ where C is a given persistence curve.

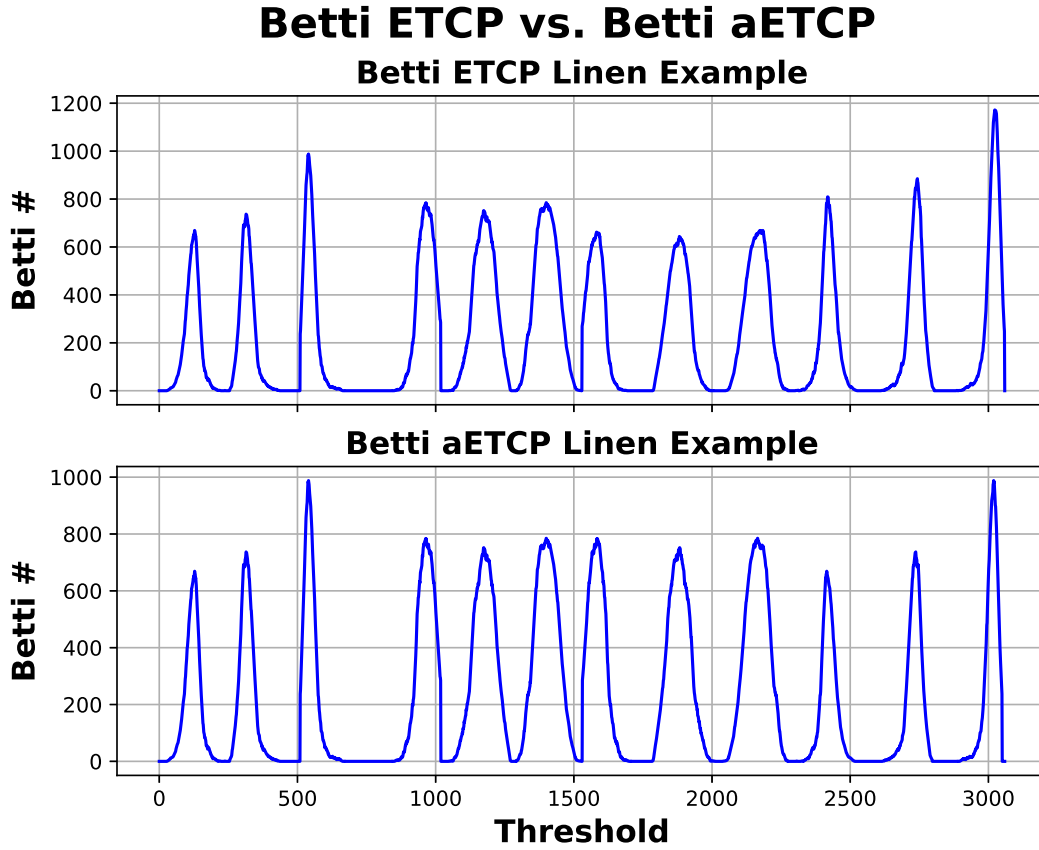


Figure 4.5: The Betti ETCP and the Betti aETCP for the linen example 3.8

While there are some noticeable differences in the ETCP and aETCPs, they bear a striking resemblance. Furthermore, as stated, the deep learning model was trained on both the ETCPs and the aETCPs. As can be seen in figures 4.6 - 4.9, the deep learning model detected no significant difference between the ETCPs and the aETCPs as it performed equally well on both data sets.

This result indicates that it suffices to compute only the TCPs which reduces the necessary TDA computations by half.

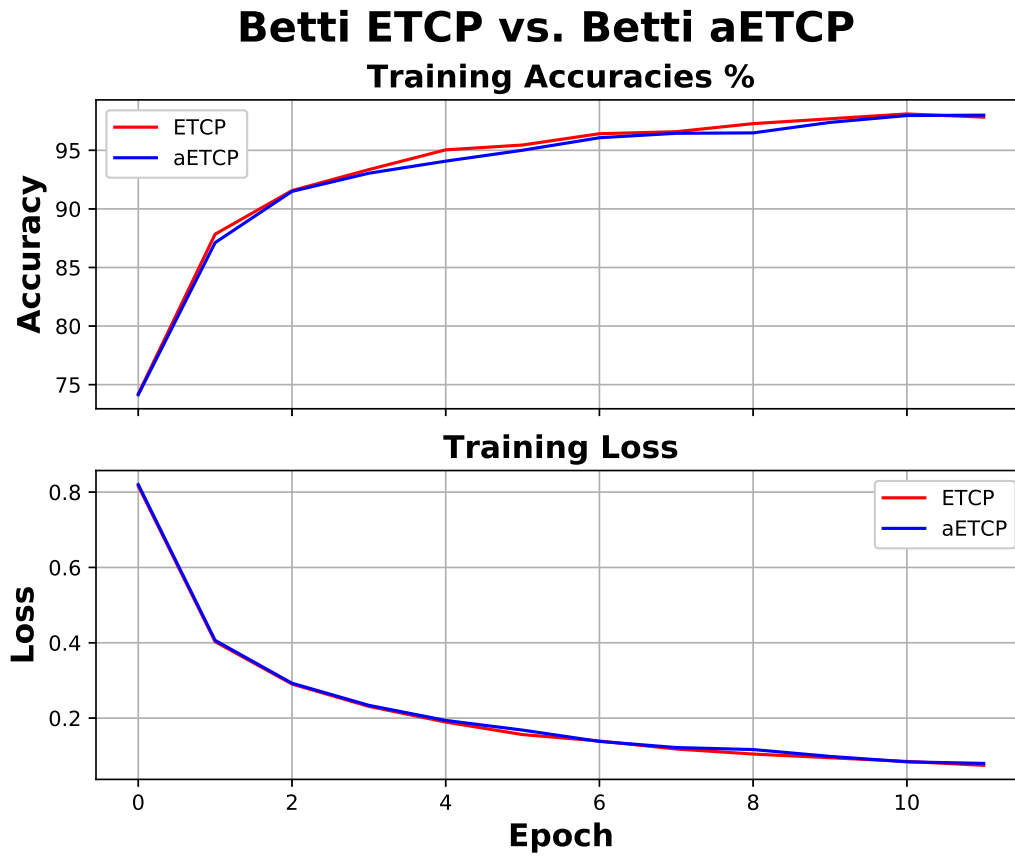


Figure 4.6: Training accuracy and loss for the Betti ETCP and the Betti aETCP. Final training accuracies for the ETCP data and the aETCP data were 97.83% and 98.00% respectively.

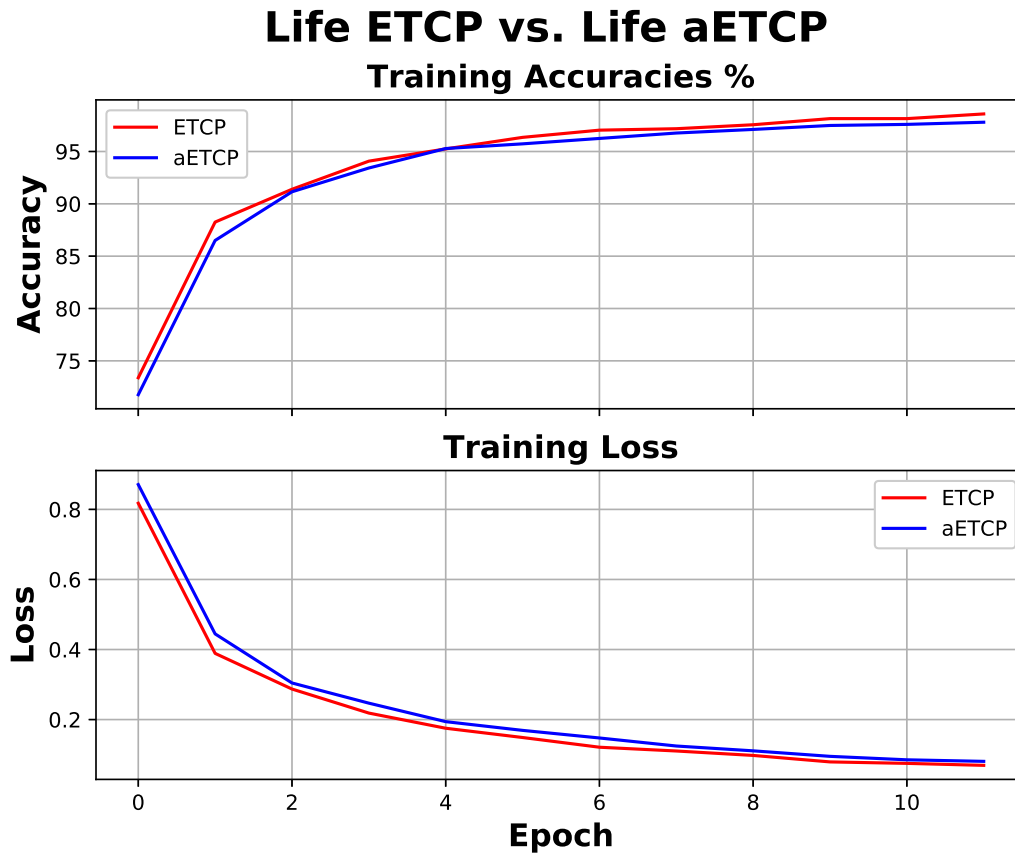


Figure 4.7: Training accuracy and loss for the Life ETCP and the Life aETCP. Final training accuracies for the ETCP data and the aETCP data were 98.59% and 97.80% respectively.

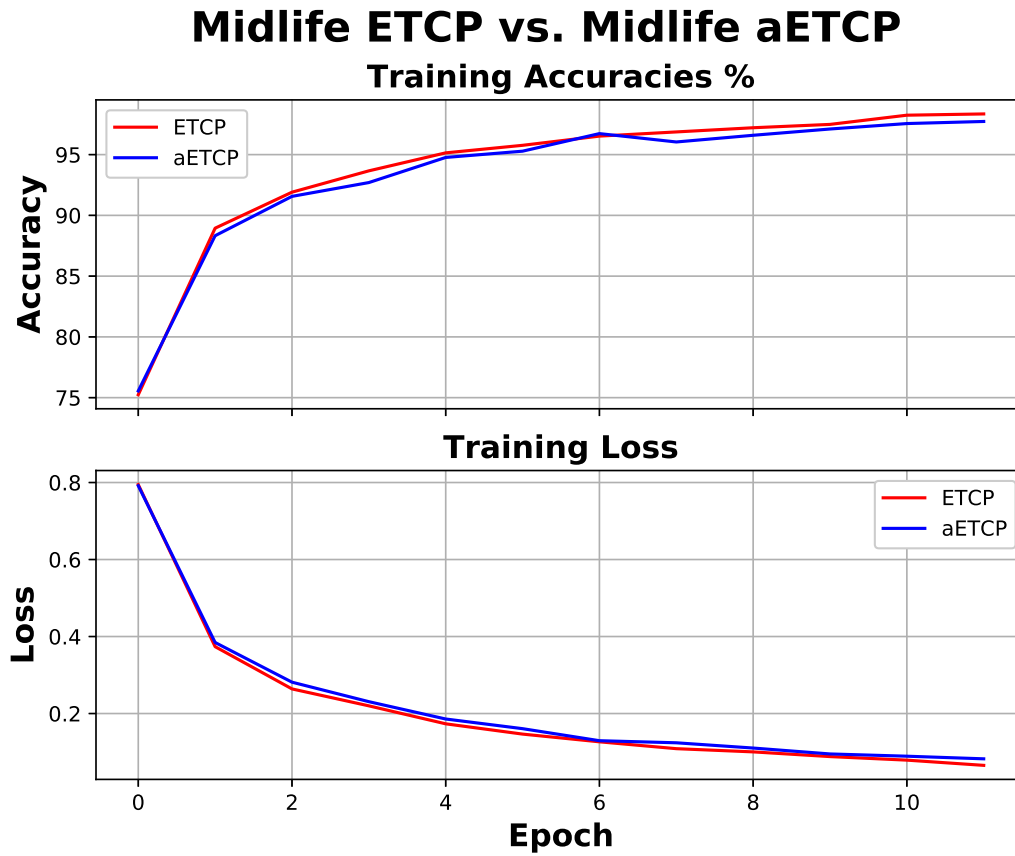


Figure 4.8: Training accuracy and loss for the Midlife ETCP and the Midlife aETCP. Final training accuracies for the ETCP data and the aETCP data were 98.35% and 97.73% respectively.

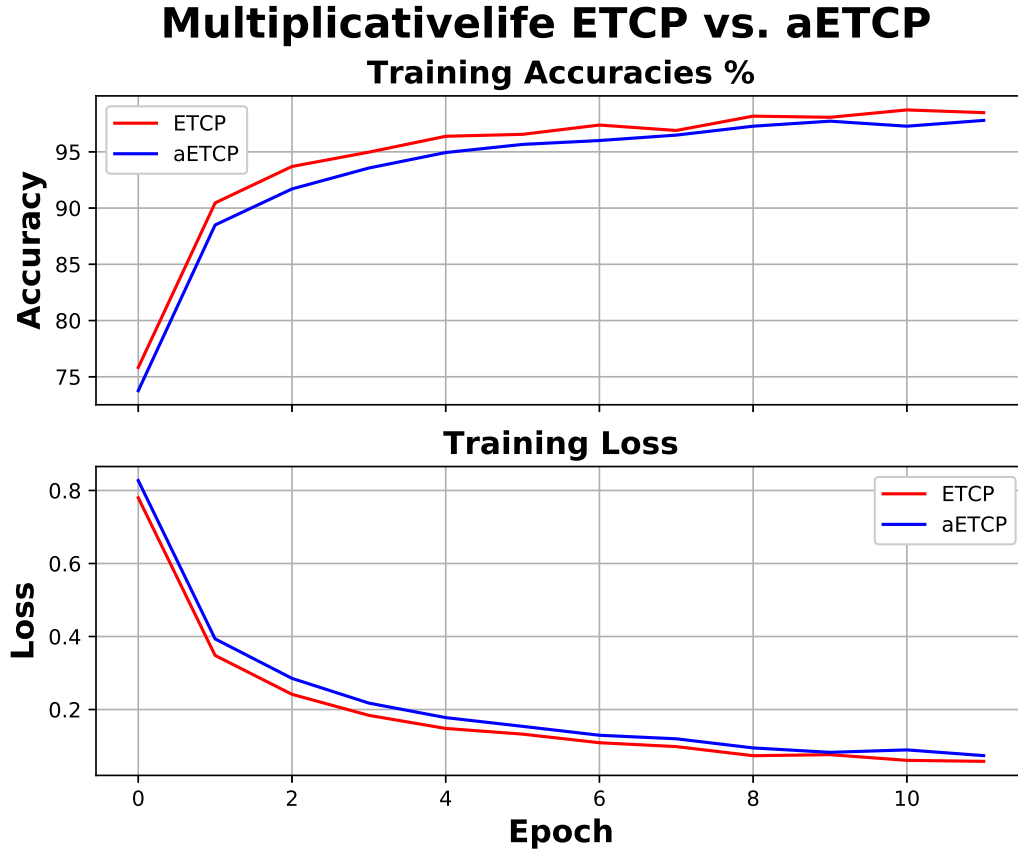


Figure 4.9: Training accuracy and loss for the Multiplicative ETCP and the Multiplicative aETCP. Final training accuracies for the ETCP data and the aETCP data were 98.48% and 97.87% respectively.

Attempts to train the model on the TCPs alone however, were far less successful; often only achieving accuracies of approximately 75%. Therefore, while the ETCPs do not carry significantly more topological information than the TCPs, the deep learning model tends to prefer the larger input vector. This could be due in part to the fact a larger input vector implies more free parameters. However, when this was accounted for by increasing the size of the hidden layer, the model still performed worse on the TCPs alone. This implies that where the free parameters appear in the deep learning model (before or after the ReLu

activation function) is just as significant as the total number of free parameters in the model.

While the author is convinced by the evidence that the ETCPs are little to no more informative than the TCPs, he is not in the mood to argue with the deep learning model. Therefore, the ETCPs will be used in the rest of the analysis.

4.1.2 The Effects of Noise

As mentioned before, in order to test the ETCPs response to noise, the images in the data set were injected with Gaussian, speckle, as well as salt&pepper noise at increasing levels of SNRdB = (1.1, 2, 4, 6, 8, 10, 12, 14, 16, 18, 20, 22, 24, 26, 28).

While the response varies for different noise and curve types, there are some pronounced commonalities. Namely, the number of generators increases with the amount of noise, and the peaks of the curves tend to drift towards the endpoints of the threshold intervals. See figure 4.10 for an example of this behavior. Note that because the PCs used in this study are computed by summing quantities over all generators alive at a given time (see table 3.1), the increase in the number of generators creates serious deviations from the noiseless ETCPs.

Another enlightening visualization are histograms of the lifespans of the generators as the amount of noise in the images increases. In line with the intuitive ranking of the significance of generators in terms of their lifespans described in 2.2.2 it is expected that image noise will contribute a disproportionate number of relatively small lifespan generators. However, figure 4.11 shows that even at relatively low levels of noise the lifespan distribution of the generators broadens and shifts to the center of the threshold interval. In fact, the noise generally decreases the number of short lived generators and increases the number long lived generators. An example of this behavior can be seen in figure 4.11.

Betti ETCP: Gaussian Noise

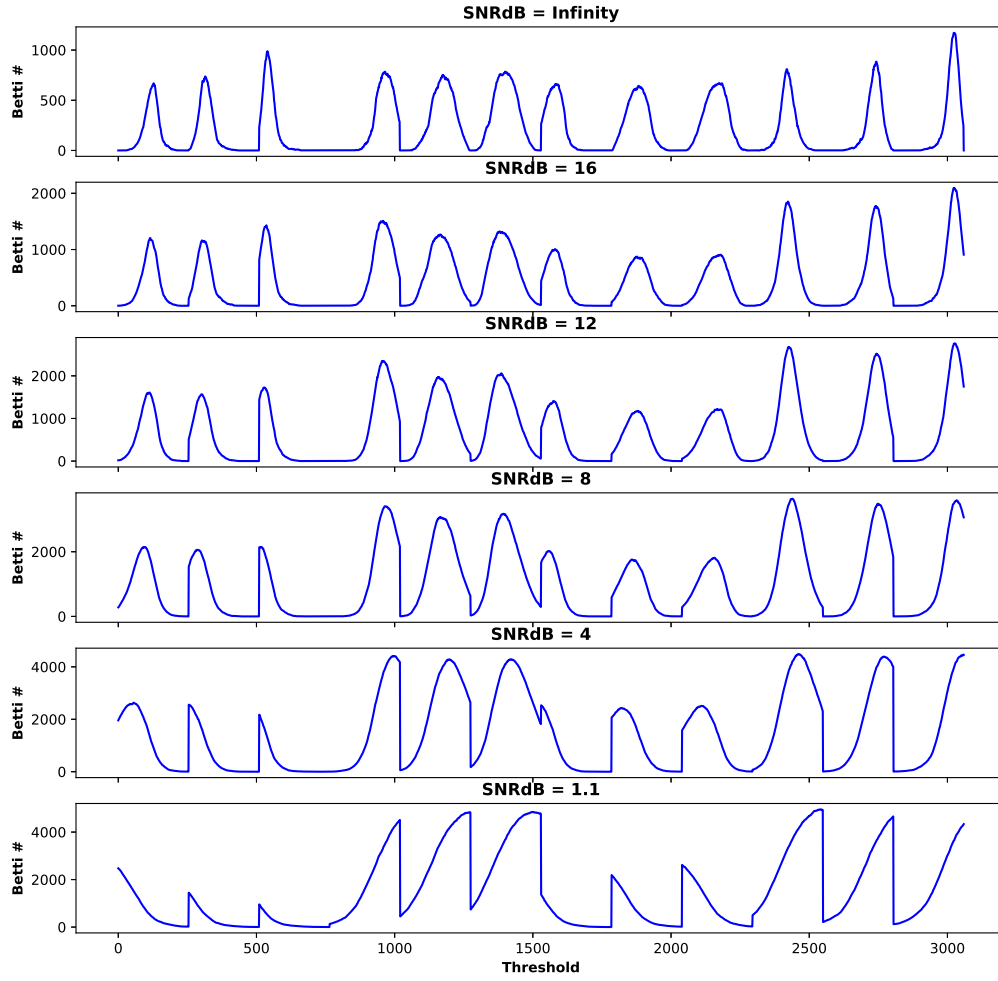


Figure 4.10: The Betti ETCPs for the linen example 3.8 with Gaussian noise injected with $\text{SNRdB} = (1.1, 4, 8, 12, 16, \infty)$. Where $\text{SNRdB} = \infty$ denotes the ETCP without any noise injection.

LifeSpan Histograms: with and without Gaussian Noise

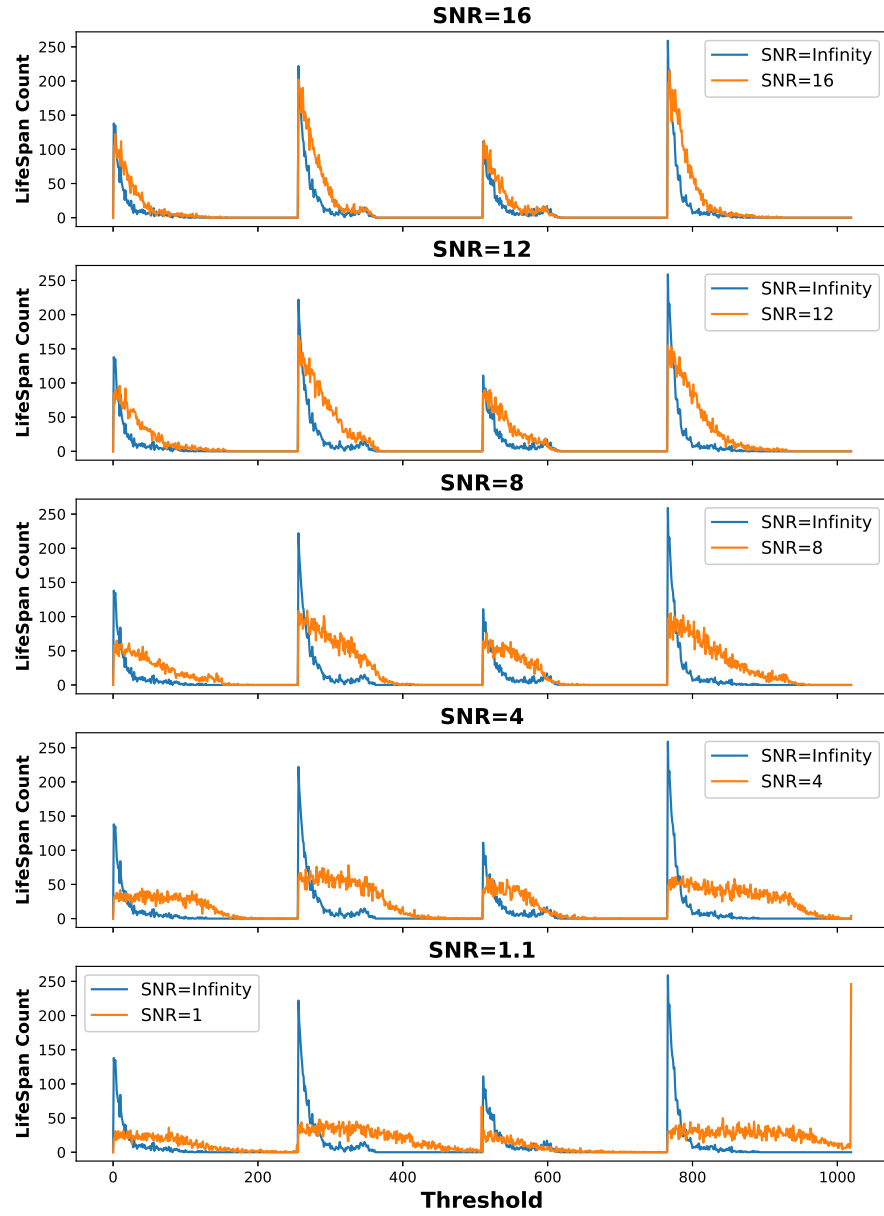


Figure 4.11: The four peaks in a given plot are four histograms of the generators according to lifespan for the linen example 3.8 in the red color channel, the first two peaks being β_0 and β_1 generators of the original image; the third and fourth peaks corresponding to the β_0 and β_1 generators of the inverse image.

4.2 Filtering Out the Noise

As seen in the previous section 4.1.2, the presence of noise in the images produces three primary effects; increases the number of generators, broadens the distribution of lifespans generally tending towards longer lifespans, shifts the constituent PCs of an ETCP towards their threshold endpoints.

The third effect is the hardest to filter because it is exactly the distribution of the constituent persistence curves that characterizes an ETCP. For instance, one could compute the center of mass of a PC (thought of as a mass density distribution on the interval $[0,255]$) and attempt to apply a transformation to shift that center of mass to the center of the interval. However, the resulting ETCPs would all look like twelve peaks evenly spaced on the interval $[0,3060]$.

However, three methods were proposed to mitigate the increase in the number of generators as well as the broadening of the lifespan distributions. First, the area under the constituent PCs were normalized to 100. This was expected to counter the effects of summing over larger numbers of generators as the SNRdB decreased.

Second, the persistence diagrams were truncated according to lifespan before the PCs were computed. That is, for a given image in the data set, the generators in each of its six associated persistence diagrams were ordered by lifespan. Then a fixed percentage of the generators were removed from the top and bottom of the lifespan-ordered list of generators. The percentages used in this study were 1%, 2%, 3%, 4%, 5%, 8%, and 10%. This was done with the expectation that it would mitigate the effects of the broadening of the lifespan distributions.

Finally, the tried and true method of "re-centering" the data by subtracting from each ETCP the average over all ETCPs was tested. The results for each method can be found in the following subsections.

However, before considering the preprocessing methods, see figure 4.12 for the effect the noise has on the model accuracy without any preprocessing of the ETCPs. Note that as the SNRdB decreases, the noise dominates the image and the models do no better than guessing ($\approx 9\%$). Similarly, as the SNRdB increases, the accuracy tends to converge to the accuracy on the noiseless ETCPs (depicted in figure 4.12 by the red dot). Lastly, note that salt&pepper noise is by far the most obstructive, particularly to the multiplicative life ETCPs.

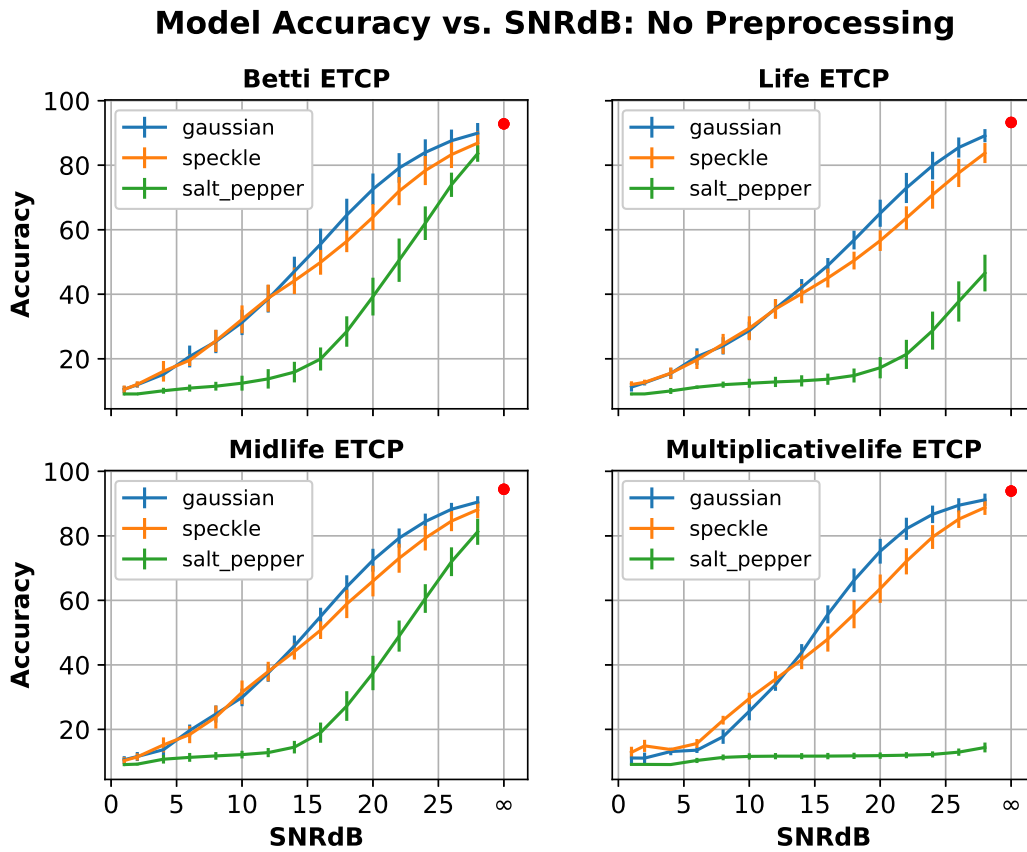


Figure 4.12: The ten pre-trained models were evaluated on the data set of noise injected ETCPs without any pre-processing. The accuracy of the ten models were average at each SNRdB and for each noise type. The red dot is the accuracy of the model on the noiseless ETCPs without pre-processing.

4.2.1 Area Normalization

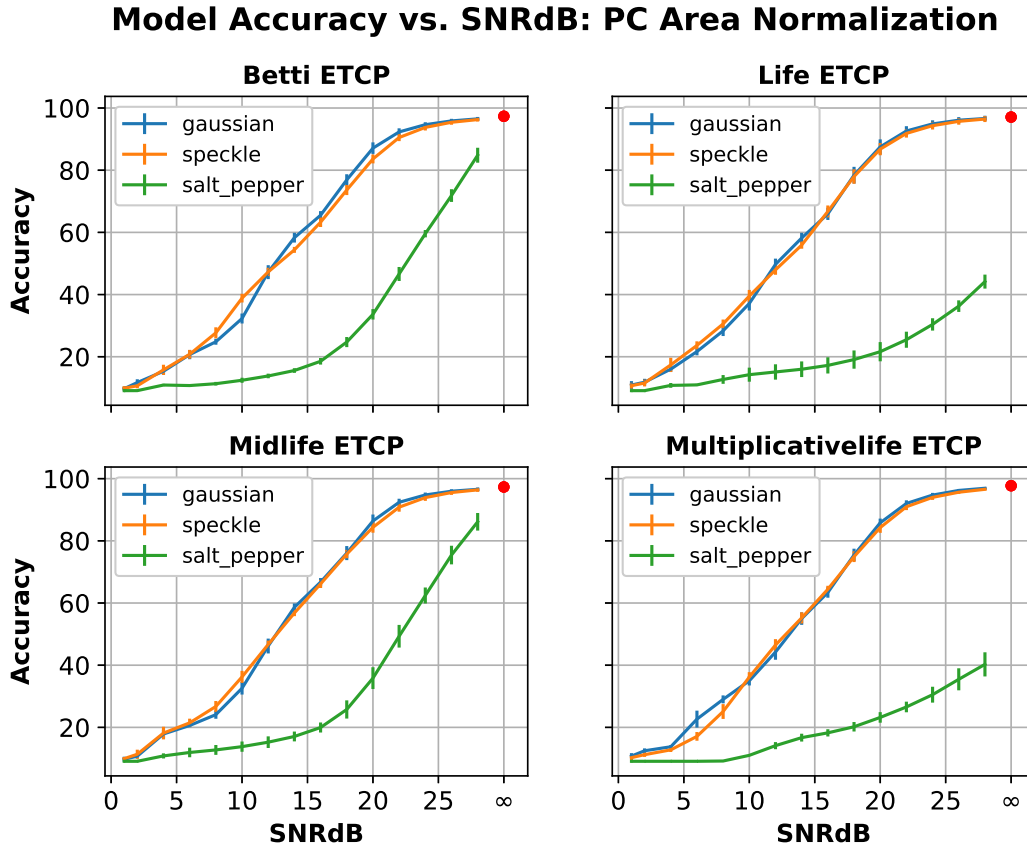


Figure 4.13: The ten pre-trained models were evaluated on the data set of ETCPs injected with noise and normalized by area. The accuracies of the ten models were average at each SNRdB and for each noise type. The red dot is the accuracy of the model on the noiseless ETCPs with area normalization.

Notice that for each of the ETCPs in figure 4.13, the disparity between Gaussian and speckle noise has essentially vanished. Furthermore, comparing to figure 4.12, the uptake in accuracy for Gaussian and Speckle noise is sharper indicating that the method is filtering out some of that noise. However, the area normalization has had little to no effect on the presence of salt & pepper noise with the exception of the multiplicative life ETCPs.

4.2.2 Lifespan Truncation

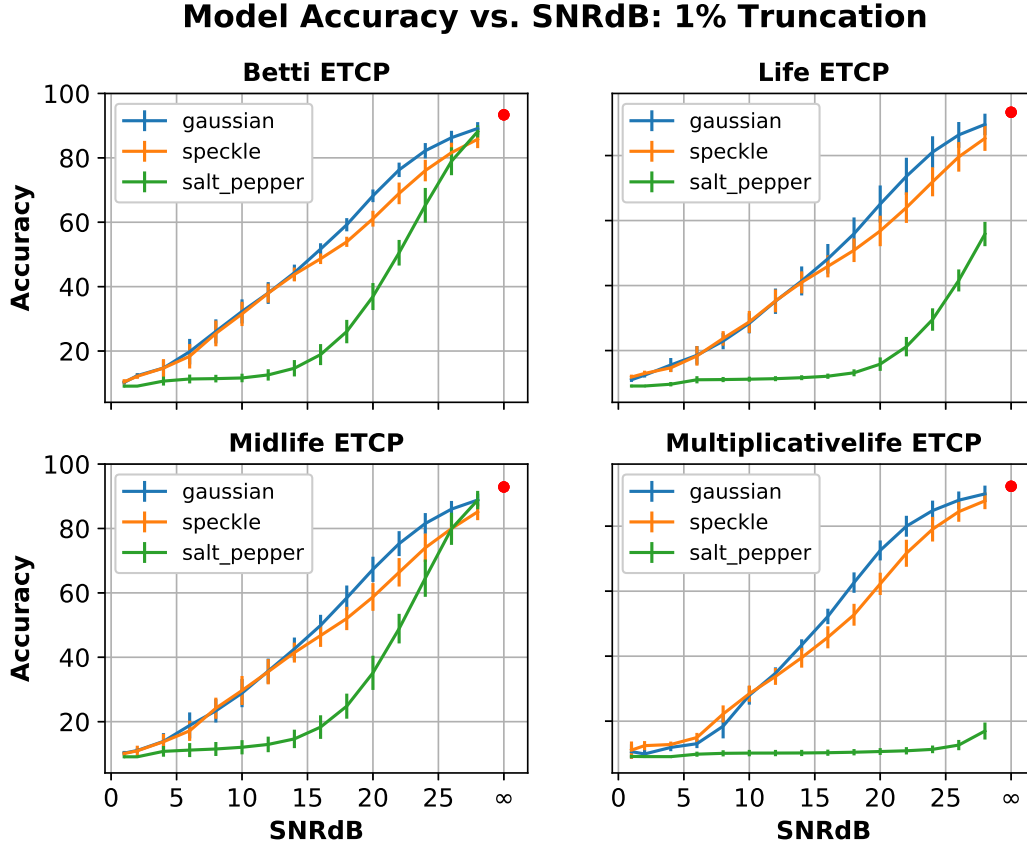


Figure 4.14: The ten pre-trained models were evaluated on the data set of ETCPs injected with noise and normalized by removing the 1% longest lived and shortest lived generators. The accuracies of the ten models were average at each SNRdB and for each noise type. The red dot is the accuracy of the model on the noiseless ETCPs with 1% truncation.

As can be seen in figure 4.14, removing as little as 1% of the generators by lifespan yields a marked increase in the accuracy of the models evaluated on the data injected with salt&pepper noise (with the exception of the multiplicative life ETCPs). It is expected that this is because salt&pepper noise min/maxs the pixel values creating generators with relatively very long lifespans. Therefore, removing some fraction of the generators with the

longest and shortest lifespans eliminates exactly those erroneous generators.

Furthermore, note that at this level of truncation, the accuracy of the models in the presence of Gaussian and speckle noise are practically unchanged.

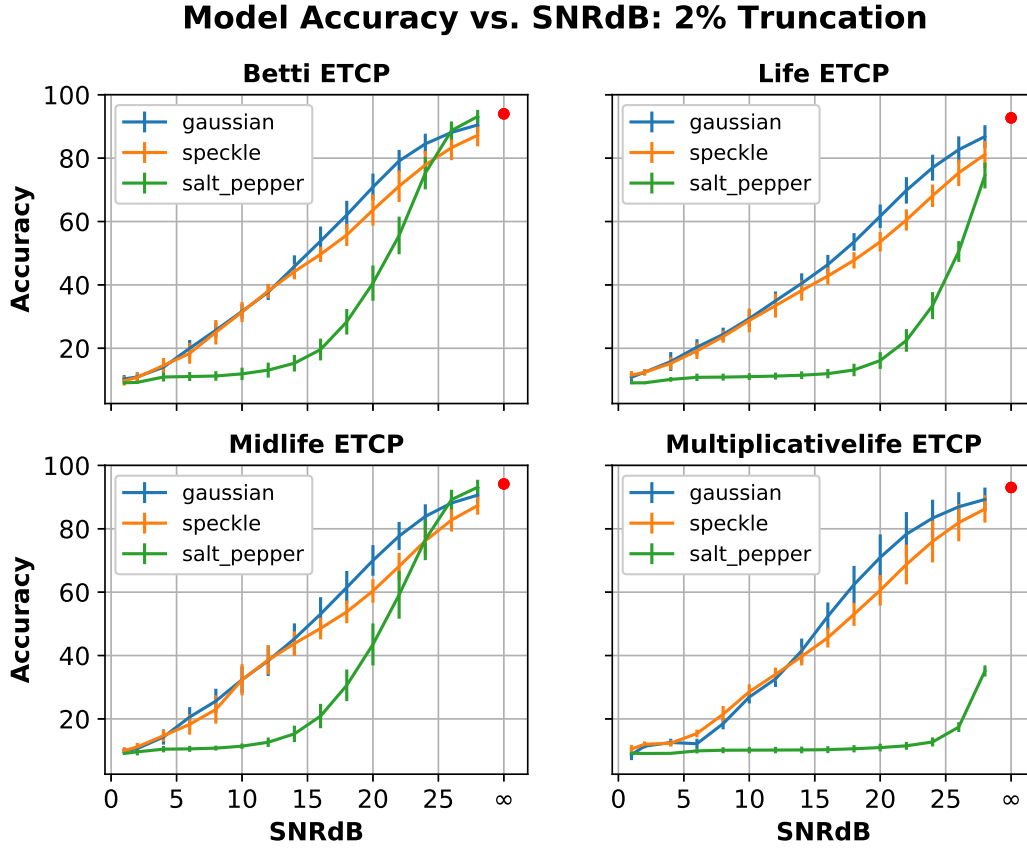


Figure 4.15: The ten pre-trained models were evaluated on the data set of ETCPs injected with noise and normalized by removing the 2% longest lived and shortest lived generators. The accuracies of the ten models were average at each SNRdB and for each noise type. The red dot is the accuracy of the model on the noiseless ETCPs with 2% truncation.

In figure 4.15, the accuracy of the models in the presence of salt&pepper noise appears to improve as more of the longest and shortest lived generators are omitted. The multiplicative life ETCPs begin showing some improvement with respect to salt&pepper noise.

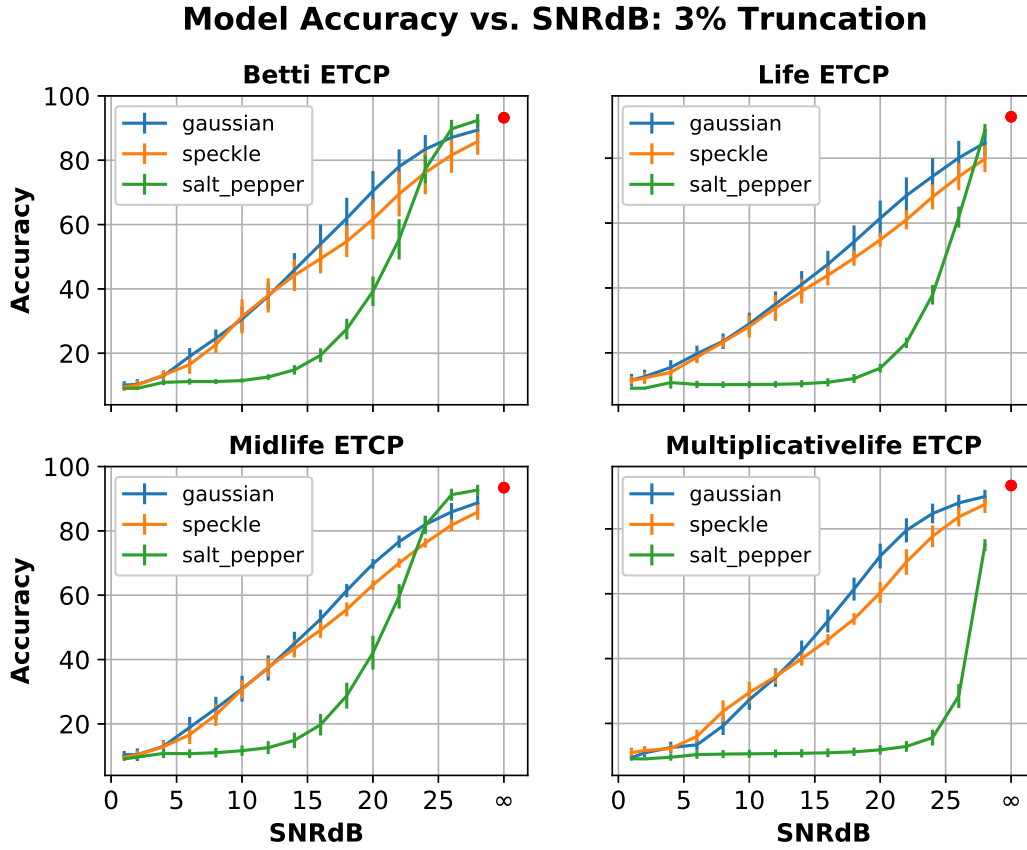


Figure 4.16: The ten pre-trained models were evaluated on the data set of ETCPs injected with noise and normalized by removing the 3% longest lived and shortest lived generators. The accuracies of the ten models were average at each SNRdB and for each noise type. The red dot is the accuracy of the model on the noiseless ETCPs with 3% truncation.

At the 3% truncation level depicted in 4.16, the improvement of the accuracy of the models with respect to salt&pepper noise is very pronounced. In fact, in the case of Betti and Midlife ETCPs, the models perform slightly better in the presence of salt&pepper noise at high SNRdB than the other noise types.

However, salt&pepper noise still demonstrates the sharpest decrease in accuracy as the SNRdb decreases. Lastly, comparing to figure 4.12, it appears that accuracy of the models in the presence of Gaussian and speckle noise is unchanged.

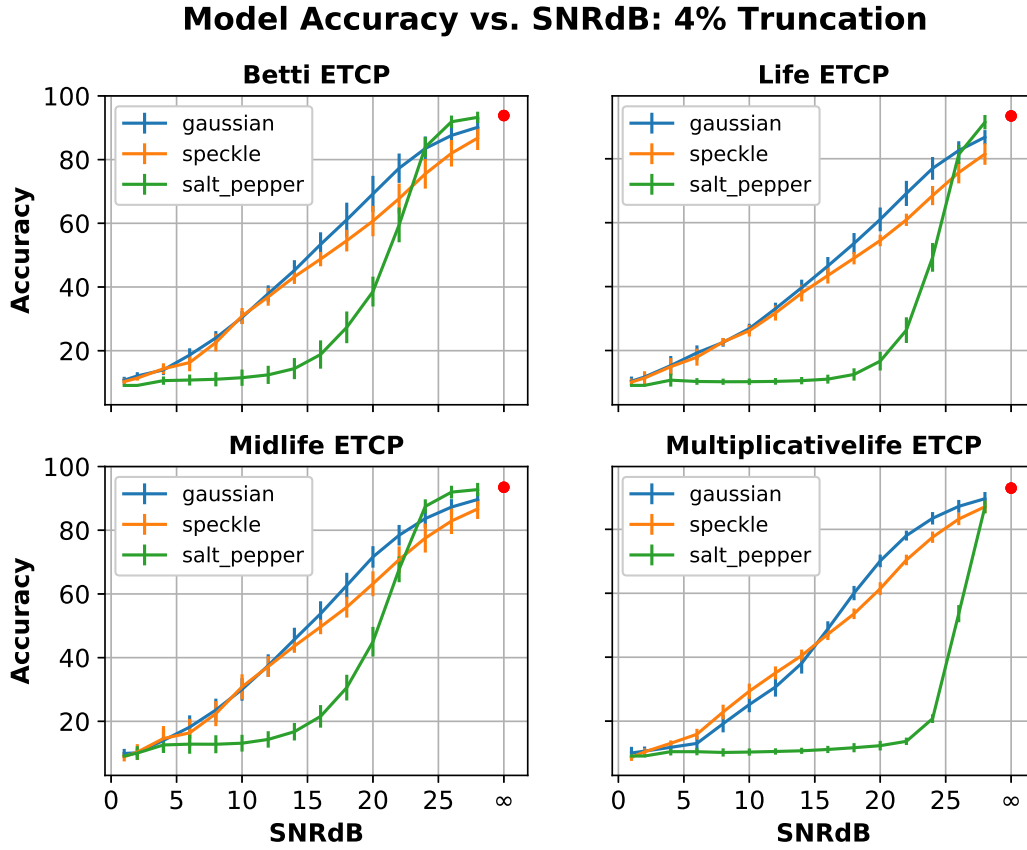


Figure 4.17: The ten pre-trained models were evaluated on the data set of ETCPs injected with noise and normalized by removing the 4% longest lived and shortest lived generators. The accuracies of the ten models were average at each SNRdB and for each noise type. The red dot is the accuracy of the model on the noiseless ETCPs with 4% truncation.

According to figure 4.17, when 4% of the longest and shortest lived generators are removed, the accuracy of the models in the presence of salt&pepper noise is better or comparable to the accuracy of the models in the presence of Gaussian and speckle noise at the highest SNRdB for all ETCPs. This likely indicates that at SNRdb=28, salt&pepper noise min/maxs approximately 3%-4% of the pixel values in a given image.

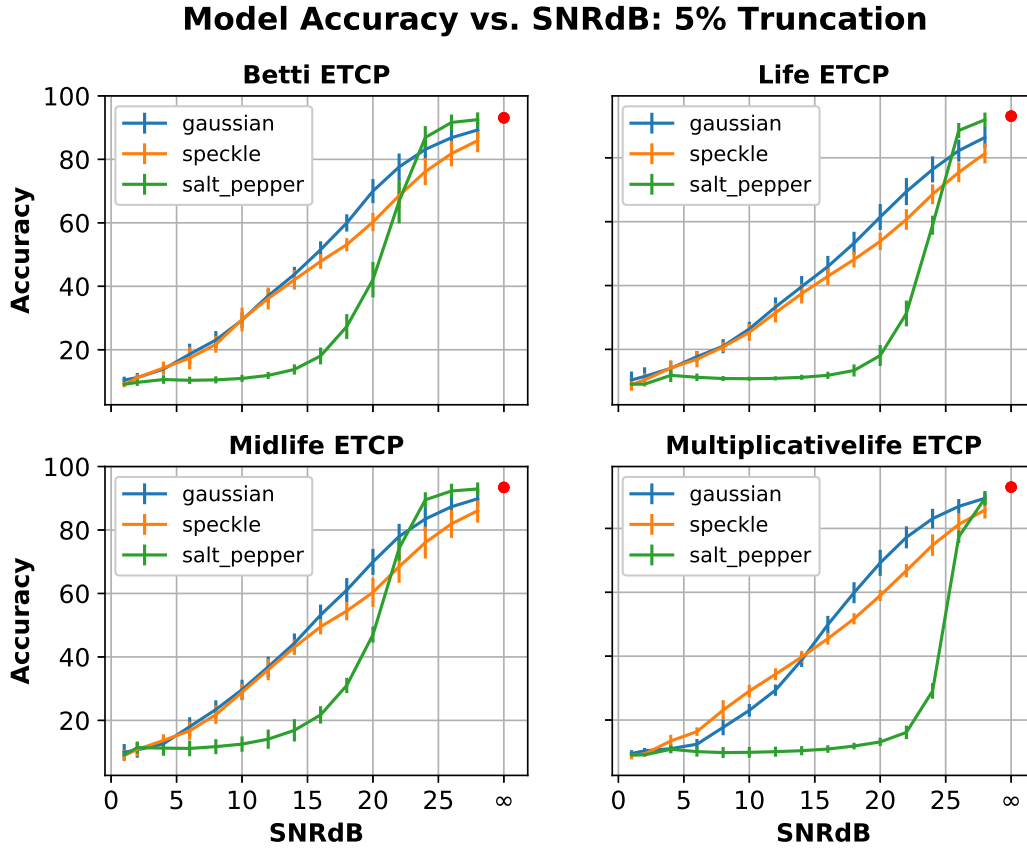


Figure 4.18: The ten pre-trained models were evaluated on the data set of ETCPs injected with noise and normalized by removing the 5% longest lived and shortest lived generators. The accuracies of the ten models were average at each SNRdB and for each noise type. The red dot is the accuracy of the model on the noiseless ETCPs with 5% truncation.

As seen in figure 4.18, the trend continues as the accuracy of the models in the presence of salt&pepper noise continues to improve for each of the ETCPs with out significantly effecting their accuracy in the presence of Gaussian and speckle noise.

Just for good measure, figures 4.19 and figure 4.20 display the result of higher levels of truncation and verify that this trend continues. While the salt&pepper noise continues to be the most obstructive noise at smaller values of SNRdB, it also continues to significantly improve at higher values of SNRdB as the truncation percentage increases.

However, at the higher truncation levels the accuracy of the models in the presence of Gaussian and speckle noise begins to suffer as compared to figure 4.12. This is particularly pronounced for the Life ETCPs.

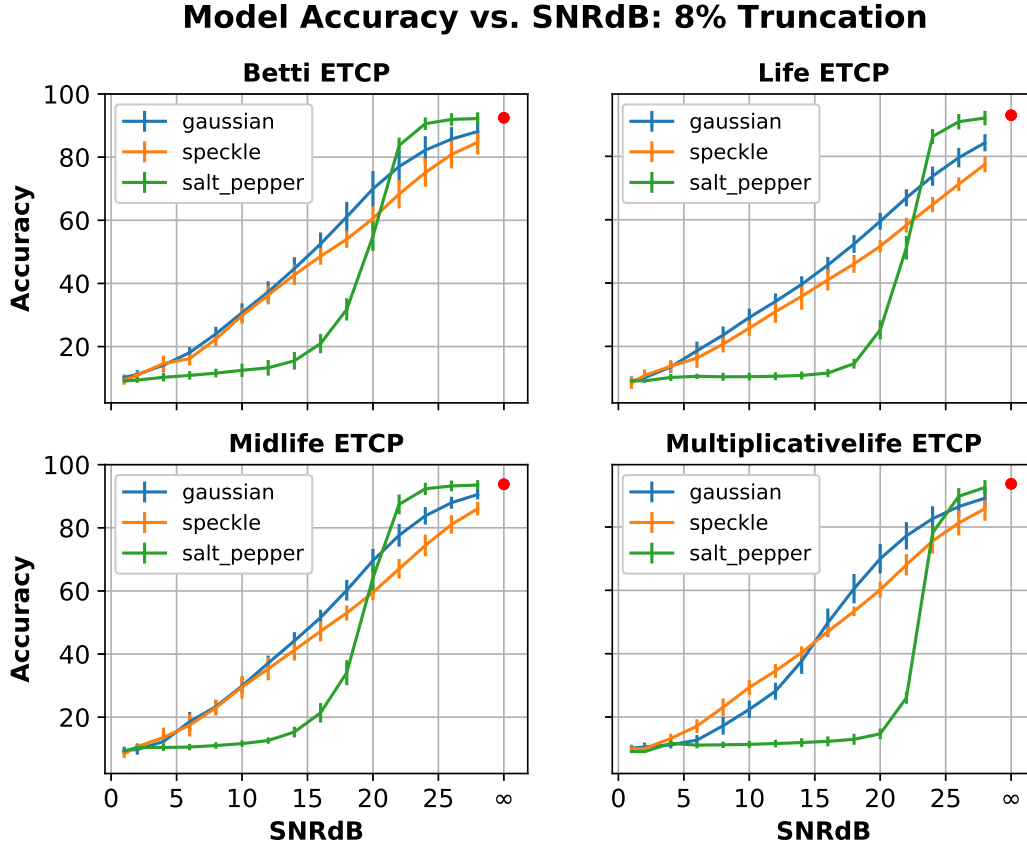


Figure 4.19: The ten pre-trained models were evaluated on the data set of ETCPs injected with noise and normalized by removing the 8% longest lived and shortest lived generators. The accuracies of the ten models were average at each SNRdB and for each noise type. The red dot is the accuracy of the model on the noiseless ETCPs with 8% truncation.

Model Accuracy vs. SNRdB: 10% Truncation

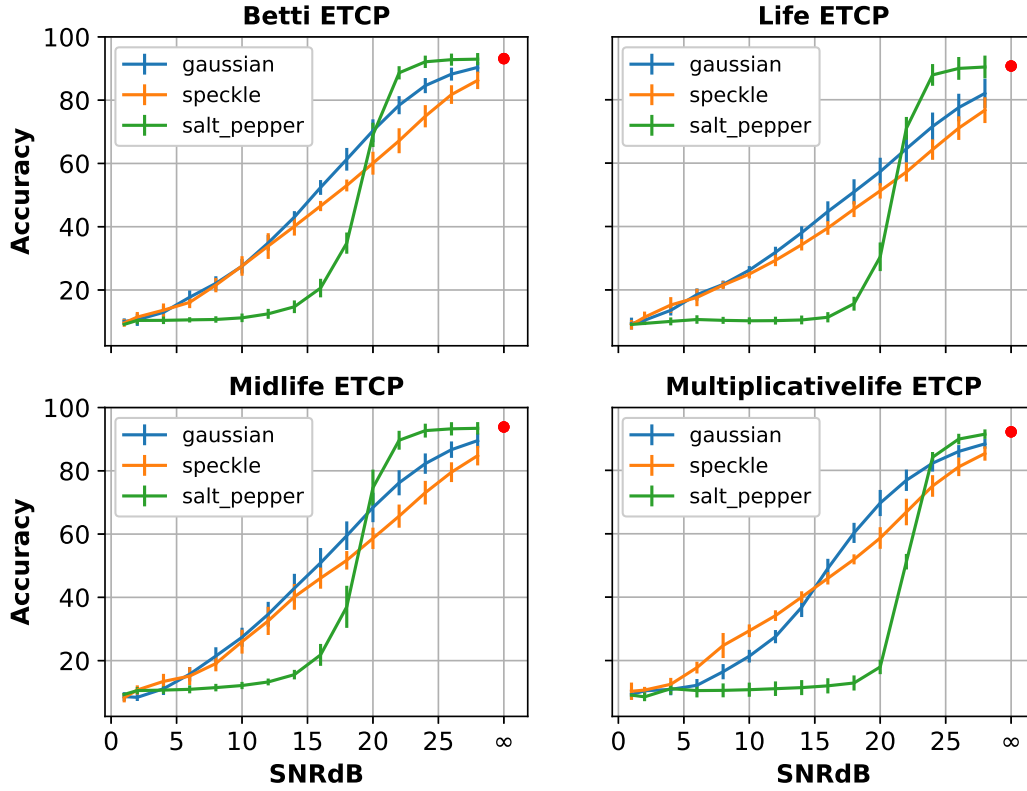


Figure 4.20: The ten pre-trained models were evaluated on the data set of ETCPs injected with noise and normalized by removing the 10% longest lived and shortest lived generators. The accuracies of the ten models were average at each SNRdB and for each noise type. The red dot is the accuracy of the model on the noiseless ETCPs with 10% truncation.

4.2.3 Re-Centering

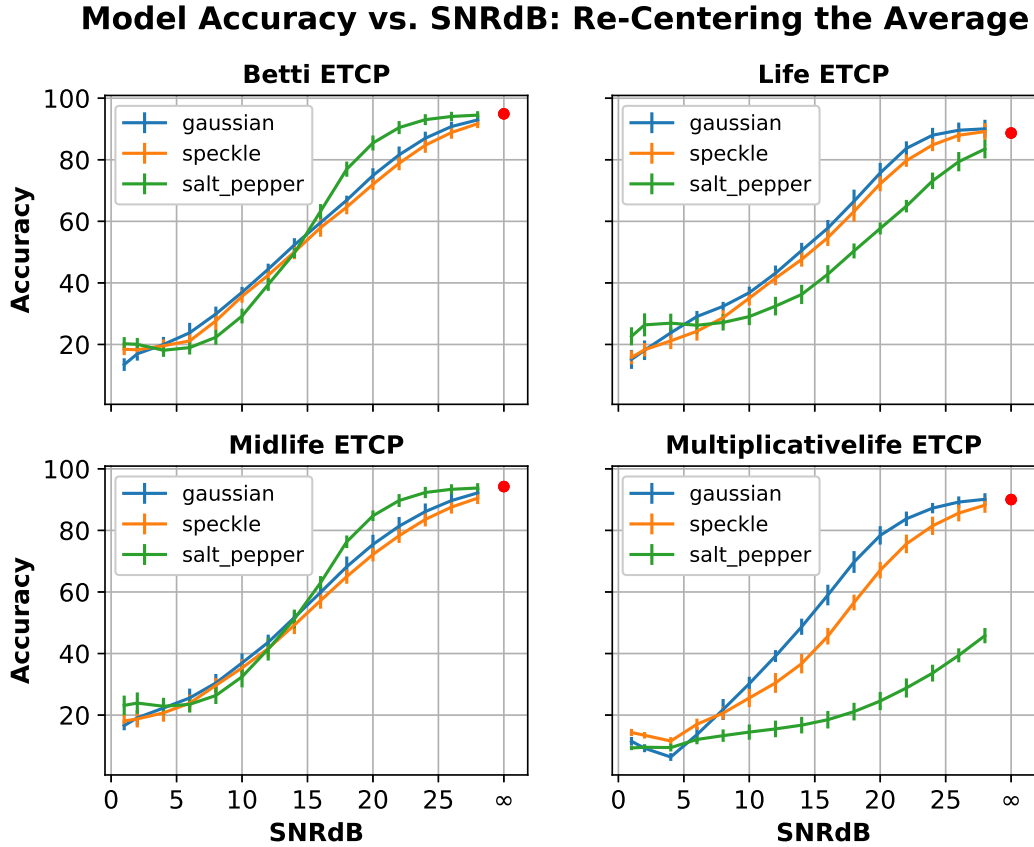


Figure 4.21: The ten pre-trained models were evaluated on the data set of ETCPs injected with noise and normalized by subtracting from each ETCPs the average over all ETCPs. The accuracies of the ten models were average at each SNRdB and for each noise type. The red dot is the accuracy of the model on the noiseless ETCPs.

As expected, re-centering the ETCPs resulted in increased performance of the models across all SNRdBs. In particular, note that in all but the multiplicative life ETCPs, the models do about two times better than guessing as the lowest SNRdB. Also, as in the area normalization case, the accuracy of the models in the presence of Gaussian and speckle noise track much closer together. Furthermore, with the exception of multiplicative life, the re-centering

method displays the greatest improvement in the presence of salt&pepper noise at lower levels of SNRdB.

4.2.4 Training on Images Directly

For a more general comparison, a model was constructed which classified the images in the KTH-TIPS2 data set by taking the images themselves directly as input. The size of the images versus the number of training samples prohibited the use of MLPs alone as the images were too large when vectorized. Therefore, a *convolutional neural network* (CNN) was required to satisfactorily classify the images.

This model consisted of two convolutional layers (with max pooling and ReLu activation functions) with a single layered MLP on top. The training, validation, and test sets were generated in the same manner as before and no pre-processing was applied. Again, ten such models were trained and evaluated on the entire data set after being injected with the three noise types at the 15 levels of SNRdB. The results of the analysis can be found below in figure 4.22.

The CNN models display the correct limiting behavior in the presence of noise. For small values of SNRdB, the images are dominated by noise and the models had to guess at the correct classification. For 11 texture classes the probability of guessing correctly is 9%. As the SNRdB increases the noise in the images reduces to zero and the accuracy of the models converged to their accuracy on the data set of noiseless images.

Comparing to figure 4.12, the CNN-based model performed better in the presence of all three noise types than any of the four unfiltered ETCPs used in this study, particularly with respect to Salt&Pepper noise. This is unsurprising as CNNs are a much more sophisticated machine learning architecture than MLPs.

However, when normalized by area, the MLPs trained on the ETCPs slightly outperform

the CNNs in the presence of Gaussian and speckle noise. Furthermore, for higher levels of lifespan truncation and higher values of SNRdB, the MLPs outperform the CNNs in the presence of Salt&Pepper noise. Lastly, after re-centering the ETCPs, the MLPs perform comparably well to the CNNs for all but the smallest values of SNRdB where the MLPs perform better.

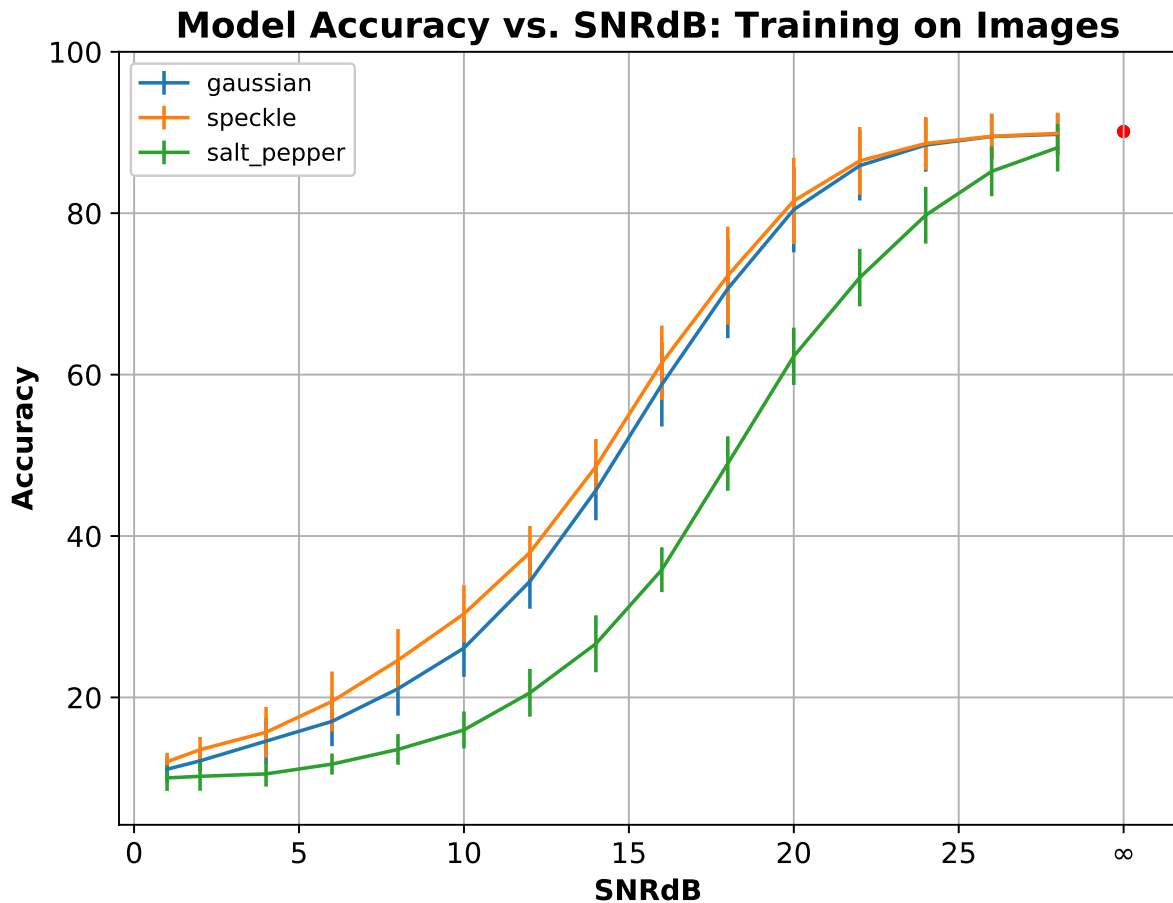


Figure 4.22: The ten pre-trained CNN models were evaluated on the data set of images injected with noise. The accuracies of the ten models were average at each SNRdB and for each noise type. The red dot is the accuracy of the model on the noiseless images.

4.2.5 Conclusions Concerning the Proposed Filtration Methods

Of the pre-processing methods attempted, the area normalization had the greatest positive impact on the accuracy of the models in the presence of Gaussian and speckle noise. However, lifespan truncation did the most to improve the accuracy in the presence of salt&pepper noise for each of the ETCs. But, the truncation methods comes with a slight trade-off in the accuracy of the models in the presence of Gaussian and speckle noise for higher levels of truncation. Finally, re-centering the ETCs produced the greatest improvement in the accuracy of the models for small values of SNRdB with the exception of the multiplicative life ETCs. The re-centering method also greatly improved the accuracy in the presence of salt&pepper noise particularly for the betti and midlife ETCs. However, the truncation method appears to have been more effective against salt&pepper noise than re-centering in the case of the life ETCs and re-centering was only comparably effective to area normalization in the case of Multiplicative life ETCs.

CHAPTER

5

ALGEBRAIC PRELIMINARIES

5.1 Differential Graded Algebras

Definition 5.1.1. Let R be a commutative ring with identity. An R -Algebra is a ring A with identity together with a ring homomorphism $f : R \rightarrow A$ mapping 1_R to 1_A such that the subring $f(R)$ is contained in the center of A .

Definition 5.1.2. A Graded R -algebra is an R -algebra with a direct sum decomposition into sub-modules, $\mathcal{A}^* = \bigoplus_{i \in \mathbb{Z}} A^i$. Elements in a given grading A^k are said to be of degree k . For $v \in A^j$ and $w \in A^k$, then $vw \in A^{j+k}$. That is to say that degrees are additive over multiplication, $\deg(vw) = \deg(v) + \deg(w)$.

Definition 5.1.3. Let \mathcal{A}^* and \mathcal{B}^* be graded R -algebras. A map $\phi : \mathcal{A}^* \rightarrow \mathcal{B}^*$ is a *morphism of graded R -algebras* if and only if it respects multiplication and degrees. That is, for $w \in A^j$ and $v \in A^k$ it holds that $\phi(w) \in B^j$, $\phi(v) \in B^k$, and $\phi(w \cdot v) = \phi(w) \cdot \phi(v) \in B^{j+k}$.

Note that the previous two definitions form the definition of the category of graded R -algebras, GRA . This perspective will be relevant later when considerations of functoriality become relevant.

Definition 5.1.4. Similarly, a *Bigraded R -algebra* is an R -algebra with a direct sum decomposition into submodules $\mathcal{A}^{**} = \bigoplus_{p,q \in \mathbb{Z}} A^{p,q}$. Elements in a given grading $A^{p,q}$ are said to be of bidegree (p, q) . For $v \in A^{p,q}$ and $w \in A^{s,t}$, then $vw \in A^{p+s, q+t}$. That is to say that bidegrees are again additive over multiplication, $\text{bideg}(vw) = \text{bideg}(v) + \text{bideg}(w)$.

Definition 5.1.5. Let \mathcal{A}^{**} and \mathcal{B}^{**} be bigraded R -algebras. A map $\phi : \mathcal{A}^{**} \rightarrow \mathcal{B}^{**}$ is a *morphism of bigraded R -algebras* if and only if it respects multiplication and degrees. That is, for $w \in A^{i,j}$ and $v \in A^{k,l}$ it holds that $\phi(w) \in B^{i,j}$, $\phi(v) \in B^{k,l}$, and $\phi(w \cdot v) = \phi(w) \cdot \phi(v) \in B^{i+k, j+l}$.

Similarly, the previous two definitions form the definition of the category of bigraded R -algebras, $BGRA$. This perspective will be relevant later when considerations of functoriality become relevant.

Definition 5.1.6. Let \mathcal{A}^* be a graded R -algebra. A *differential* on \mathcal{A}^* is a map $d : \mathcal{A}^* \rightarrow \mathcal{A}^*$ such that d has degree $+1$, $d \circ d = 0$, and for products $d(vw) = d(v)w + (-1)^{\deg(v)} v d(w)$.

A graded R -algebra equipped with a differential is called a *Differential Graded R -algebra* (*DGA*, or *cochain complex*) and is denoted (\mathcal{A}^*, d) .

Definition 5.1.7. Let (\mathcal{A}^*, d) be a DGA. Then the condition that $d \circ d = 0$ implies that $\text{Img}(d) \subseteq \text{Ker}(d)$. Therefore, the *Cohomology* of a DGA is a graded R -algebra given by $H^*(\mathcal{A}^*, d) = \bigoplus_{i \in \mathbb{Z}} H^i(\mathcal{A}^*, d)$ where

$$H^i(\mathcal{A}, d) = \frac{\text{Ker}(d : A^i \rightarrow A^{i+1})}{\text{Img}(d : A^{i-1} \rightarrow A^i)}$$

and multiplication on $H^*(\mathcal{A}^*, d)$ is induced by the multiplication on \mathcal{A}^* .

Similarly, a *digraded differential R -algebra*, (\mathcal{A}^{**}, d) , is a bigraded R -algebra with a map $d : \mathcal{A}^{**} \rightarrow \mathcal{A}^{**}$ with bidegree (n, k) such that $d \circ d = 0$. The cohomology of a bigraded differential R -algebra is given in the same manner as in definition 5.1.7.

Definition 5.1.8. Let (\mathcal{A}^*, d) and (\mathcal{B}^*, δ) be two DGAs. Then a map between them $\phi : \mathcal{A}^* \rightarrow \mathcal{B}^*$ is a *morphism of DGAs* (commonly referred to as a *co-chain map*) is a morphism between them as graded R -algebras with the additional condition that it commutes with the differentials.

In other words, a graded R -algebra morphism $\phi : \mathcal{A}^* \rightarrow \mathcal{B}^*$ is a co-chain map if and only if the following diagram commutes for each i .

$$\begin{array}{ccc} A^{i+1} & \xrightarrow{\phi} & B^{i+1} \\ d \uparrow & & \uparrow \delta \\ A^i & \xrightarrow{\phi} & B^i \end{array}$$

Definition 5.1.9. Let $\mathcal{A}^* = \bigoplus_{k \in \mathbb{Z}} A_k$ be a graded R -algebra such that each A_k is finitely generated. Then the q -Dimension of \mathcal{A}^* is given by

$$qdim(\mathcal{A}) = \sum_{k=0}^{\infty} q^k \text{rank}(A_k)$$

where

$$\text{rank}(A_k) = \dim_Q(A_k \otimes_R Q)$$

and Q is the field of fractions over R .

The q -dimension is often used in categorifications because it has the following very useful properties.

Lemma 5.1.1. Let \mathcal{A}^* and \mathcal{B}^* be graded R -algebras. Then

$$qdim(\mathcal{A}^* \oplus \mathcal{B}^*) = qdim(\mathcal{A}^*) + qdim(\mathcal{B}^*)$$

$$qdim(\mathcal{A}^* \otimes \mathcal{B}^*) = qdim(\mathcal{A}^*) \cdot qdim(\mathcal{B}^*)$$

Example 5.1.1. Consider the graded R -algebra $\mathcal{A}^* = \mathbb{Z}[x] / \langle x^2 \rangle$. Then the q -dimension of \mathcal{A}^* is given by

$$qdim(\mathcal{A}^*) = 1 + q$$

Furthermore, the q -dimension of its k^{th} tensor power is given by

$$qdim(\mathcal{A}^{\otimes k}) = (1 + q)^k$$

Finally, the Graded Euler Characteristic of a graded R -algebra \mathcal{A}^* is given by

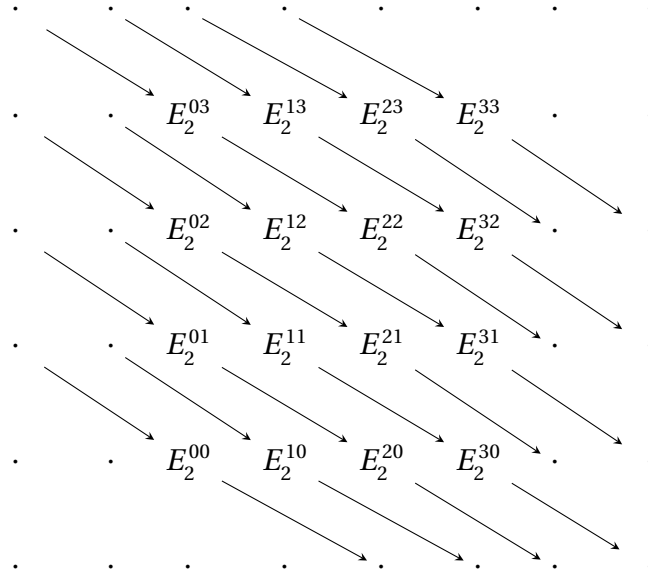
$$\chi_q(\mathcal{A}^*) = \sum_{k=0}^{\infty} (-1)^k qdim(A_k)$$

5.2 Spectral Sequences

Definition 5.2.1. A *cohomological spectral sequence* is a collection of bigraded differential R -algebras $\{E_r^{**}, d_r\}_{r \in \mathbb{N}}$ where the differentials are all of bidegree $(r, 1-r)$ and $E_{r+1}^{p,q}$ is isomorphic to $H^{p,q}(E_r^{**}, d_r)$. Furthermore, the multiplication maps on each page are induced by the multiplication maps on the preceding page.

Each bigraded R -algebra E_r^{**} of a spectral sequence $\{E_r^{**}, d_r\}_{r \in \mathbb{N}}$ is called the r^{th} -page of the spectral sequence.

Example 5.2.1. The 2^{nd} -page, (E_2^{**}, d_2) , of a typical cohomological spectral sequence where arrows represent the d_2 differentials



Definition 5.2.2. The r^{th} -total complex of a spectral sequence $\{E_r^{**}, d_r\}_{r \in \mathbb{N}}$ is given by $Tot_r^*(E_r^{**}) = \bigoplus_n Tot_r^n(E_r^{**})$ where

$$Tot_r^n(E_r^{**}) = \bigoplus_{p+q=n} E_r^{p,q}$$

i.e. take direct sums along lines of slope of negative-one on the r^{th} -page.

Theorem 5.2.1. *McCleary (1985) Each page of a cohomological spectral sequence $E_r^{p,q}$ is isomorphic to a quotient of submodules of the zero-th page $E_0^{p,q}$.*

Proof. Consider the differentials coming into and out of the $(p, q)^{th}$ grading on the r^{th} and $(r+1)^{st}$ pages of the spectral sequence

$$E_r^{p-r, q-(1-r)} \xrightarrow{d_r} E_r^{p, q} \xrightarrow{d_r} E_r^{p+r, q+(1-r)}$$

$$E_{r+1}^{p-(r+1), q-(1-(r+1))} \xrightarrow{d_{r+1}} E_{r+1}^{p, q} \xrightarrow{d_{r+1}} E_{r+1}^{p+(r+1), q+(1-(r+1))}$$

and denote

$$Z_r^{p, q} = \text{Ker}(d_r) \text{ and } B_r^{p, q} = \text{Img}(d_r)$$

$$Z_{r+1}^{p, q} = \text{Ker}(d_{r+1}) \text{ and } B_{r+1}^{p, q} = \text{Img}(d_{r+1})$$

Then the condition that $d_r \circ d_r = 0$ implies that

$$B_r^{p, q} \subset Z_r^{p, q} \subset E_r^{p, q}$$

$$B_{r+1}^{p, q} \subset Z_{r+1}^{p, q} \subset E_{r+1}^{p, q}$$

Furthermore, by definition

$$E_{r+1}^{p, q} \cong Z_r^{p, q} / B_r^{p, q}$$

$$E_{r+2}^{p, q} \cong Z_{r+1}^{p, q} / B_{r+1}^{p, q}$$

However, since $Z_{r+1}^{p, q}$ is a submodule of $E_{r+1} \cong Z_r^{p, q} / B_r^{p, q}$, it can be written as $Z_{r+1}^{p, q} \cong \tilde{Z}_{r+1}^{p, q} / B_2^{p, q}$ where $\tilde{Z}_{r+1}^{p, q}$ is some submodule of $Z_r^{p, q}$. Similary, since B_{r+1} is a submodule of $E_{r+1} \cong Z_r^{p, q} / B_r^{p, q}$, it can be written as $B_{r+1} \cong \tilde{B}_{r+1}^{p, q} / B_2^{p, q}$ where $\tilde{B}_{r+1}^{p, q}$ is some submodule of $Z_r^{p, q}$.

Therefore $E_{r+2}^{p,q}$ can be written as subquotient of submodules of $E_{r+1}^{p,q}$ in the following way.

$$E_{r+2}^{p,q} \cong Z_{r+1}^{p,q} / B_{r+1}^{p,q} \cong (\tilde{Z}_{r+1}^{p,q} / B_2^{p,q}) / (\tilde{B}_{r+1}^{p,q} / B_2^{p,q}) \cong \tilde{Z}_{r+1}^{p,q} / \tilde{B}_{r+1}^{p,q}$$

Iterating this process, we get a tower of submodules on the E_0^{**} page

$$\tilde{B}_0^{p,q} \subset \tilde{B}_1^{p,q} \subset \dots \subset \tilde{B}_r^{p,q} \subset \dots \subset \tilde{Z}_r^{p,q} \subset \dots \tilde{Z}_1^{p,q} \subset \tilde{Z}_0^{p,q} \subset E_0^{p,q}$$

such that for each r , $E_{r+1}^{p,q} \cong \tilde{Z}_r^{p,q} / \tilde{B}_r^{p,q}$. □

In addition each differential is a map

$$d_{r+1} : \tilde{Z}_r^{p,q} / \tilde{B}_r^{p,q} \longrightarrow \tilde{Z}_r^{p,q} / \tilde{B}_r^{p,q}$$

such that $\text{Ker}(d_{r+1}) = \tilde{Z}_{r+1}^{p,q} / \tilde{B}_r^{p,q}$ and $\text{Img}(d_{r+1}) = \tilde{B}_{r+1}^{p,q} / \tilde{B}_r^{p,q}$.

Definition 5.2.3. An element of $E_0^{p,q}$ which is also in $\tilde{Z}_r^{p,q}$ is said to be an r -cocycle. An element of $E_0^{p,q}$ which is also an element of $\tilde{B}_r^{p,q}$ is said to be an r -coboundary. Denote $\tilde{Z}_\infty^{p,q} = \bigcap_{r=0}^\infty \tilde{Z}_r^{p,q}$ and call an element of $\tilde{Z}_\infty^{p,q}$ an ∞ -cocycle. Similarly, denote $\tilde{B}_\infty^{p,q} = \bigcup_{r=0}^\infty \tilde{B}_r^{p,q}$ and call an element of $\tilde{B}_\infty^{p,q}$ an ∞ -coboundary. From the proof of Thm 5.2.1, it is clear that $\tilde{B}_\infty^{p,q} \subset \tilde{Z}_\infty^{p,q}$. Then, the ∞ -page of the cohomological spectral sequence is defined to be $E_\infty^{p,q} \cong \tilde{Z}_\infty^{p,q} / \tilde{B}_\infty^{p,q}$.

Definition 5.2.4. The r^{th} -page of a spectral sequence $\{E_r^{**}, d_r\}_{r \in \mathbb{N}}$ is said to be *bounded* if there exist $n, m \in \mathbb{N}$ such that

$$E_r^{p,q} = \begin{cases} \neq 0 & \text{if } |p| \leq n \text{ and } |q| < m \\ = 0 & \text{otherwise} \end{cases}$$

That is, the r^{th} page is only non-zero inside of some finite sub-rectangle on the.

Note that by Thm 5.2.1, if the r^{th} -page is bounded, then so is every subsequent page.

It is often the case that the calculation of a spectral sequence terminates after a finite number of pages. That is, there exists some smallest $N \in \mathbb{N}$ such that for all $m \geq N$, $E_m^{**} \cong E_\infty^{**}$. In this case we say that the spectral sequence *collapses* on the N^{th} -page.

For instance, suppose that a spectral sequence is bounded on its r^{th} page. Since the magnitude of the slopes of the differentials increases, after a finite number of pages either the domain or codomain of every differential map will lie outside of the finite subrectangle in which the spectral sequence is exclusively non-zero. At this point all of the differentials (and all subsequent differentials on all subsequent pages) will be zero maps. Thus every page thereafter will be isomorphic to one another. Therefore, if the spectral sequence is bounded on its r^{th} page, then it will collapse after a finite number of pages.

5.3 Filtrations of DGAs

Definition 5.3.1. Let \mathcal{A}^* be a graded R -algebra. Then a *filtration* of \mathcal{A}^* is a family of subalgebras $\{F^p(\mathcal{A}^*)\}_{p \in \mathbb{Z}}$, such that either,

$$\dots \subset F^{p+1}(\mathcal{A}^*) \subset F^p(\mathcal{A}^*) \subset F^{p-1}(\mathcal{A}^*) \subset \dots \quad (\text{decreasing filtration})$$

$$\text{or } \dots \subset F^{p-1}(\mathcal{A}^*) \subset F^p(\mathcal{A}^*) \subset F^{p+1}(\mathcal{A}^*) \subset \dots \quad (\text{increasing filtration})$$

Furthermore, if (\mathcal{A}^*, d) is a DGA, then the filtration must also be such that it is preserved by the differential, $d : F^p(\mathcal{A}^*) \rightarrow F^p(\mathcal{A}^*)$.

Let $F^*(\mathcal{A}^*) = \{F^p(\mathcal{A}^*)\}_{p \in \mathbb{Z}}$ be a filtration of the graded R -algebra \mathcal{A}^* . Furthermore, denote $F^p(A^n) = F^p(\mathcal{A}^*) \cap A^n$.

Definition 5.3.2. A filtration of a DGA $\{F^p(\mathcal{A}^*)\}_{p \in \mathbb{Z}}$ is said to be *bounded* if and only if for each n there exists some $s = s(n)$ and $t = t(n)$ such that

$$\{0\} = F^s(A^n) \subset F^{s+1}(A^n) \subset \dots \subset F^{t+1}(A^n) \subset F^t(A^n) = A^n, \quad F^* \text{ is decreasing}$$

$$\{0\} = F^s(A^n) \subset F^{s+1}(A^n) \subset \dots \subset F^{t-1}(A^n) \subset F^t(A^n) = A^n, \quad F^* \text{ is increasing}$$

Definition 5.3.3. The *associated bigraded R -algebra* of \mathcal{A}^* with respect to F^* is given as follows

$$E_{assoc}^{p,q}(\mathcal{A}^*, F^*) = \begin{cases} F^p(A^{p+q})/F^{p+1}(A^{p+q}), & F^* \text{ is decreasing} \\ F^p(A^{p+q})/F^{p-1}(A^{p+q}), & F^* \text{ is increasing} \end{cases}$$

Definition 5.3.4. A spectral sequence $\{E_r^{**}, d_r\}_{r \in \mathbb{N}}$ is said to *converge* to a graded R -algebra \mathcal{A}^* if and only if there is a filtration F^* of \mathcal{A}^* such that

$$E_{\infty}^{p,q} \cong E_{assoc}^{p,q}(\mathcal{A}^*, F^*)$$

Theorem 5.3.1. *McCleary (1985) Let (\mathcal{A}^*, d) be a DGA such that $\deg(d) = +1$. Then a decreasing filtration $F^*(\mathcal{A}^*)$ on (\mathcal{A}^*, d) determines a spectral sequence $\{E_r^{**}, d_r\}_{r \in \mathbb{N}}$ where $\deg(d_r) = (r, 1-r)$ and*

$$E_0^{p,q} = E_{assoc}^{p,q}(\mathcal{A}^*, F^*)$$

$$E_1^{p,q} = H^{p+q}\left(F^p(\mathcal{A}^*)/F^{p+1}(\mathcal{A}^*)\right)$$

Furthermore, if the filtration is bounded, then the spectral sequence converges to $H^(\mathcal{A}^*, d)$,*

$$E_{\infty}^{p,q} \cong E_{assoc}^{p,q}(H^*(\mathcal{A}^*, d), F^*)$$

Note that a filtration F^* on a DGA (\mathcal{A}^*, d) induces a filtration on its cohomology $H^*(\mathcal{A}^*, d)$

because F^* is preserved by the differential. Therefore, $E_{assoc}^{p,q}(H^*(\mathcal{A}^*, d), F^*)$ is well defined.

The goal here is that the ∞ -total complex of the spectral sequence be isomorphic to $H^*(\mathcal{A}^*, d)$.

$$Tot_{\infty}^*(E_{\infty}^{**}) \cong H^*(\mathcal{A}^*, d)$$

However, this may only be true up to some extensions for arbitrary DGAs.

5.4 Bicomplexes and Their Filtrations

Definition 5.4.1. A bigraded R -algebra \mathcal{A}^{**} is a *bicomplex* if there are two maps ∂ and d such that for each i , $(\mathcal{A}^{i,*}, d)$ and $(\mathcal{A}^{*,i}, \partial)$ are DGAs and $d \circ \partial + \partial \circ d = 0$.

Example 5.4.1. A typical bicomplex $(\mathcal{A}^{**}; d, \partial)$.

$$\begin{array}{ccccccc}
 & \uparrow & & \uparrow & & \uparrow & & \uparrow \\
 & \cdot & & \cdot & & \cdot & & \cdot \\
 \cdot & \longrightarrow & A^{03} & \xrightarrow{\partial} & A^{13} & \xrightarrow{\partial} & A^{23} & \xrightarrow{\partial} & A^{33} & \longrightarrow & \cdot \\
 & \uparrow d & & \uparrow d & & \uparrow d & & \uparrow d \\
 \cdot & \longrightarrow & A^{02} & \xrightarrow{\partial} & A^{12} & \xrightarrow{\partial} & A^{22} & \xrightarrow{\partial} & A^{32} & \longrightarrow & \cdot \\
 & \uparrow d & & \uparrow d & & \uparrow d & & \uparrow d \\
 \cdot & \longrightarrow & A^{01} & \xrightarrow{\partial} & A^{11} & \xrightarrow{\partial} & A^{21} & \xrightarrow{\partial} & A^{31} & \longrightarrow & \cdot \\
 & \uparrow d & & \uparrow d & & \uparrow d & & \uparrow d \\
 \cdot & \longrightarrow & A^{00} & \xrightarrow{\partial} & A^{10} & \xrightarrow{\partial} & A^{20} & \xrightarrow{\partial} & A^{30} & \longrightarrow & \cdot \\
 & \uparrow & & \uparrow & & \uparrow & & \uparrow \\
 & \cdot & & \cdot & & \cdot & & \cdot
 \end{array}$$

The total complex of a bicomplex is defined in the same manner as the r^{th} -total complex of a spectral sequence and is itself a DGA. Namely, it is given by $Tot^*(\mathcal{A}^{**}) = \bigoplus_n Tot^n(\mathcal{A}^{**})$

where:

$$\text{Tot}^n(\mathcal{A}^{**}) = \bigoplus_{p+q=n} \mathcal{A}^{p,q} \text{ and } D = d + \partial$$

Note that the condition in the definition that $d \circ \partial + \partial \circ d = 0$ is necessary to ensure the that map D is a genuine differential on the total complex.

Definition 5.4.2. Let $(\mathcal{A}^{**}, d_{\mathcal{A}}, \partial_{\mathcal{A}})$ and $(\mathcal{B}^{**}, d_{\mathcal{B}}, \partial_{\mathcal{B}})$ be two bicomplexes. Then a map $\phi : \mathcal{A}^{**} \rightarrow \mathcal{B}^{**}$ is a *morphism of bicomplexes* if it is a morphism from \mathcal{A}^{**} to \mathcal{B}^{**} as bigraded R -algebras that also commutes with the differentials $d_{\mathcal{A}}$ and $d_{\mathcal{B}}$.

Note that, as in the case with DGAs, commuting with the differential means that a bicomplex morphism will induced maps on the bigraded space resulting from computing cohomology with respect to those differentials.

Theorem 5.4.1. Let $(\mathcal{B}^*, \delta_{\mathcal{B}})$ and $(\mathcal{C}^*, \delta_{\mathcal{C}})$ be DGAs. Then their tensor product $\mathcal{B}^* \otimes \mathcal{C}^*$ is the total complex of a bicomplex with total differential given by $D = (-1)^p \text{Id}_{\mathcal{B}} \otimes \delta_{\mathcal{C}} + \delta_{\mathcal{B}} \otimes \text{Id}_{\mathcal{C}}$.

Proof. Given $(\mathcal{B}^*, \delta_{\mathcal{B}})$ and $(\mathcal{C}^*, \delta_{\mathcal{C}})$, recall that their tensor product is given by

$$\mathcal{B}^* \otimes \mathcal{C}^* = \bigoplus_n \left(\bigoplus_{p+q=n} (B^p \otimes C^q) \right)$$

Define a bigraded space \mathcal{A}^{**} where $A^{p,q} = B^p \otimes C^q$. The differentials $\delta_{\mathcal{B}}$ and $\delta_{\mathcal{C}}$ induce the differentials on the bigraded R -algebra $\partial = \delta_{\mathcal{B}} \otimes \text{Id}_{\mathcal{C}}$ and $d = (-1)^p \text{Id}_{\mathcal{B}} \otimes \delta_{\mathcal{C}}$. Multiplication on \mathcal{A}^{**} is induced by multiplication on \mathcal{B}^* and \mathcal{C}^* , $(b_1 \otimes c_1)(b_2 \otimes c_2) = (b_1 b_2) \otimes (c_1 c_2)$. Therefore $(\mathcal{A}^{**}, d, \partial)$ is a bicomplex.

From the \mathcal{A}^{**} , the total

$$\text{Tot}^*(\mathcal{A}^{**}) = \bigoplus_n \left(\bigoplus_{p+q=n} A^{p,q} \right) = \bigoplus_n \left(\bigoplus_{p+q=n} (B^p \otimes C^q) \right) = \mathcal{B}^* \otimes \mathcal{C}^*$$

and total differential $D = (-1)^p \text{Id}_{\mathcal{B}} \otimes \delta_{\mathcal{C}} + \delta_{\mathcal{B}} \otimes \text{Id}_{\mathcal{C}}$ are given by Def 5.2.2. □

The sign factor $(-1)^p$ in the definition of d in the preceding theorem is called the *sign trick* in some texts. It is a convention which guarantees that the the total differentials d and ∂ are anti-commutative as required by the definition of a bicomplex. Note that without it they are commutative.

Theorem 5.4.2. *A finite tensor product of DGAs is a DGA.*

Proof. Let $(\mathcal{B}^*, \delta_{\mathcal{B}})$, $(\mathcal{C}^*, \delta_{\mathcal{C}})$, and $(\mathcal{D}^*, \delta_{\mathcal{D}})$ be DGAs and consider the triple tensor product $\mathcal{B}^* \otimes \mathcal{C}^* \otimes \mathcal{D}^*$. The first pair of factors can be realized as a single DGA, $\mathcal{B}^* \otimes \mathcal{C}^* = \text{Tot}^*(\mathcal{A}^{**})$ as in Thm 5.4.1. Then $\mathcal{B}^* \otimes \mathcal{C}^* \otimes \mathcal{D}^* = \text{Tot}^*(\mathcal{A}^{**}) \otimes \mathcal{D}^*$ which is again a tensor product of two DGAs. Repeating the process reduces it to a single DGA.

For a finite tensor product of DGAs, iterating the process resolves it into a single DGA. \square

Lemma 5.4.3. *Given two DGAs $(\mathcal{B}^*, \delta_{\mathcal{B}})$ and $(\mathcal{C}^*, \delta_{\mathcal{C}})$, their direct sum is a DGA given by*

$$\mathcal{A}^* = \bigoplus_i (B^i \oplus C^i), d = \delta_{\mathcal{B}} + \delta_{\mathcal{C}}$$

Multiplication on \mathcal{A}^ is given by $(b_1, c_1)(b_2, c_2) = (b_1 b_2, c_1 c_2)$.*

Definition 5.4.3. Let $(\mathcal{A}^{**}; d, \partial)$ be a bicomplex and $(\text{Tot}^*(\mathcal{A}^{**}), D)$ be its total complex. The *horizontal filtration* of the $(\text{Tot}^*(\mathcal{A}^{**}), D)$ is induced by a filtration on the rows of $(\mathcal{A}^{**}, d, \partial)$ as follows.

$$\left(F_h^i(\text{Tot}^*(\mathcal{A}^{**})) \right)^{p,q} = \begin{cases} A^{p,q} & \text{if } q \geq i \\ 0 & \text{else} \end{cases}$$

Definition 5.4.4. Let $(\mathcal{A}^{**}; d, \partial)$ be a bicomplex and $(\text{Tot}^*(\mathcal{A}^{**}), D)$ be its total complex. Then the *vertical filtration* of the total complex is induced by a filtration on the columns of the bicomplex. Specifically, it is given by

$$\left(F_v^i(\text{Tot}^*(\mathcal{A}^{**})) \right)^{p,q} = \begin{cases} A^{p,q} & \text{if } p \geq i \\ 0 & \text{else} \end{cases}$$

Example 5.4.2. $F_h^1(\text{Tor}^*(\mathcal{A}^{**}))$ and $F_h^2(\text{Tor}^*(\mathcal{A}^{**}))$ of a typical bicomplex are obtained by taking the total complex of the following bicomplexes respectively.

Example 5.4.3. $F_v^1(\text{Tot}^*(\mathcal{A}^{**}))$ and $F_v^2(\text{Tot}^*(\mathcal{A}^{**}))$ of a typical bicomplex are obtained by taking the total complex of the following bicomplexes respectively.

90

Theorem 5.4.4. *Let $(\mathcal{A}^{**}; d, \partial)$ be a bounded bicomplex and F_h^* denote the horizontal filtration. There exists a spectral sequence $\{E_r^{**}, d_r\}_{r \in \mathbb{N}}$ arising from the application of F_h^* to $(\mathcal{A}^{**}; d, \partial)$ given by*

$$E_0^{p,q} = \mathcal{A}^{q,p} \text{ where } d_0 = \partial$$

$$E_1^{p,q} = H^{q,p}(\mathcal{A}^{**}) \text{ where } d_1 = d$$

where

$$H^{q,p}(\mathcal{A}^{**}) = \frac{\text{Ker}(\mathcal{A}^{q,p} \xrightarrow{\partial} \mathcal{A}^{q,p+1})}{\text{Img}(\mathcal{A}^{q,p-1} \xrightarrow{\partial} \mathcal{A}^{q,p})}$$

Furthermore, the spectral sequence converges and

$$E_\infty^{p,q} \cong E_{assoc}^{p,q} \left(H^*(\text{Tot}^*(\mathcal{A}^{**}), D), F_h^* \right)$$

Proof. We wish to apply Thm 5.3.1 where the filtration is the horizontal filtration F_h^* and the DGA is the total complex with its total differential $\text{Tot}^*(A^{**}, D)$. Then it must be shown that F_h^* is a bounded decreasing filtration and that $\deg(D) = +1$.

Recall that $\deg(d) = +1 = \deg(\partial)$ by assumption. Therefore the differential $D = d + \partial$ has bidegree $(+1, +1)$ in the bicomplex. It is clear then from Ex 5.4.2 that D preserves the horizontal filtration of $(\mathcal{A}^{**}; d, \partial)$. Therefore, the total differential D on the total complex of the bicomplex $\text{Tot}^*(\mathcal{A}^{**})$ preserves the induced filtrations on the total complex and has total degree $+1$.

$$D : F_h^i(\text{Tot}^j(\mathcal{A}^{**})) \rightarrow F_h^i(\text{Tot}^{j+1}(\mathcal{A}^{**}))$$

Furthermore, notice that the multiplication on \mathcal{A}^{**} also respects the filtration since bidegrees are additive.

Since $F_h^i(\text{Tot}^*(\mathcal{A}^{**})) \subseteq F_h^{i-1}(\text{Tot}^*(\mathcal{A}^{**}))$ for all i , F_h^* is a decreasing filtration. Furthermore, since the bicomplex $(\mathcal{A}^{**}; d, \partial)$ is bounded by assumption, the horizontal filtration of the

total complex is a bounded filtration.

Lastly, notice from Ex 5.4.2 that only one of the two differentials of the bicomplex preserves the quotient of subsequent filtrations.

$$\partial : F_h^i(\text{Tot}^*(\mathcal{A}^{**})) / F_h^{i+1}(\text{Tot}^*(\mathcal{A}^{**})) \rightarrow F_h^i(\text{Tot}^*(\mathcal{A}^{**})) / F_h^{i+1}(\text{Tot}^*(\mathcal{A}^{**}))$$

It follows from Thm 5.3.1 that the horizontal filtration gives rise to a spectral sequence. The differential $d_0 = \partial$ on E_0^{**} is the differential which preserves the quotient of subsequent filtrations. Furthermore, since \mathcal{A}^{**} is bounded by assumption, the horizontal filtration will be bounded.

Therefore, by Thm 5.3.1 the horizontal filtration induces a spectral sequence $\{E_r^{**}, d_r\}_{r \in \mathbb{N}}$ where $\deg(d_r) = (r, 1 - r)$ and

$$E_0^{p,q} = E_{assoc}^{p,q}(\text{Tot}^*(\mathcal{A}^{**}), F_h^*) \text{ where } d_0 = \partial$$

$$E_1^{p,q} = H^{p+q}\left(F_h^p(\text{Tot}^*(\mathcal{A}^{**})) / F_h^{p+1}(\text{Tot}^*(\mathcal{A}^{**}))\right)$$

$$E_\infty^{p,q} \cong E_{assoc}^{p,q}\left(H^*(\text{Tot}^*(\mathcal{A}^{**}), D), F_h^*\right)$$

Note that the convergence claim follows directly from Thm 5.3.1.

Therefore, the first thing to show is that

$$E_{assoc}^{p,q}(\text{Tot}^*(\mathcal{A}^{**}), F_h^*) = \mathcal{A}^{q,p}$$

This can be done by unwinding the definitions as follows. First, recall from Def 5.3.3 that

$$E_{assoc}^{p,q}(\text{Tot}^*(\mathcal{A}^{**}), F_h^*) = F_h^p(\text{Tot}^{p+q}(\mathcal{A}^{**})) / F_h^{p+1}(\text{Tot}^{p+q}(\mathcal{A}^{**}))$$

$$F_h^p(\text{Tot}^{p+q}(\mathcal{A}^{**})) = F_h^p(\text{Tot}^*(\mathcal{A}^{**})) \cap \text{Tot}^{p+q}(\mathcal{A}^{**})$$

$$F_h^{p+1}(\text{Tot}^{p+q}(\mathcal{A}^{**})) = F_h^{p+1}(\text{Tot}^*(\mathcal{A}^{**})) \cap \text{Tot}^{p+q}(\mathcal{A}^{**})$$

Now, by Def 5.4.3 and Def 5.2.2 respectively that

$$F_h^p(\text{Tot}^*(\mathcal{A}^{**}))^{i,j} = \begin{cases} \mathcal{A}^{i,j} & \text{if } j \geq p \\ 0 & \text{else} \end{cases}$$

$$F_h^{p+1}(\text{Tot}^*(\mathcal{A}^{**}))^{i,j} = \begin{cases} \mathcal{A}^{i,j} & \text{if } j \geq p+1 \\ 0 & \text{else} \end{cases}$$

$$\text{Tot}^{p+q}(\mathcal{A}^{**}) = \bigoplus_{i+j=p+q} \mathcal{A}^{i,j}$$

Therefore, we find that

$$F_h^p(\text{Tot}^{p+q}(\mathcal{A}^{**})) = \bigoplus_{\substack{i+j=p+q \\ j \geq p}} \mathcal{A}^{i,j}$$

$$F_h^{p+1}(\text{Tot}^{p+q}(\mathcal{A}^{**})) = \bigoplus_{\substack{i+j=p+q \\ j \geq p+1}} \mathcal{A}^{i,j}$$

Then we get that.

$$\begin{aligned} E_{assoc}^{p,q}(\text{Tot}^*(\mathcal{A}^{**}), F_h^*) &= \left(\bigoplus_{\substack{i+j=p+q \\ j \geq p}} \mathcal{A}^{i,j} \right) / \left(\bigoplus_{\substack{i+j=p+q \\ j \geq p+1}} \mathcal{A}^{i,j} \right) \\ &= \bigoplus_{\substack{i+j=p+q \\ j=p}} \mathcal{A}^{i,j} \\ &= \mathcal{A}^{q,p} \end{aligned}$$

As for the claims about E_1^{**} and d_1 . By Def 5.2.1, E_1^{**} is given by cohomology on E_0^{**} . As for d_1 , it is induced by \bar{d} in the natural way.

Now, the second claim to be proved is that

$$E_1^{p,q} = H^{q,p}(\mathcal{A}^{**}) \quad \text{where} \quad H^{q,p}(\mathcal{A}^{**}) = \frac{\text{Ker}(\mathcal{A}^{q,p} \xrightarrow{\partial} \mathcal{A}^{q,p+1})}{\text{Img}(\mathcal{A}^{q,p-1} \xrightarrow{\partial} \mathcal{A}^{q,p})}.$$

We have just shown that $(E_0^{p,q}, d_0) = (\mathcal{A}^{q,p}, \partial)$. By Thm 5.3.1, the 1^{st} -page of the spectral sequence is given by computing cohomology on the 0^{th} -page. However, that is exactly $H^{q,p}(\mathcal{A}^{**})$ as described. \square

Theorem 5.4.5. *Let $(\mathcal{A}^{**}, d, \partial)$ be a bounded bicomplex and F_v^* denote the vertical filtration. There exists a spectral sequence $\{E_r^{**}, d_r\}_{r \in \mathbb{N}}$ arising from the application of F_v^* to $(\mathcal{A}^{**}, d, \partial)$ given by*

$$E_0^{p,q} = \mathcal{A}^{p,q} \text{ where } d_0 = d$$

$$E_1^{p,q} = H^{p,q}(\mathcal{A}^{**}) \text{ where } d_1 = \partial$$

where

$$H^{p,q}(\mathcal{A}^{**}) = \frac{\text{Ker}(\mathcal{A}^{p,q} \xrightarrow{d} \mathcal{A}^{p,q+1})}{\text{Img}(\mathcal{A}^{p,q-1} \xrightarrow{d} \mathcal{A}^{p,q})}$$

Furthermore, the spectral sequence converges and

$$E_\infty^{p,q} \cong E_{assoc}^{p,q} \left(H^*(\text{Tot}^*(\mathcal{A}^{**}), D), F_v^* \right)$$

Proof. The proof is analogous to that of Thm 5.4.4. \square

Given a bounded bicomplex $(\mathcal{A}^{**}, d, \partial)$ with total complex $(\text{Tot}^*(\mathcal{A}^{**}), D)$, the spectral sequences arising from the vertical and horizontal filtrations of $(\mathcal{A}^{**}, d, \partial)$ both converge to $H^*(\text{Tot}^*(\mathcal{A}^{**}))$. That is, the total complex of the infinity page of both spectral sequences are isomorphic to the cohomology of the total complex of the bicomplex.

CHAPTER

6

GRAPH COLORINGS AND BICOMPLEXES

6.1 Preliminary on Graphs

Definition 6.1.1. A *Graph* is a pair $G = (V(G), E(G))$ consisting of a finite set $V(G) = \{v_i\}_{i=0}^n$ and a set of two-element subsets of $V(G)$, $e = \{v_i, v_j\} \in E(G)$. Elements of $V(G)$ are called vertices and elements of $E(G)$ are called edges.

Let G and H be graphs. Then a morphism of graphs is a set map $f : V(G) \rightarrow V(H)$ such that if $\{v_i, v_j\} \in E(G)$ then $\{f(v_i), f(v_j)\} \in E(H)$ and is denoted $f : G \rightarrow H$.

The objects which have been defined as *graphs* here are more commonly called *finite simple graphs* in graph theory literature as they do not contain loops or multi-edges and have

a finite number of vertices. Furthermore, note that for a given graph morphism $f : G \rightarrow H$, the set map $f : V(G) \rightarrow V(H)$ induces a set map $f : E(G) \rightarrow E(H)$.

Definition 6.1.2. A graph G is a *subgraph* of H if and only if there exists a graph morphism $f : G \rightarrow H$ such that $f : V(G) \rightarrow V(H)$ is injective.

Definition 6.1.3. Two vertices $v_i, v_j \in V(G)$ of a graph G are *connected* if and only if there exists a sequence of edges $\{e_k\}_{k=0}^n \subseteq E(G)$ such that $v_i \in e_1, v_j \in e_n$, for each $k \in \{0, \dots, n-1\}$ $e_k \cap e_{k+1} \neq \emptyset$, and each vertex in $V(G)$ appears in at most two edges in the sequence. Furthermore, each vertex in $V(G)$ is connected to itself.

Lemma 6.1.1. Let G be a graph. Then the connectedness relation is an equivalence relation on the vertex set $V(G)$.

Definition 6.1.4. Given a graph G , an equivalence class in $V(G)$ under the connectedness relation is called a *connected component*. Denote the set of connected components of G by $\pi_0(G) = \{C_i\}_{i=0}^n$.

Each connected component of a graph G has a unique associated subgraph. Let $C_i \in \pi_0(G)$. Then $C_i \subseteq V(G)$. Define the subgraph G^{C_i} as given by $V(G^{C_i}) = C_i$ and $E(G^{C_i}) = \{e \in E(G) \mid \text{there exists } v_i \in C_i \text{ s.t. } v_i \in e\}$.

Lemma 6.1.2. Let G and H be graphs and $f : G \rightarrow H$ be a graph morphism. Then there is an induced map $f_* : \pi_0(G) \rightarrow \pi_0(H)$.

Proof. It is enough to show that $f : G \rightarrow H$ preserves the connectedness relation. Therefore, let $v_i \in V(G)$ be connected to $v_j \in V(G)$ by the sequence of edges $S = \{e_k\}_{k=0}^n \subseteq E(G)$. If $f(v_i) = f(v_j) \in V(H)$, then connectedness is preserved since each vertex is connected to itself by definition.

Suppose that $f(v_i) \neq f(v_j) \in V(H)$. Then let $S_r = \{e_{k_r}\}_{r=0}^m$ be the maximal subsequence of S such that the induced map on the edge sets is such that $f|_{S_r} : S_r \rightarrow E(H)$ is injective. Then $f(v_i)$ is connected to $f(v_j)$ by the sequence of edges $\{f(e_{k_r})\}_{r=0}^m \subseteq E(H)$. \square

6.2 The Chromatic Complex

The contents of this section can be found in the literature at Helme-Guizon and Rong (2005a) and Helme-Guizon and Rong (2005b).

Definition 6.2.1. Let G be a graph and $S \subseteq E(G)$. Then G_S is defined as the subgraph of G given by $V(G_S) = V(G)$ and $E(G_S) = S \subseteq E(G)$.

If $V(G)$ is given a total ordering $V(G) = \{v_0, \dots, v_m\}$, then $E(G)$ will inherit a lexicographical ordering, $E(G) = \{e_0, \dots, e_n\}$. Similarly, the connected components of a given subgraph G_S inherit a total order wherein two components bear the same relation as their least vertices. Finally, for a given subgraph G_S , let k_S denote its number of connected components, $k_S = |\pi_0(G_S)|$.

Definition 6.2.2. A subgraph G_S is said to be in the i^{th} -state if G_S has exactly i -many edges, $|S| = i$.

Definition 6.2.3. Given a graph G , a *graph coloring* of G with λ -many colors is a map $c : V(G) \rightarrow \{i\}_{i=1}^\lambda$ such that if $\{v_j, v_k\} \in E(G)$, then $c(v_j) \neq c(v_k)$.

Definition 6.2.4. For a given graph G the *Chromatic Polynomial*, $P_G(\lambda)$, is a function which returns the number colorings of a graph G using λ -many colors.

Note that for the empty graph on n vertices, all possible colorings of the vertices are permissible since there are no edges. In this case, $P_G(\lambda) = \lambda^n$. Furthermore, the chromatic polynomial obeys the following recursive relation.

Lemma 6.2.1. (Deletion-Contraction Rule) Given a graph G and edge $e \in E(G)$, let $G \setminus e$ denote the subgraph of G such that $V(G \setminus e) = V(G)$ and $E(G \setminus e) = E(G) \setminus e$ (i.e. the e -edge is deleted from G). Let G/e denote the graph obtained by contracting the e -edge in G and identifying its vertices.

The chromatic polynomial for the graph G then has the following property:

$$P_G(\lambda) = P_{G \setminus e}(\lambda) - P_{G/e}(\lambda) \quad (6.1)$$

Proof. (Sketch) For motivation, it is enough to consider the graph G where $V(G) = \{v, w\}$ and $E(G) = \{e = \{v, w\}\}$ (two vertices connected by one edge). In this case it is clear what effect the presence of e , its deletion, and its contraction have on the possible colorings of G . In $G \setminus e$ all colorings of v and w are allowed. The number of all colorings is the sum of colorings in which v and w have the same color plus the number of colorings in which v , and w have different colors. In G/e , v and w must have the same color while in G they must have different colors. We therefore find that

$$P_{G \setminus e}(\lambda) = P_G(\lambda) + P_{G/e}(\lambda)$$

A simple rearrangement of terms yields the desired relation. The reader is directed to ?? for more details. □

Corollary 6.2.1.1. Using the result for the empty graph as a base case, the Deletion Contraction Rule can be resolved into an explicit form called the **State Sum Formula** which is given by:

$$P_G(\lambda) = \sum_{i \geq 0} (-1)^i \sum_{\substack{S \subseteq E(G) \\ |S|=i}} \lambda^{k_S}$$

Suppose that $|E(G)| = n$. Then the collection of all subsets $S \subseteq E(G)$ is in bijection with

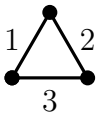
the collection of all binary n -tuples ε wherein the j^{th} element of ε is '1' if the j^{th} edge of $E(G)$ is in S and '0' otherwise. In this way, the subgraphs G_S can be equivalently denoted $G_S = G_\varepsilon$.

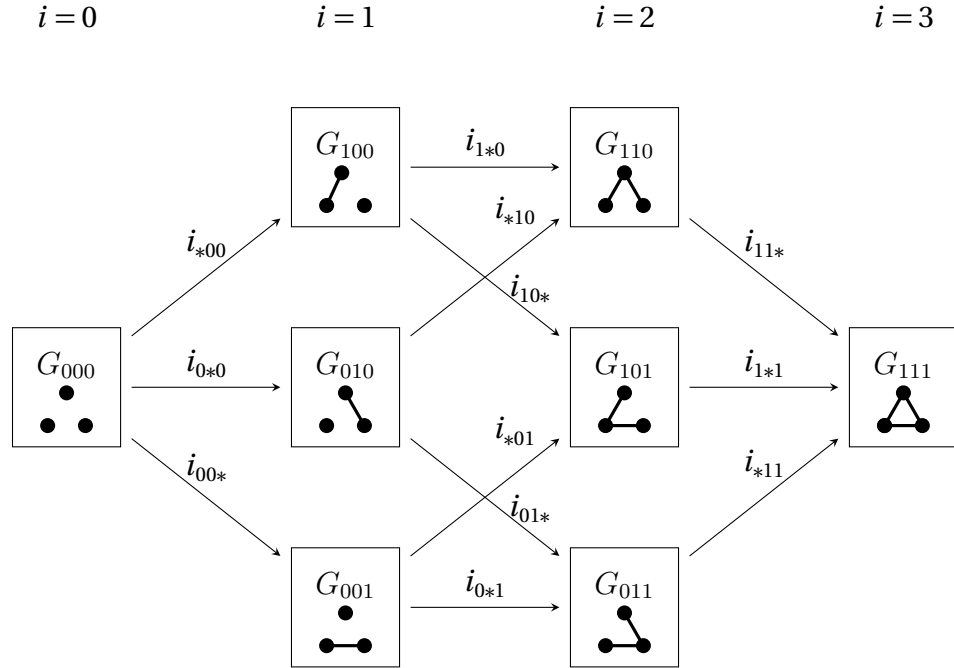
Let G be a graph and G_S be a subgraph in the i^{th} -state. For each edge $e \in E(G) \setminus S$, let $S' = S \cup \{e\}$. Then $G_{S'}$ is a subgraph of G in the $(i+1)^{st}$ -state. Furthermore, G_S is a subgraph of $G_{S'}$.

Suppose $e \in E(G) \setminus S$ is the j^{th} edge in $E(G)$. Then we can equivalently denote $G_S = G_\varepsilon$ and $G_{S'} = G_{\varepsilon'}$ where ε' is obtain from ε by altering the j^{th} element of ε from a '0' to a '1'. Then the graph homomorphism which realizes G_ε as a subgraph of $G_{\varepsilon'}$ can be denoted $i_{\varepsilon^*} : G_\varepsilon \rightarrow G_{\varepsilon'}$ where ε^* is obtained from ε by altering the j^{th} element of ε from a '0' to an '*'. Similarly, let k_ε denote the number of connected components of the subgraph G_ε ,

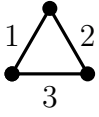
Definition 6.2.5. Given a graph G , all of its subgraphs of the form G_ε and their respective inclusion maps i_{ε^*} can be organized into a cubic lattice called the *Chromatic Diagram*. The subgraphs G_ε form the vertices, the inclusion maps i_{ε^*} form the edges, and subgraphs are organized into columns of increasing state.

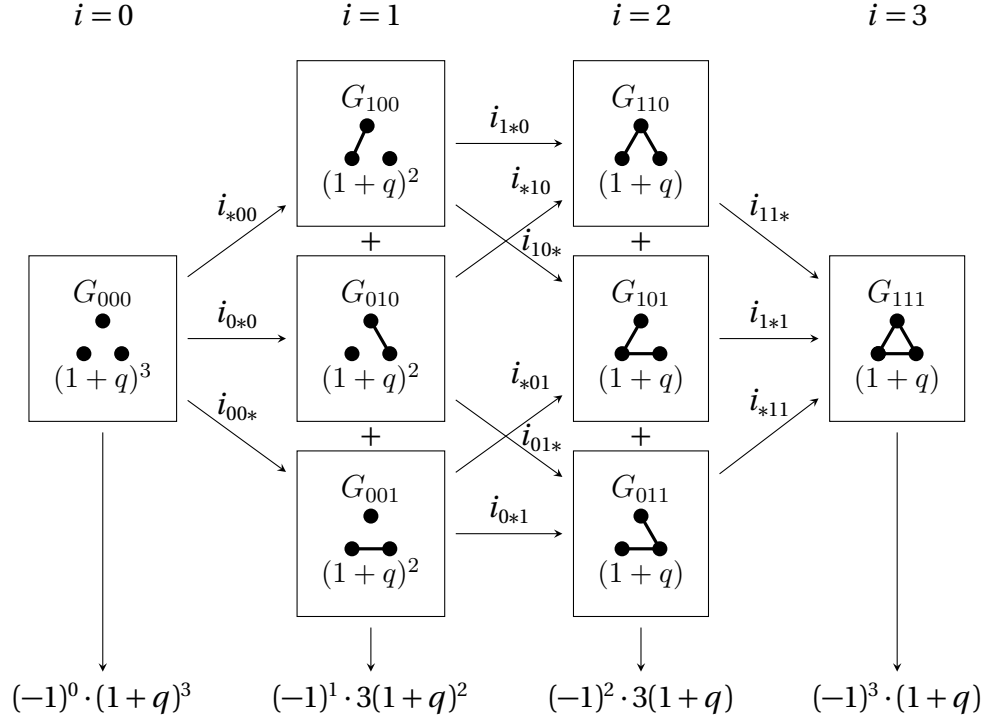
The Chromatic Diagram of a graph G is often called its Hasse Diagram in other literature where the subgraphs are organized into rows of increasing state. See Example 6.2.1 below.

Example 6.2.1. $G =$ 



With this technology, the state sum formula has the advantage that it can be expressed diagrammatically. Consider this representation in the following example 6.2.2 where the chromatic polynomial of the complete graph on three vertices is computed. The substitution $\lambda = 1 + q$ has been made for reasons which will be made clear shortly.

Example 6.2.2. $G =$  & $\lambda = 1 + q$



$$P_G(1+q) = (1+q)^3 - 3(1+q)^2 + 3(1+q) - (1+q)$$

The Chromatic Diagram of a graph can be made into a DGA with the following definitions and prescriptions which effectively categorifies the chromatic polynomial.

Definition 6.2.6. Given a graded R -algebra \mathcal{A}^* and a graph G , to each subgraph G_ϵ assign the graded R -algebra $\mathcal{A}^{\otimes k_\epsilon} = (\mathcal{A}^*)^{\otimes k_\epsilon}$. Then the i^{th} Chromatic Co-Chain Group is given by

$$CHR^i(G, \mathcal{A}) = \bigoplus_{|\epsilon|=i} \mathcal{A}^{\otimes k_\epsilon}$$

That is, take direct sums of the assigned graded R -algebras along subgraphs of the same state (along columns of the diagram).

Notice that each inclusion map i_{ϵ^*} represents adding an edge to some G_ϵ in state j to obtain some other $G_{\epsilon'}$ in state $j+1$. Adding an edge does one of two things to the connected components of G_ϵ . It either decreases k_ϵ by one, or it preserves k_ϵ . That is to say, either $k_{\epsilon'} = k_\epsilon - 1$ or $k_{\epsilon'} = k_\epsilon$.

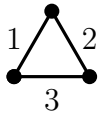
Therefore, to each inclusion $i_{\epsilon^*} : G_\epsilon \rightarrow G_{\epsilon'}$ assign the following map between the graded R -algebras assigned to G_ϵ and $G_{\epsilon'}$.

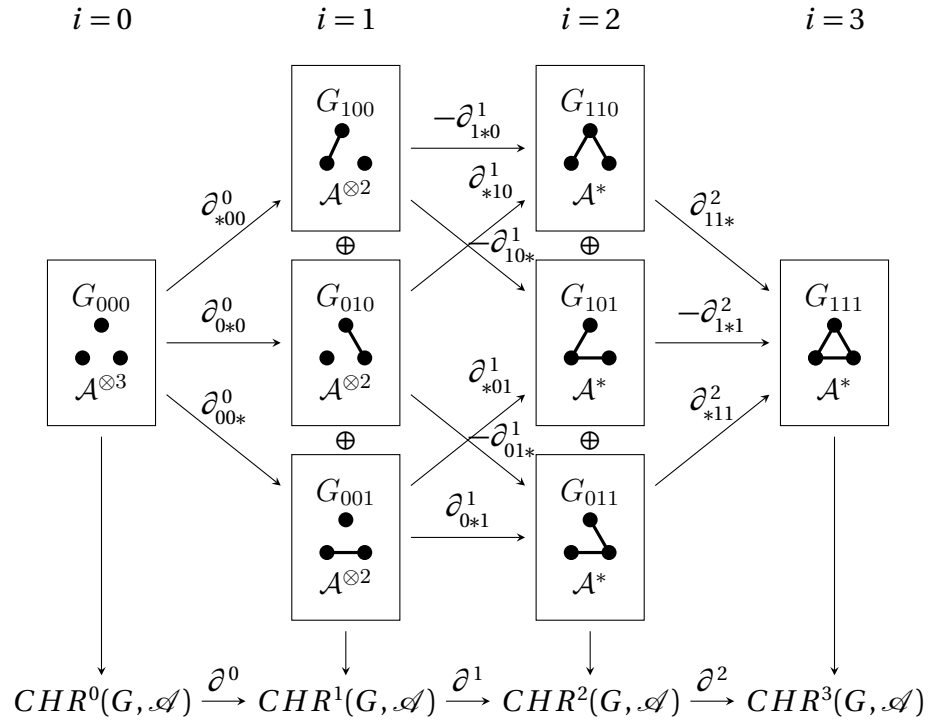
Definition 6.2.7. To each i_{ϵ^*} assign the map $(-1)^{\epsilon_*} \partial_{\epsilon_*}^i : \mathcal{A}^{\otimes k_\epsilon} \rightarrow \mathcal{A}^{\otimes k_{\epsilon'}}$. Each $(-1)^{\epsilon_*} \partial_{\epsilon_*}^i$ is called a *per-edge map* and is given by the following:

1. $(-1)^{\epsilon_*}$ is 1 if the number of ones in ϵ_* before the asterisk is even, and -1 if the number of such ones on odd.
2. If $k_{\epsilon'} = k_\epsilon$, then $\partial_{\epsilon_*}^i = \text{Id}_{\mathcal{A}^{\otimes k_\epsilon}}$.
3. If $k_{\epsilon'} = k_\epsilon - 1$, then $\partial_{\epsilon_*}^i = \text{Id}_{\mathcal{A}^{\otimes k_\epsilon}}$ on all of the tensor factors except the two corresponding to the components of G_ϵ which become connected upon adding the edge. On those two tensor factors $\partial_{\epsilon_*}^i$ is given by the multiplication, $m : \mathcal{A}^* \otimes \mathcal{A}^* \rightarrow \mathcal{A}^*$ which maps to the tensor factor in the codomain $\mathcal{A}^{\otimes k_{\epsilon'}}$ which corresponds to the connected component in $G_{\epsilon'}$ which resulted from adding the edge to G_ϵ .

Definition 6.2.8. Note that the Chromatic Diagram is always a cubic lattice and the assignment $(-1)^{\varepsilon_*}$ to the per-edge maps gives it a balanced coloring. Therefore, summing the per-edge maps along the columns produces a differential on the co-chain groups. The result is a co-chain complex called the *Chromatic Complex* and is denote $(CHR^*(G, \mathcal{A}), \partial)$ where each differential ∂ is a signed sum of per-edge maps.

Note that the chromatic complex is always bounded by the number of edges in the graph which is finite for finite graphs.

Example 6.2.3. $G =$ 



Where:

$$CHR^0(G, \mathcal{A}) = \mathcal{A}^{\otimes 3}$$

$$CHR^1(G, \mathcal{A}) = \bigoplus_3 \mathcal{A}^{\otimes 2}$$

$$CHR^2(G, \mathcal{A}) = \bigoplus_3 \mathcal{A}$$

$$CHR^3(G, \mathcal{A}) = \mathcal{A}$$

$$CHR^*(G, \mathcal{A}) = \bigoplus_{i=0}^3 CHR^i(G, \mathcal{A})$$

$$\partial^0 = \partial_{*00}^0 + \partial_{0*0}^0 + \partial_{00*}^0$$

$$\partial^1 = -\partial_{1*0}^1 + \partial_{*10}^1 - \partial_{10*}^1 + \partial_{*01}^1 - \partial_{01*}^1 + \partial_{0*1}^1$$

$$\partial^2 = \partial_{11*}^2 - \partial_{1*1}^2 + \partial_{*11}^2$$

Example 6.2.4. Specifically, recalling Ex 5.1.1, let $\mathcal{A}^* = \mathbb{Z}[x]/\langle x^2 \rangle$. Then the categorification of the chromatic polynomial is demonstrated by

$$\begin{aligned} P_G(1+q) &= \sum_{i \geq 0} (-1)^i \sum_{\substack{S \subseteq E(G) \\ |S|=i}} (1+q)^{k_S} \\ &= \sum_{i \geq 0} (-1)^i \sum_{\substack{S \subseteq E(G) \\ |S|=i}} qdim(\mathcal{A}^{\otimes k_S}) \\ &= \sum_{i \geq 0} (-1)^i qdim \left(\bigoplus_{|S|=i} \mathcal{A}^{\otimes k_S} \right) \\ &= \chi_q(CHR^*(G, \mathcal{A})) \end{aligned}$$

Furthermore (and more generally), if \mathcal{A}^* is a graded R -module such that the ring R is a principal ideal domain and for each i , \mathcal{A}^i is finitely generated, then $\chi_q(CHR^*(G, \mathcal{A})) = \chi_q(H_{CHR}^*(G, \mathcal{A}))$ where $H_{CHR}^*(G, \mathcal{A})$ is the graded R -algebra resulting from computing the cohomology of the chromatic complex.

6.3 The Chromatic Bicomplex

Theorem 6.3.1. (Baranovsky and Sazdanovic 2012) Let G be a graph and (\mathcal{A}^*, δ) be a DGA. Then the chromatic complex $CHR^*(G, (\mathcal{A}^*, \delta))$ defines a bicomplex $(CHR^{**}(G, (\mathcal{A}^*, \delta)); \bar{d}, \partial)$ called the **Chromatic Bicomplex** of G with respect to (\mathcal{A}^*, δ) . The differential \bar{d} is induced by δ and differential ∂ is the chromatic differential.

Proof. First note that the i^{th} co-chain group of the Chromatic Complex, $CHR^i(G, (\mathcal{A}^*, \delta))$ is a direct sum of tensor products of (\mathcal{A}^*, δ) with itself. By Thm 5.4.1 and Def 5.4.3, this is itself a DGA $(CHR^i(G, (\mathcal{A}^*, \delta))^*, \bar{d})$ where the differential \bar{d} is induced by δ .

Therefore $CHR^*(G, (\mathcal{A}^*, \delta))^*$ is a bigraded space where one grading is given by the chromatic complex and the other is given by the total grading on direct sums of tensor powers of (\mathcal{A}^*, δ) .

For consistency of notation, we will denote the bigraded space by

$$CHR^{**}(G, (\mathcal{A}, \delta)) = CHR^*(G, (\mathcal{A}^*, \delta))^*$$

where the first $*$ is the grading on the chromatic complex and the second $*$ is the grading on each $(CHR^i(G, (\mathcal{A}^*, \delta))^*, \bar{d})$

$$CHR^{i*}(G, (\mathcal{A}, \delta)) = CHR^i(G, (\mathcal{A}^*, \delta))^*$$

$$CHR^{*j}(G, (\mathcal{A}, \delta)) = CHR^*(G, (\mathcal{A}^*, \delta))^j$$

Furthermore, we have just shown that for each i , $(CHR^{i*}(G, (\mathcal{A}, \delta)), \bar{d})$ is a DGA.

Now it remains to show that $CHR^{*j}(G, (\mathcal{A}, \delta))$ is a DGA for each j . It is enough to show that the chromatic differential preserves $CHR^{*j}(G, (\mathcal{A}, \delta))$. Recall that the total degree of a tensor product of elements of a DGA is the sum of the degrees of the factors. The chromatic

differential is a signed sum of per-edge maps. Each per-edge map is either the identity map, or multiplication both of which preserves the total degree. Therefore, the chromatic differential preserves the total degree as well.

Therefore, $(CHR^{*j}(G, (\mathcal{A}, \delta)), \partial)$ is a DGA for each j where the differential is just the chromatic differential.

Finally, it remains to be shown that the differentials \bar{d} and ∂ anti-commute. However, as shown in the following lemma, they in fact commute. This issue is resolved shortly after the lemma by the addition of a sign convention. \square

In the following lemma, it is assumed that the multiplication in the DGA (\mathcal{A}^*, δ) is super-commutative. That is, for $w \in A^k$ and $v \in A^l$ it is the case that $w \cdot v = (-1)^{kl} v \cdot w$. This assumption will require an additional sign factor in the definition of the chromatic differential. However, if the multiplication in the DGA (\mathcal{A}^*, δ) is commutative, then this sign factor may be omitted and the lemma still holds.

Lemma 6.3.2. *The differentials \bar{d} and ∂ commute.*

Proof. An element of a chain group in $CHR^{**}(G, (\mathcal{A}, \delta))$ is a direct sum of tensor products over R of elements in \mathcal{A}^* . It will be enough to check the desired properties on a basic element $\bigotimes_{n=1}^k \alpha_n$. The more general properties will then follow from the linearity of the differentials.

Recall that the chromatic differential, ∂ , is given by a signed sum of per edge maps ∂_{e^*} . Therefore, it suffices to show that \bar{d} commutes with the per-edge maps ∂_{e^*} which are given on a basis element by

$$\partial_{e^*} \left(\bigotimes_{n=1}^k \alpha_n \right) = \begin{cases} \bigotimes_{n=1}^k \alpha_n & \text{if } k_{e'} = k_e \\ s(i, j) \alpha_1 \otimes \dots \otimes \alpha_i \wedge \alpha_j \otimes \dots \hat{\alpha}_j \dots \otimes \alpha_k & \text{if } k_{e'} = k_e - 1 \end{cases}$$

$$\text{where: } s(i, j) = (-1)^{\deg(\alpha_j) \cdot \sum_{n=i+1}^{j-1} \deg(\alpha_n)}$$

where in the first case the edge being added preserves the number of connected components of the subgraph ($k_{\varepsilon'} = k_{\varepsilon}$) and thus the per edge map is the identity map. In the second case, the edge being added reduces the number of connected components by 1 by connecting the i^{th} component to the j^{th} component. The additional sign factor $s(i, j)$ is exactly the one alluded to in the preceding remarks.

Recall that the differential \bar{d} of a basic element in the formal tensor product is given by the extended Leibniz rule as follows

$$\bar{d} \left(\bigotimes_{n=1}^k \alpha_n \right) = \sum_{n=1}^k (-1)^{\sum_{m=1}^{n-1} \deg(\alpha_m)} \alpha_1 \otimes \dots \otimes \delta \alpha_n \otimes \dots \otimes \alpha_k$$

The induced differential \bar{d} clearly commutes with the per-edge map in the case that $k_{\varepsilon'} = k_{\varepsilon}$ since the per-edge map is the identity map. Consider the case in which adding the edge connects the i^{th} and j^{th} components.

First consider $\bar{d} \circ \partial_{\varepsilon^*} \left(\bigotimes_{n=1}^k \alpha_n \right)$:

$$\begin{aligned} \bar{d} \circ \partial_{\varepsilon^*} \left(\bigotimes_{n=1}^k \alpha_n \right) &= \bar{d} \left((-1)^{\deg(\alpha_j) \cdot \sum_{n=i+1}^{j-1} \deg(\alpha_n)} \alpha_1 \otimes \dots \otimes \alpha_i \wedge \alpha_j \otimes \dots \otimes \alpha_k \right) \\ &= (-1)^{\deg(\alpha_j) \cdot \sum_{n=i+1}^{j-1} \deg(\alpha_n)} \left(\sum_{n=1}^{i-1} (-1)^{\sum_{m=1}^{n-1} \deg(\alpha_m)} \alpha_1 \otimes \dots \otimes \delta \alpha_n \otimes \dots \otimes \alpha_i \wedge \alpha_j \otimes \dots \otimes \alpha_k \right. \\ &\quad + (-1)^{\sum_{m=1}^{i-1} \deg(\alpha_m)} \alpha_1 \otimes \dots \otimes \delta(\alpha_i \wedge \alpha_j) \otimes \dots \otimes \alpha_k \\ &\quad + \sum_{n=i+1}^{j-1} (-1)^{\deg(\alpha_j) + \sum_{m=1}^{n-1} \deg(\alpha_m)} \alpha_1 \otimes \dots \otimes \alpha_i \wedge \alpha_j \otimes \dots \otimes \delta \alpha_n \otimes \dots \otimes \alpha_k \\ &\quad \left. + \sum_{n=j+1}^k (-1)^{\sum_{m=1}^{n-1} \deg(\alpha_m)} \alpha_1 \otimes \dots \otimes \alpha_i \wedge \alpha_j \otimes \dots \otimes \alpha_n \otimes \dots \otimes \alpha_k \right) \end{aligned}$$

Note that the term

$$(-1)^{\sum_{m=1}^{i-1} \deg(\alpha_m)} \alpha_1 \otimes \dots \otimes \delta(\alpha_i \wedge \alpha_j) \otimes \dots \hat{\alpha}_j \dots \otimes \alpha_k$$

expands under the product rule to become

$$(-1)^{\sum_{m=1}^{i-1} \deg(\alpha_m)} \alpha_1 \otimes \dots \otimes \delta(\alpha_i) \wedge \alpha_j \otimes \dots \hat{\alpha}_j \dots \otimes \alpha_k + (-1)^{\sum_{m=1}^i \deg(\alpha_m)} \alpha_1 \otimes \dots \otimes \alpha_i \wedge \delta(\alpha_j) \otimes \dots \hat{\alpha}_j \dots \otimes \alpha_k$$

Therefore, the composition $\bar{d} \circ \partial_{\varepsilon^*} \left(\bigotimes_{n=1}^k \alpha_n \right)$ becomes

$$\begin{aligned} &= (-1)^{\deg(\alpha_j) + \sum_{n=i+1}^{j-1} \deg(\alpha_n)} \left(\sum_{n=1}^{i-1} (-1)^{\sum_{m=1}^{n-1} \deg(\alpha_m)} \alpha_1 \otimes \dots \otimes \delta \alpha_n \otimes \dots \otimes \alpha_i \wedge \alpha_j \otimes \dots \hat{\alpha}_j \dots \otimes \alpha_k \right. \\ &\quad + (-1)^{\sum_{m=1}^{i-1} \deg(\alpha_m)} \alpha_1 \otimes \dots \otimes \delta(\alpha_i) \wedge \alpha_j \otimes \dots \hat{\alpha}_j \dots \otimes \alpha_k \\ &\quad + (-1)^{\sum_{m=1}^i \deg(\alpha_m)} \alpha_1 \otimes \dots \otimes \alpha_i \wedge \delta(\alpha_j) \otimes \dots \hat{\alpha}_j \dots \otimes \alpha_k \\ &\quad + \sum_{n=i+1}^{j-1} (-1)^{\deg(\alpha_j) + \sum_{m=1}^{n-1} \deg(\alpha_m)} \alpha_1 \otimes \dots \otimes \alpha_i \wedge \alpha_j \otimes \dots \otimes \delta \alpha_n \otimes \dots \hat{\alpha}_j \dots \otimes \alpha_k \\ &\quad \left. + \sum_{n=j+1}^k (-1)^{\sum_{m=1}^{n-1} \deg(\alpha_m)} \alpha_1 \otimes \dots \otimes \alpha_i \wedge \alpha_j \otimes \dots \hat{\alpha}_j \dots \otimes \delta \alpha_n \otimes \dots \otimes \alpha_k \right) \end{aligned}$$

Now compute the composition $\partial_{\varepsilon^*} \circ \bar{d} \left(\bigotimes_{n=1}^k \alpha_n \right)$ and show it is equivalent.

$$\partial_{\varepsilon^*} \circ \bar{d} \left(\bigotimes_{n=1}^k \alpha_n \right) = \partial_{\varepsilon^*} \left(\sum_{n=1}^k (-1)^{\sum_{m=1}^{n-1} \deg(\alpha_m)} \alpha_1 \otimes \dots \otimes \delta \alpha_n \otimes \dots \otimes \alpha_k \right)$$

$$\begin{aligned}
&= (-1)^{\deg(\alpha_j) \cdot \sum_{n=i+1}^{j-1} \deg(\alpha_n)} \sum_{n=1}^{i-1} (-1)^{\sum_{m=1}^{n-1} \deg(\alpha_m)} \alpha_1 \otimes \dots \otimes \delta \alpha_n \otimes \dots \otimes \alpha_i \wedge \alpha_j \otimes \dots \hat{\alpha}_j \dots \otimes \alpha_k \\
&\quad + (-1)^{\deg(\alpha_j) \cdot \sum_{n=i+1}^{j-1} \deg(\alpha_n)} (-1)^{\sum_{m=1}^{i-1} \deg(\alpha_m)} \alpha_1 \otimes \dots \otimes \delta \alpha_i \wedge \alpha_j \otimes \dots \hat{\alpha}_j \dots \otimes \alpha_k \\
&\quad + (-1)^{\deg(\alpha_j) \cdot \left(1 + \sum_{n=i+1}^{j-1} \deg(\alpha_n)\right)} \sum_{n=i+1}^{j-1} (-1)^{\sum_{m=1}^{n-1} \deg(\alpha_m)} \alpha_1 \otimes \dots \otimes \alpha_i \wedge \alpha_j \otimes \dots \otimes \delta \alpha_n \otimes \dots \hat{\alpha}_j \dots \otimes \alpha_k \\
&\quad + (-1)^{(\deg(\alpha_j)+1) \cdot \sum_{n=i+1}^{j-1} \deg(\alpha_n)} (-1)^{\sum_{m=1}^{j-1} \deg(\alpha_m)} \alpha_1 \otimes \dots \otimes \alpha_i \wedge \delta \alpha_j \otimes \dots \hat{\alpha}_j \dots \otimes \alpha_k \\
&\quad + (-1)^{\deg(\alpha_j) \cdot \sum_{n=i+1}^{j-1} \deg(\alpha_n)} \sum_{n=j+1}^k (-1)^{\sum_{m=1}^{n-1} \deg(\alpha_m)} \alpha_1 \otimes \dots \otimes \alpha_i \wedge \alpha_j \otimes \dots \hat{\alpha}_j \dots \otimes \delta \alpha_n \otimes \dots \otimes \alpha_k \\
&= (-1)^{\deg(\alpha_j) \cdot \sum_{n=i+1}^{j-1} \deg(\alpha_n)} \left(\sum_{n=1}^{i-1} (-1)^{\sum_{m=1}^{n-1} \deg(\alpha_m)} \alpha_1 \otimes \dots \otimes \delta \alpha_n \otimes \dots \otimes \alpha_i \wedge \alpha_j \otimes \dots \hat{\alpha}_j \dots \otimes \alpha_k \right. \\
&\quad + (-1)^{\sum_{m=1}^{i-1} \deg(\alpha_m)} \alpha_1 \otimes \dots \otimes \delta \alpha_i \wedge \alpha_j \otimes \dots \hat{\alpha}_j \dots \otimes \alpha_k \\
&\quad + (-1)^{\deg(\alpha_j)} \sum_{n=i+1}^{j-1} (-1)^{\sum_{m=1}^{n-1} \deg(\alpha_m)} \alpha_1 \otimes \dots \otimes \alpha_i \wedge \alpha_j \otimes \dots \otimes \delta \alpha_n \otimes \dots \hat{\alpha}_j \dots \otimes \alpha_k \\
&\quad + (-1)^{\sum_{n=i+1}^{j-1} \deg(\alpha_n)} (-1)^{\sum_{m=1}^{j-1} \deg(\alpha_m)} \alpha_1 \otimes \dots \otimes \alpha_i \wedge \delta \alpha_j \otimes \dots \hat{\alpha}_j \dots \otimes \alpha_k \\
&\quad \left. + \sum_{n=j+1}^k (-1)^{\sum_{m=1}^{n-1} \deg(\alpha_m)} \alpha_1 \otimes \dots \otimes \alpha_i \wedge \alpha_j \otimes \dots \hat{\alpha}_j \dots \otimes \delta \alpha_n \otimes \dots \otimes \alpha_k \right)
\end{aligned}$$

Notice that the following product simplifies:

$$\begin{aligned}
&(-1)^{\sum_{n=i+1}^{j-1} \deg(\alpha_n)} (-1)^{\sum_{m=1}^{j-1} \deg(\alpha_m)} = (-1)^{\sum_{n=i+1}^{j-1} \deg(\alpha_n) + \sum_{m=1}^{j-1} \deg(\alpha_m)} \\
&= (-1)^{\sum_{n=i+1}^{j-1} \deg(\alpha_n) + \sum_{m=i+1}^{j-1} \deg(\alpha_m) + \sum_{m=1}^i \deg(\alpha_m)} \\
&= (-1)^{2 \sum_{n=i+1}^{j-1} \deg(\alpha_n) + \sum_{m=1}^i \deg(\alpha_m)} \\
&= (-1)^{\sum_{m=1}^i \deg(\alpha_m)}
\end{aligned}$$

Therefore we find the composition becomes:

$$\begin{aligned}
&= (-1)^{\deg(\alpha_j) \cdot \sum_{n=i+1}^{j-1} \deg(\alpha_n)} \left(\sum_{n=1}^{i-1} (-1)^{\sum_{m=1}^{n-1} \deg(\alpha_m)} \alpha_1 \otimes \dots \otimes \delta \alpha_n \otimes \dots \otimes \alpha_i \wedge \alpha_j \otimes \dots \hat{\alpha}_j \dots \otimes \alpha_k \right. \\
&\quad + (-1)^{\sum_{m=1}^{i-1} \deg(\alpha_m)} \alpha_1 \otimes \dots \otimes \delta \alpha_i \wedge \alpha_j \otimes \dots \hat{\alpha}_j \dots \otimes \alpha_k \\
&\quad + \sum_{n=i+1}^{j-1} (-1)^{\deg(\alpha_j) + \sum_{m=1}^{n-1} \deg(\alpha_m)} \alpha_1 \otimes \dots \otimes \alpha_i \wedge \alpha_j \otimes \dots \otimes \delta \alpha_n \otimes \dots \hat{\alpha}_j \dots \otimes \alpha_k \\
&\quad + (-1)^{\sum_{m=1}^i \deg(\alpha_m)} \alpha_1 \otimes \dots \otimes \alpha_i \wedge \delta \alpha_j \otimes \dots \hat{\alpha}_j \dots \otimes \alpha_k \\
&\quad \left. + \sum_{n=j+1}^k (-1)^{\sum_{m=1}^{n-1} \deg(\alpha_m)} \alpha_1 \otimes \dots \otimes \alpha_i \wedge \alpha_j \otimes \dots \hat{\alpha}_j \dots \otimes \delta \alpha_n \otimes \dots \otimes \alpha_k \right)
\end{aligned}$$

Comparing this to what was computed earlier, we see they are equivalent. Thus $\bar{d} \circ \partial_{\varepsilon^*} = \partial_{\varepsilon^*} \circ \bar{d}$ from which it follows that $\bar{d} \circ \partial = \partial \circ \bar{d}$. \square

In order for $CHR^{**}(G, (\mathcal{A}, \delta))$ to be a bicomplex, the differentials d and ∂ must anti-commute. The preceding lemma shows that \bar{d} and ∂ in fact commute. However, this can be fixed with the sign-trick mentioned in Thm 5.4.1. Therefore define $d = (-1)^p \bar{d}$. Then $(CHR^{**}(G, (\mathcal{A}, \delta)); d, \partial)$ is a genuine bicomplex and the proof of Thm 6.3.1 is complete.

Theorem 6.3.3. *Applying the horizontal filtration F_h^* to the chromatic bicomplex results in a spectral sequence $\{E_r^{**}, d_r\}_{r \in \mathbb{N}}$ given by*

$$E_0^{p,q} = CHR^{q,p}(G, (\mathcal{A}, \delta)) \text{ where } d_0 = \partial$$

$$E_1^{p,q} = H^{q,p}(CHR^{**}(G, (\mathcal{A}, \delta))) \text{ where } d_1 = \bar{d}$$

where

$$H^{q,p}(CHR^{**}(G, (\mathcal{A}, \delta))) = \frac{\text{Ker}(CHR^{q,p} \xrightarrow{\partial} CHR^{q,p+1})}{\text{Img}(CHR^{q,p-1} \xrightarrow{\partial} CHR^{q,p})}$$

Furthermore, the spectral sequence converges and

$$E_{\infty}^{p,q} \cong E_{assoc}^{p,q} \left(H^* \left(Tot^*(CHR^{**}), D \right), F_h^* \right)$$

Proof. The result follows directly from Thm 5.4.4. □

Theorem 6.3.4. *Applying the vertical filtration F_v^* to the chromatic bicomplex results in a spectral sequence given by*

$$E_0^{p,q} = CHR^{p,q}(G, (\mathcal{A}, \delta)) \text{ where } d_0 = \bar{d}$$

$$E_1^{p,q} = H^{p,q}(CHR^{**}(G, (\mathcal{A}, \delta))) \text{ where } d_1 = \partial$$

where

$$H^{p,q}(CHR^{**}(G, (\mathcal{A}, \delta))) = \frac{Ker(CHR^{p,q} \xrightarrow{d} CHR^{p,q+1})}{Im(CHR^{p,q-1} \xrightarrow{d} CHR^{p,q})}$$

Furthermore, the spectral sequence converges and

$$E_{\infty}^{p,q} \cong E_{assoc}^{p,q} \left(H^* \left(Tot^*(CHR^{**}), D \right), F_v^* \right)$$

Proof. The result follows directly from Thm 5.4.5. □

6.4 de Rham Cohomology in Particular

Definition 6.4.1. Let M be a smooth manifold. The *de Rham Complex* associated to M is the space of smooth differential forms on M with coefficients in \mathbb{R} along with the derivative, $(\Omega^*(M), d)$.

Note that $\Omega^*(M)$ is a DGA with a super-commutative multiplication given by the wedge product of differential forms and where $\deg(d) = +1$. Letting $\phi \in \Omega^k(M)$ and $\psi \in \Omega^l(M)$, then multiplication is given by $\phi \wedge \psi = (-1)^{kl} \psi \wedge \phi$ and the derivative acts on products by $d(\phi \wedge \psi) = d(\phi) \wedge \psi + (-1)^k \phi \wedge d(\psi)$. In fact, each grading of $\Omega^*(M)$ is an infinite dimensional real vector space.

The cohomology of the de Rham complex is denoted $H^*(M)$.

Theorem 6.4.1. *(Bott and Tu 1982) Let $(\Omega^*(M), d_M)$ and $(\Omega^*(N), d_N)$ be the de Rham complexes of smooth manifold M and N respectively. Then the following isomorphism holds*

$$H^*(\Omega^*(M) \otimes \Omega^*(N)) \xleftarrow{\cong} H^*(M) \otimes H^*(N) \xleftarrow{\cong} H^*(M \times N)$$

Proof. This is a standard result of the Kunneth isomorphism in the context of de Rham cohomology. However, it will be useful later to be familiar with the details of the map chain map $K : \Omega^*(M) \otimes \Omega^*(N) \rightarrow \Omega^*(M \times N)$ which realizes the isomorphism $H^*(M) \otimes H^*(N) \cong H^*(M \times N)$. It is described in the following.

Consider the product manifold $M \times N$. There are natural projection maps from $M \times N$ onto the first and second factors which induce maps on the de Rham complexes as follows

$$\begin{array}{ccc} M \times N & \xrightarrow{\pi_2} & N \\ \pi_1 \downarrow & & \uparrow \pi_1^* \\ M & & \Omega^*(M) \end{array} \quad \begin{array}{ccc} \Omega^*(M \times N) & \xleftarrow{\pi_2^*} & \Omega^*(N) \\ & & \uparrow \pi_1^* \\ & & \Omega^*(M) \end{array}$$

Then the map $K : \Omega^*(M) \otimes \Omega^*(N) \rightarrow \Omega^*(M \times N)$ is given by

$$w \otimes v \mapsto \pi_1^*(w) \wedge \pi_2^*(v)$$

This map is clearly a well defined chain map since pullbacks commute with the derivative

which also obeys a product rule over wedge products.

The claim that it is an isomorphism on the level of cohomology is omitted here as it is a standard result and quite technical. The reader is referred to Bott and Tu (1982) for details in the de Rham cohomology setting specifically and Hatcher (2001) more generally. \square

Theorem 6.4.2. *Let M and N be smooth manifolds. Then there is an isomorphism*

$$\Omega^*(M \sqcup N) \cong \Omega^*(M) \oplus \Omega^*(N)$$

which induces the following isomorphism

$$H^*(\Omega^*(M \sqcup N)) \cong H^*(\Omega^*(M) \oplus \Omega^*(N)) \cong H^*(M) \oplus H^*(N)$$

Proof. The isomorphisms are induced via pullbacks of the inclusions

$$\begin{array}{ccc} M \sqcup N & \xleftarrow{i_2} & N \\ i_1 \uparrow & & \\ M & & \end{array} \quad \begin{array}{ccc} \Omega^*(M \sqcup N) & \xrightarrow{i_2^*} & \Omega^*(N) \\ i_1^* \downarrow & & \\ \Omega^*(M) & & \end{array}$$

$$\Omega^*(M \sqcup N) \xleftarrow{I^*} \Omega^*(M) \oplus \Omega^*(N)$$

For $(w, v) \in \Omega^*(M) \oplus \Omega^*(N)$, $(w, v) \mapsto w + v \in \Omega^*(M \sqcup N)$. Since $M \sqcup N$ is a disjoint union, every element of $\Omega^*(M \sqcup N)$ is uniquely written as $w + v$ for $w \in \Omega^*(M)$ and $v \in \Omega^*(N)$. \square

Theorem 6.4.3. *Let G be a graph and (Ω^*, d) the de Rham complex of a smooth manifold. Applying the horizontal filtration F_h^* to the chromatic bicomplex*

$$(CHR^{**}(G, (\Omega, d)); d, \partial)$$

results in a spectral sequence $\{E_r^{**}, d_r\}_{r \in \mathbb{N}}$ given by

$$E_0^{p,q} = CHR^{q,p}(G, (\Omega^*, d)) \text{ where } d_0 = \partial$$

$$E_1^{p,q} = H^{q,p}(CHR^{**}(G, (\Omega^*, d))) \text{ where } d_1 = \bar{d}$$

where

$$H^{q,p}(CHR^{**}(G, (\Omega^*, d))) = \frac{\text{Ker}(CHR^{q,p} \xrightarrow{\partial} CHR^{q,p+1})}{\text{Img}(CHR^{q,p-1} \xrightarrow{\partial} CHR^{q,p})}$$

Furthermore, the spectral sequence converges and

$$E_\infty^{p,q} \cong E_{assoc}^{p,q} \left(H^*(\text{Tot}^*(CHR^{**}), D), F_h^* \right)$$

Proof. The result follow directly from Thm 5.4.4. □

Theorem 6.4.4. Let G be a graph and (Ω^*, d) the de Rham complex of a smooth manifold.

Applying the vertical filtration F_v^* to the chromatic bicomplex

$$(CHR^{**}(G, (\Omega, d)); d, \partial)$$

results in a spectral sequence $\{E_r^{**}, d_r\}_{r \in \mathbb{N}}$ given by

$$E_0^{p,q} = CHR^{p,q}(G, (\Omega^*, d)) \text{ where } d_0 = \bar{d}$$

$$E_1^{p,q} = CHR^{p,q}(G, H^*) \text{ where } d_1 = \partial$$

Furthermore, the spectral sequence converges and

$$E_\infty^{p,q} \cong E_{assoc}^{p,q} \left(H^*(\text{Tot}^*(CHR^{**}(G, (\Omega, d))), D), F_v^* \right)$$

Proof. The existence of the spectral sequence itself, the claim concerning the first page and its differential, as well as the convergence claim all follow directly from Thm 5.4.5. It remains to show that $E_1^{p,q} = CHR^{p,q}(G, H^*)$ where $d_1 = \partial$.

Recall from Thm 5.4.5 that $E_1^{**} = H^{p,q}(CHR^{**}(G, (\Omega^*, d)))$ where

$$H^{p,q}(CHR^{**}(G, (\Omega^*, d))) = \frac{\text{Ker}(CHR^{p,q} \xrightarrow{d} CHR^{p,q+1})}{\text{Img}(CHR^{p,q-1} \xrightarrow{d} CHR^{p,q})}$$

Therefore, by definition, to obtain $E_1^{p,q}$ from $E_0^{p,q}$ the de Rham cohomology of

$$CHR^{p*}(G, (\Omega_c^*, d))$$

is computed for each p considered as a DGA.

However, for each p , $CHR^{p*}(G, (\Omega^*, d))$ is the direct sum of tensor products of Ω^* with itself. By Thm 6.4.1 and Thm 6.4.2 the cohomology is isomorphic to the same direct sum of tensor products of H^* with itself. Therefore letting $\mathcal{A}^* = \Omega^*$ on the first page and computing the second page from the first is equivalent to letting $\mathcal{A}^* = H^*$ on the first page. \square

CHAPTER

7

MANIFOLDS AND SIMPLICIES

7.1 Simplicial Manifolds

Definition 7.1.1. A *Simplicial Space* is a sequence of topological spaces

$\mathbf{X} = \{X_n\}_{n=0}^{\infty}$ equipped with continuous maps

$$\partial_{n-1}^i : X_n \rightarrow X_{n-1} \quad \text{and} \quad \delta_{n+1}^i : X_n \rightarrow X_{n+1}$$

for each $0 \leq i \leq n$ which obey the following face and degeneracy map relations

$$\left\{ \begin{array}{ll} \partial_{n-1}^i \circ \partial_n^j = \partial_{n-1}^{j-1} \circ \partial_n^i & , \quad i < j \\ \delta_{n+1}^i \circ \delta_n^j = \delta_{n+1}^{j+1} \circ \delta_n^i & , \quad i \leq j \\ \partial_{n+1}^j \circ \delta_n^j = \partial_{n+1}^{j+1} \circ \delta_n^j = Id_n & , \quad \text{for all } j \\ \partial_{n+1}^i \circ \delta_n^j = \delta_{n-1}^{j-1} \circ \partial_n^i & , \quad i < j \\ \partial_{n+1}^i \circ \delta_n^j = \delta_{n-1}^j \circ \partial_n^{i-1} & , \quad i > j+1 \end{array} \right\}$$

For brevity, a *simplicial manifold* will refer to a simplicial space where the topological spaces are smooth manifolds and where the face and degeneracy maps are smooth maps.

Definition 7.1.2. (The Nerve Construction)

Let M be a manifold and $\{U_i\}_{i \in A}$ be an open cover of M . For $I = (i_1, \dots, i_k)$ a sequence of integers $i_1 \leq \dots \leq i_k$ in A , define $l(I) = k$ as the length of I and $U_I = U_{i_1} \cap \dots \cap U_{i_k}$ when the intersection is non-empty.

Now let $N_n = \bigsqcup_{l(I)=n+1} U_I$, so that $N_0 = \bigsqcup_i U_i$ is the disjoint union of the elements of $\{U_i\}_{i \in A}$, $N_1 = \bigsqcup_{l(I)=2} U_i \cap U_j$ is the disjoint union of all non-empty pair-wise intersections of sequential elements ($i \leq j$) of $\{U_i\}_{i \in A}$, ect.

Then $\mathbf{N} = \{N_n\}_{n=0}^\infty$ is a simplicial manifold with induced face and degeneracy maps given by inclusions and repetitions. The face and degeneracy maps between N_0 and N_1 are given by

$$\partial_0^0 : U_i \cap U_j \rightarrow U_j, \partial_0^1 : U_i \cap U_j \rightarrow U_i, \delta_0^0 : U_i \rightarrow U_i \cap U_i$$

The simplicial manifold \mathbf{N} is called the *Nerve* of the open cover $\{U_i\}_{i \in A}$ of M .

Theorem 7.1.1. (The Nerve Theorem, Borsuk (1948))

Let M be a manifold and $\{U_i\}_{i \in A}$ be an enumerable open cover of M . If for any non-empty subsets of the open cover $\{U_{i_k}\} \subseteq \{U_i\}_{i \in A}$ it is the case that $\bigcap_k U_{i_k}$ is either empty or contractible, then the geometric realization of the nerve of $\{U_i\}_{i \in A}$, $\|\mathbf{N}\|$ is homotopy equivalent to M .

For more details on simplicial objects and how they induce (co)homological structures, see Section 2.1.

7.2 The Simplicial Bicomplex

Definition 7.2.1. (Eastwood and Hugget 2007) Let G be a graph and M be a smooth manifold. The *Graph Configuration Space* M_G of M with respect to G is given as follows.

For $|V(G)| = n$, denote the n -fold Cartesian product of M with itself by $M^n = M^{\times n}$. Then each factor of M in M^n corresponds to a vertex in $V(G)$. Each $e \in E(G)$ consists of two vertices in $V(G)$, $e = \{v_i, v_j\}$. Therefore for each $e \in E(G)$ defines a subspace of M^n as follows

$$D_e = \{(m_1, \dots, m_n) \in M^n \mid m_i = m_j \text{ where } e = \{v_i, v_j\}\}$$

Now let $D_{E(G)} = \bigcup_{e \in E(G)} D_e$ and define $M_G = M^n \setminus D_{E(G)}$.

Lemma 7.2.1. (Bendersky and Gitler 1991) Let G be a graph, M be a smooth manifold. There is a bicomplex called the **Simplicial Bicomplex** $(SIM^{**}(G, M); d, \partial)$ associated to $D_{E(G)} \subset M^n$ arising from the nerve construction Ex 7.1.2 and the de Rham complex.

Proof. Let G be a graph and M a smooth manifold. Suppose $|V(G)| = n$ and the $E(G)$ has a total order and consider the topological subspace $D_{E(G)} \subset M^n$. Since the collection of sub-diagonals $\{D_e\}_{e \in E(G)}$ is an open cover of $D_{E(G)}$, it has an associated simplicial space given by its nerve with respect $\{D_e\}_{e \in E(G)}$.

Namely, for $S \subseteq E(G)$, define $\bar{D}_S = \bigcap_{e \in S} D_e$. Then following the procedure in Ex 7.1.2, for each j ,

$$N_j = \bigsqcup_{|S|=j+1} \bar{D}_S$$

Furthermore, it is clear that for each $S \subset E(G)$, $\bar{D}_S \cong M^{r(S)}$ for some function $r(S)$. For

example, when S is a singleton set $S = \{e\}$, then $\bar{D}_S = D_e \cong M^{n-1}$.

The function $r(S)$ is the number of connected components of the subgraph G_S . Recalling notation from Sec 6.2, $G_S = G_e$ and $k_S = k_e$, it is the case that

$$N_j \equiv \bigsqcup_{|S|=j+1} \bar{D}_S = \bigsqcup_{|\varepsilon|=j+1} M^{k_\varepsilon}$$

Therefore the nerve $\mathbf{N} = \{V_j\}_{j=0}^\infty$ is in fact a simplicial manifold.

Since N_j is a smooth manifold for each j , consider the de Rham complex for each j , $\Omega^*(N_j)$. Since the de Rham complex is a contravariant functor, the simplicial face maps $\partial_{j-1}^i : N_j \rightarrow N_{j-1}$ induce maps on the de Rham complexes $\partial_j^i : \Omega^*(N_j) \rightarrow \Omega^*(N_{j+1})$. Appropriately signed sums of the induced maps produce the usual simplicial differentials $\partial_j : \Omega^*(N_j) \rightarrow \Omega^*(N_{j+1})$.

Lastly, note that since $D_{E(G)} \subset M^n$, the simplicial structure can be augmented by defining $N_{-1} = M^n$ and a differential $\partial_{-1} : \Omega^*(N_{-1}) \rightarrow \Omega^*(N_0)$ which is the signed sum of pullbacks of the inclusions $i_e : D_e \rightarrow M^n$.

Now define

$$SIM^{p,q}(G, M) = \Omega^q(N_p)$$

by construction, it is clear that for each p and q , $SIM^{p,*}(G, M) = \Omega^*(N_p)$ and $SIM^{*,q}(G, M) = \Omega^q(N_*)$ are DGAs with differentials given by the derivative d and simplicial map ∂ respectively. Lastly, because the de Rham complex is functorial, the differentials d and ∂ commute. Applying the sign trick guarantees that they anti-commute. \square

Note that the simplicial bicomplex $SIM^{**}(G, M)$ is not entirely contained in the second quadrant ($p, q \geq 0$) because it incorporates the augmentation $N_{-1} = M^n$ so that $SIM^{-1,*}(G, M) = \Omega^*(N_{-1}) = \Omega^*(M^n)$. To facilitate later exposition it is helpful to rectify this with a degree shift of $+1$ in the simplicial grading.

Now, the induced face maps ∂_j^i (of which the simplicial differential ∂_j is a signed sum) are pullbacks under inclusions of sub-diagonals considered as intersections of higher dimensional sub-diagonals.

Example 7.2.1. Suppose the graph G consisted of three vertices $V(G) = \{v_1, v_2, v_3\}$ and two edges $E(G) = \{e_1 = \{v_1, v_2\}, e_2 = \{v_2, v_3\}\}$.

Then $N_0 = M^3$, $N_1 = D_{e_1} \sqcup D_{e_2}$, and $N_2 = D_{e_1} \cap D_{e_2}$ where

$$D_{e_1} = \{(m_1, m_1, m_3) \in M^3\} \cong M^2$$

$$D_{e_2} = \{(m_1, m_2, m_2) \in M^3\} \cong M^2$$

$$D_{e_1} \cap D_{e_2} = \{(m_1, m_1, m_1) \in M^3\} \cong M$$

Then the two simplicial face maps are given by the inclusion of subspaces as diagonals

$$\partial_1^0 \equiv i_{D_0} : D_{e_1} \cap D_{e_2} \rightarrow D_{e_2}, \partial_1^1 \equiv i_{D_1} : D_{e_1} \cap D_{e_2} \rightarrow D_{e_1}$$

Then the induced maps, after applying the de Rham complex, are pullbacks under these inclusions of subdiagonals.

In order to more easily recall the nature of the simplicial differential in this case, we will equivalently denote $\partial \equiv D^*$ whenever convenient.

Theorem 7.2.2. *Let G be a graph and M be a smooth manifold. Applying the horizontal filtration F_h^* to the simplicial bicomplex*

$$(SIM^{**}(G, M); d, \partial)$$

*results in a spectral sequence $\{E_r^{**} d_r\}_{r \in \mathbb{N}}$ given by*

$$E_0^{p,q} = SIM^{q,p}(G, M) \text{ where } d_0 = \partial$$

$$E_1^{p,q} = H^{q,p}(SIM^{**}(G, M)) \text{ where } d_1 = \bar{d}$$

where

$$H^{q,p}(SIM^{**}(G, M)) = \frac{Ker(SIM^{q,p} \xrightarrow{\partial} SIM^{q,p+1})}{Img(SIM^{q,p-1} \xrightarrow{\partial} SIM^{q,p})}$$

Furthermore, the spectral sequence converges and

$$E_\infty^{p,q} \cong E_{assoc}^{p,q} \left(H^* \left(Tot^*(SIM^{**}(G, M)), D \right), F_h^* \right)$$

$$\begin{aligned} Tot_\infty^*(E_\infty^{**}) &\cong H^* \left(Tot^*(SIM^{**}(G, M)), D \right) \\ &\cong H^*(M^n, D_{E(G)}) \end{aligned}$$

Proof. The existence and claims concerning the first and second pages follow directly from Thm 5.4.4. The additional claim about convergence follows from the fact that this is an Anderson Spectral Sequence (Anderson 1972).

In short, the geometric realization of the simplicial space $\|\mathbf{V}\|$ is weakly equivalent to the pair $(M, D_{E(G)})$, so the spectral sequence converges to the relative cohomology, $H^*(M^n, D_{E(G)})$. □

Theorem 7.2.3. *Let G be a graph and M be a smooth manifold. Applying the vertical filtration F_v^* to the simplicial bicomplex*

$$(SIM^{**}(G, M); d, \partial)$$

*results in a spectral sequence $\{E_r^{**}, d_r\}_{r \in \mathbb{N}}$ given by*

$$E_0^{p,q} = SIM^{p,q}(G, M) \text{ where } d_0 = \bar{d}$$

$$E_1^{p,q} = H^{p,q}(SIM^{**}(G, M)) \text{ where } d_1 = \partial$$

where

$$H^{p,q}(SIM^{**}(G, M)) = \frac{\text{Ker}(SIM^{p,q} \xrightarrow{\bar{d}} SIM^{p+1,q})}{\text{Img}(SIM^{p-1,q} \xrightarrow{\bar{d}} SIM^{p,q})}$$

Furthermore, the spectral sequence converges and

$$E_\infty^{p,q} \cong E_{assoc}^{p,q} \left(H^* \left(\text{Tot}^*(SIM^{**}(G, M)), D \right), F_v^* \right)$$

$$\begin{aligned} \text{Tot}_\infty^*(E_\infty^{**}) &\cong H^* \left(\text{Tot}^*(SIM^{**}(G, M)), D \right) \\ &\cong H^*(M^n, D_{E(G)}) \end{aligned}$$

Proof. Same as in the previous theorem, the existence and claims concerning the first and second pages follow directly from Thm 5.4.5. The additional claim about convergence follows from the fact that this is an Anderson Spectral Sequence (Anderson 1972).

In short, the geometric realization of the simplicial space $\|\mathbf{V}\|$ is weakly equivalent to the pair $(M, D_{E(G)})$, so the spectral sequence converges to the relative cohomology, $H^*(M^n, D_{E(G)})$. □

Lemma 7.2.4. (*Eastwood and Hugget 2007*) Let G be a graph and M be a compact orientable smooth manifold of dimension m . Then the following isomorphism holds

$$H^*(M^n, D_{E(G)}) \cong H_{mn-*}(M_G)$$

Proof. By Lefschetz Duality, if A is a compact, locally contractible subspace of a closed orientable n -manifold X , then for all i ,

$$H_i(X, X \setminus A; \mathbb{Z}) \cong H^{n-i}(A; \mathbb{Z})$$

Letting $A = M_G \equiv M^{\times n} \setminus D_{E(G)}$ and $X = M^{\times n}$ and $X = M^{\times n}$. Then $X \setminus A = M^{\times n} \setminus (M^{\times n} \setminus D_{E(G)}) = D_{E(G)}$, and thus $H^*(M^{\times n}, D_{E(G)}; \mathbb{R}) \cong H_{mn-*}(M_G; \mathbb{R})$. \square

The requirement that M be compact can be relaxed if the deRham complex is restricted to the sub-complex of compactly supported forms called the *compactly supported de Rham complex*, $\Omega_c^*(M)$. This is because the compactness requirements of the Lefschetz duality theorem can be relaxed by restricting to compact supports.

CHAPTER

8

SIMPLICIAL AND CHROMATIC RELATIONS

8.1 A Morphism of Bicomplexes

Recall from Ex 7.2.1, that we equivalently denote $\partial \equiv D^*$ in the simplicial bicomplex. We will do so in the following theorem to avoid confusion with the chromatic differential. There is no threat from confusing the differential d in the two bicomplexes as they are indeed the same smooth derivative albeit induced slightly differently in the different contexts although not in anyways that matter significantly as will be shown.

Theorem 8.1.1. *Given a graph G and smooth manifold M , there exists a map from the chromatic bicomplex to the simplicial bicomplex*

$$\psi : (CHR^{**}(G, (\Omega, d)); d, \partial) \rightarrow (SIM^{**}(G, M); d, D^*)$$

Proof. Let G be a graph and M be a manifold and recall from Thm 6.4.1 and Lemma 6.4.2 that there are maps

$$\Omega^*(M) \otimes \Omega^*(M) \xrightarrow{K} \Omega^*(M \times M)$$

$$\Omega^*(M) \oplus \Omega^*(M) \xleftarrow{I^*} \Omega^*(M \sqcup M)$$

By definition $CHR^{i,*}$ is the direct sum of tensor powers of $\Omega^*(M)$ corresponding to connected components of all subgraphs G_ε in the i^{th} state. Furthermore, recall that the subgraphs are ordered by their least vertex. Suppose that there are n subgraphs in the i^{th} state and denote the number of connected components of the j^{th} subgraph in the i^{th} state by k_{ε_j} .

Now recall that $SIM^{i,*}$ is the de Rham complex of a disjoint union of cartesian powers of M with itself. Each term in the disjoint union corresponds to a subgraph in the i^{th} state and the cartesian power of a given term is the number of connected components of the corresponding subgraph.

We can therefore generically write

$$CHR^{i,*} = \bigoplus_{j=1}^n (\Omega^*(M)^{\otimes k_{\varepsilon_j}}) \xrightarrow{K} \bigoplus_{j=1}^n (\Omega^*(M^{k_{\varepsilon_j}})) \xleftarrow{I^*} \Omega^*\left(\bigsqcup_{j=1}^n M^{k_{\varepsilon_j}}\right) = SIM^{i,*}$$

To demonstrated that this is a morphism of bicomplexes, it remains to show that K and I^* commute with the differentials. In the case of the derivatives d , K and I^* were shown to be de Rham chain maps in Thm 6.4.1 in such a way that they naturally take the derivative d

on CHR^{**} to the derivative d on SIM^{**} .

Therefore it remains to show that K and s commute with the chromatic differential ∂ . However, recall that ∂ is a signed sum of per-edge maps. Therefore, it is sufficient to demonstrate that K commutes with per-edge maps. Furthermore, each per-edge map is either identity or the wedge product. Since everything commutes with identity, the problem reduces to showing K commutes with wedge products.

Now, the wedge product $\mathcal{A}^* \otimes \mathcal{A}^* \xrightarrow{\wedge} \mathcal{A}^*$ is formally defined as the image of the alternation map from the formal tensor product to its exterior algebra. However, for the de Rham complex of a manifold the wedge product can be equivalently defined by the composition

$$\wedge = D^* \circ K : \Omega^*(M) \otimes \Omega^*(M) \rightarrow \Omega^*(M)$$

where D^* is the pullback under the diagonal embedding $D : M \rightarrow M \times M$. That is to say that it is defined as the map which makes the following diagram commute

$$\begin{array}{ccc} \Omega^*(M) \otimes \Omega^*(M) & \xrightarrow{K} & \Omega^*(M \times M) \\ & \searrow \wedge \quad \swarrow D^* & \\ & \Omega^*(M) & \end{array}$$

Recall that $K = \pi_1^* \wedge \pi_2^*$ was define in Thm 6.4.1. So it seems that this definition is circular in that it is definining the wedge product in terms of a map K which is itself defined in terms of the wedge product. However, this is resolved by defining the wedge product in the definition $K = \pi_1^* \wedge \pi_2^*$ as formal wedge product (thought of as the image of the alternation map) and then taking the above diagram to define the per-edge maps which are simply inconveniently labeled by the same symbol.

With this definition of the per-edge maps, K commutes with them by definition. Furthermore, the diagram also includes the diagonal pullback maps in such a way that it is

clear that K takes ∂ to D^* as needed. □

Theorem 8.1.2. *(Baranovsky and Sazdanovic 2012) Given a graph G and a smooth manifold M . The spectral sequences arising from the vertical filtrations of the chromatic and simplicial bicomplexes are isomorphic on their 1^{st} -pages, $E_1^{**}(CHR, F_v) \cong E_1^{**}(SIM, F_v)$.*

Proof. By Thm 8.1.1, the map between the chromatic and simplicial bicomplexes $\psi = I^* \circ K$ induces a map ψ^* on the 1^{st} -pages of the spectral sequences because it commutes with the differentials.

By Thm 6.4.1 and Thm 6.4.2, the maps K and I^* induce isomorphisms on cohomology when computed with respect to the de Rham differential. Under the vertical filtration, cohomology is computed with respect to the de Rham differential in order to obtain the 1^{st} -page from the 0^{th} -page. Therefore, $\psi^* : E_1^{**}(CHR, F_v) \rightarrow E_1^{**}(SIM, F_v)$ is an isomorphism which takes direct sums of tensor powers of $H^*(M)$ to the de Rham cohomology of the disjoint unions of Cartesian powers of M . □

Corollary 8.1.2.1. *(Baranovsky and Sazdanovic 2012) Given a graph G and a smooth manifold M , the spectral sequences arising from the vertical filtrations of the chromatic and simplicial bicomplexes converge to $H^*(M^n, D_{E(G)}) \cong H_{mn-*}(M_G)$.*

Conjecture 8.1.1. *Given a graph G and a smooth manifold M , the spectral sequences arising from the horizontal filtrations of the chromatic and simplicial bicomplexes are isomorphic on their 2^{nd} -pages $E_2^{**}(CHR, F_h) \cong E_2^{**}(SIM, F_h)$.*

It is clear that the E_1 pages of the spectral sequences arising from the horizontal filtrations of the bicomplexes will in general not be isomorphic. However, they have the same limit. Therefore, it is an open question as to under what circumstances they become isomorphic (if any) before the limit is achieved. The conjecture that they are isomorphic on and after their E_2 pages is based on the fact that the reduction from infinitely generated

algebras to finitely generated algebras occurs after cohomology has been computed with respect to the deRham differential. In the case of the horizontal filtration, this would be on the E_2 page. In conjunction with the commutativity of the differentials in the underlying bicomplexes, this hints that an isomorphism is likely on their E_2 pages.

8.2 An Example Vertical Filtration Computation

In the following, let G be the two-vertex one-edge graph, $M = \mathbb{R}^1$, and $\Omega_c^*(M)$ be the de Rham complex of compactly supported differential forms on M with coefficients in \mathbb{R} .

Then the chromatic complex is given by

Example 8.2.1. $G = \bullet \text{---} \bullet$

$$0 \longrightarrow \begin{array}{c} i=0 \\ \boxed{\begin{array}{c} \bullet \\ \bullet \end{array}} \xrightarrow{\partial_*^0} \begin{array}{c} i=1 \\ \boxed{\begin{array}{c} \bullet \\ \text{---} \\ \bullet \end{array}} \longrightarrow 0 \end{array}$$

$$0 \longrightarrow \Omega_c^*(M) \otimes \Omega_c^*(M) \xrightarrow{\partial^0} \Omega_c^*(M) \longrightarrow 0$$

Where:

$$\partial^0(\alpha \otimes \beta) = \alpha \wedge \beta$$

The de Rham complex can be written more explicitly as follows

$$\Omega_c^*(M) = \Omega_c^0(M) \oplus \Omega_c^1(M)$$

$$\Omega_c^*(M) \otimes \Omega_c^*(M) = \left(\Omega_c^0(M) \otimes \Omega_c^0(M) \right) \oplus \left(\begin{array}{c} \Omega_c^0(M) \otimes \Omega_c^1(M) \\ \oplus \\ \Omega_c^1(M) \otimes \Omega_c^0(M) \end{array} \right) \oplus \left(\Omega_c^1(M) \otimes \Omega_c^1(M) \right)$$

The chromatic bicomplex is formed by substituting in the above expansions of $\Omega_c^*(M)$ and $\Omega_c^*(M) \otimes \Omega_c^*(M)$ in the chromatic complex with the smooth differentials. Note that by Thm 6.3.4 this is also the 0^{th} -page of the spectral sequence arising from the vertical filtration.

Example 8.2.2. $CHR^{**}(G, (\Omega_c, d)) = E_0^{**}(CHR, F_v)$

where $G = \mathbf{I}$ & $M = \mathbb{R}^1$

$$\begin{array}{ccccccc}
 & & 0 & & 0 & & \\
 & & \uparrow & & \uparrow & & \\
 0 & \longrightarrow & \Omega_c^1(M) \otimes \Omega_c^1(M) & \xrightarrow{\partial} & 0 & \longrightarrow & 0 \\
 & & \bar{d} \uparrow & & \bar{d} \uparrow & & \\
 0 & \longrightarrow & \begin{array}{c} \Omega_c^0(M) \otimes \Omega_c^1(M) \\ \oplus \\ \Omega_c^1(M) \otimes \Omega_c^0(M) \end{array} & \xrightarrow{\partial} & \Omega_c^1(M) & \longrightarrow & 0 \\
 & & \bar{d} \uparrow & & \bar{d} \uparrow & & \\
 0 & \longrightarrow & \Omega_c^0(M) \otimes \Omega_c^0(M) & \xrightarrow{\partial} & \Omega_c^0(M) & \longrightarrow & 0 \\
 & & \uparrow & & \uparrow & & \\
 & & 0 & & 0 & &
 \end{array}$$

Similarly the simplicial bicomplex is given by the following. Again, note that by Thm 7.2.3 the simplicial bicomplex is the 0^{th} -page of the spectral sequence arising from the vertical filtration.

Example 8.2.3. $SIM^{**}(G, M) = E_0^{**}(SIM, F_v)$

where $G = \mathbb{I}$ & $M = \mathbb{R}^1$

$$\begin{array}{ccccccc}
 & & 0 & & 0 & & \\
 & & \uparrow & & \uparrow & & \\
 0 & \longrightarrow & \Omega_c^2(M \times M) & \xrightarrow{\partial} & 0 & \longrightarrow & 0 \\
 & & \bar{d} \uparrow & & \bar{d} \uparrow & & \\
 0 & \longrightarrow & \Omega_c^1(M \times M) & \xrightarrow{\partial} & \Omega_c^1(M) & \longrightarrow & 0 \\
 & & \bar{d} \uparrow & & \bar{d} \uparrow & & \\
 0 & \longrightarrow & \Omega_c^0(M \times M) & \xrightarrow{\partial} & \Omega_c^0(M) & \longrightarrow & 0 \\
 & & \uparrow & & \uparrow & & \\
 & & 0 & & 0 & &
 \end{array}$$

Now, the spectral sequences arising from the vertical filtrations can be computed and their convergence results verified. By Thm 8.1.2, the spectral sequences are isomorphic on their 1^{st} -pages. It is therefore enough to compute one of them.

Consider $E_0^{**}(SIM, F_v)$. Computing the 1^{st} -page from the 0^{th} page is equivalent to computing the de Rham cohomology of each column. Since the compactly supported de Rham cohomologies of $M = \mathbb{R}^1$ and $M \times M \cong \mathbb{R}^2$ are known (Lee 2013), the 1^{st} -pages of the spectral sequences arising from the vertical filtrations are given by the following.

Example 8.2.4. $E_1^{**}(SIM, F_\nu) \cong E_1^{**}(CHR, F_\nu)$

where $G = \mathbf{I}$ & $M = \mathbb{R}^1$

$$\begin{array}{ccccc}
 & 0 & & 0 & \\
 & \uparrow & & \uparrow & \\
 0 \longrightarrow & H_c^2(M \times M) & \xrightarrow{\partial} & 0 & \longrightarrow 0 \\
 & \uparrow & & \uparrow & \\
 0 \longrightarrow & H_c^1(M \times M) & \xrightarrow{\partial} & H_c^1(M) & \longrightarrow 0 \\
 & \uparrow & & \uparrow & \\
 0 \longrightarrow & H_c^0(M \times M) & \xrightarrow{\partial} & H_c^0(M) & \longrightarrow 0 \\
 & \uparrow & & \uparrow & \\
 & 0 & & 0 &
 \end{array}
 \quad
 \begin{array}{ccccc}
 & 0 & & 0 & \\
 & \uparrow & & \uparrow & \\
 0 \longrightarrow & \mathbb{R} & \xrightarrow{\partial} & 0 & \longrightarrow 0 \\
 & \uparrow & & \uparrow & \\
 0 \longrightarrow & 0 & \xrightarrow{\partial} & \mathbb{R} & \longrightarrow 0 \\
 & \uparrow & & \uparrow & \\
 0 \longrightarrow & 0 & \xrightarrow{\partial} & 0 & \longrightarrow 0 \\
 & \uparrow & & \uparrow & \\
 & 0 & & 0 &
 \end{array}$$

In this case the spectral sequence collapses on the 1^{st} -page. The ∞ -total complex is therefore equal to the 1^{st} -total complex and is given by

$$Tot_\infty^2 = \mathbb{R} \oplus \mathbb{R}, Tot_\infty^n = 0 \text{ else}$$

In this example $M^n \setminus D_{E(G)}$ is just \mathbb{R}^2 set-minus the diagonal. Therefore the singular homology of $M^n \setminus D_{E(G)}$ is readily apparent and given by

$$H_0 = \mathbb{R} \oplus \mathbb{R}, H_n = 0 \text{ else}$$

Therefore, $Tot_\infty^* \cong H_{mn-*}(M^n \setminus D_{E(G)})$ exactly in accordance with Thm 7.2.2 and Thm 7.2.4.

8.3 Functoriality in the Bicomplexes

Both the chromatic and simplicial bicomplexes are constructions that takes two inputs, a graph G and a smooth manifold M . They output bicomplexes, $(CHR^{**}(G, (\Omega, d)); d, \partial)$ and $(SIM^{**}(G, M); d, D^*)$ respectively. A natural question (pun intended) is whether or not these constructions are functorial in any sense. That is, which morphisms (if any) of graphs and smooth manifolds induce maps between their associated bicomplexes? Addressing this question is subject of this section.

8.3.1 Functoriality in the Manifold

Let's start with a discussion of the functoriality of the chromatic bicomplex with respect to smooth manifolds. Since the chromatic bicomplex arises from the chromatic complex (which takes a graph G and a graded R -algebra \mathcal{A}^*), it makes sense to begin by establishing the functoriality of the chromatic complex with respect to the input algebra.

Theorem 8.3.1. *Let G be a graph, \mathcal{A}^* and \mathcal{B}^* be graded R -algebras, and $\phi : \mathcal{A}^* \rightarrow \mathcal{B}^*$ be a graded R -algebra morphism. Then there is an induced morphism $\phi^* : CHR^*(G, \mathcal{A}) \rightarrow CHR^*(G, \mathcal{B})$ which in turn induces a map on chromatic cohomology, $\phi^* : H_{CHR}^*(G, \mathcal{A}) \rightarrow H_{CHR}^*(G, \mathcal{B})$.*

Proof. First, the induced map $\phi^* : CHR^*(G, \mathcal{A}) \rightarrow CHR^*(G, \mathcal{B})$ is given as follows. By definition $CHR^i(G, \mathcal{A})$ is the direct sum of tensor powers of \mathcal{A}^* corresponding to connected components of all subgraphs G_ϵ in the i^{th} state. Furthermore, recall that the subgraphs are ordered by their least vertex. Suppose that there are n subgraphs in the i^{th} state and denote the number of connected components of the j^{th} subgraph in the i^{th} state by k_{ϵ_j} .

Then $CHR^i(G, \mathcal{A})$ and $CHR^i(G, \mathcal{B})$ can be written as follows.

$$CHR^i(G, \mathcal{A}) = \bigoplus_{j=1}^n ((\mathcal{A}^*)^{\otimes k_{\varepsilon_j}}) \quad \text{and} \quad CHR^i(G, \mathcal{B}) = \bigoplus_{j=1}^n ((\mathcal{B}^*)^{\otimes k_{\varepsilon_j}})$$

Then the induced map $\phi_i^* : CHR^i(G, \mathcal{A}) \rightarrow CHR^i(G, \mathcal{B})$ is just the corresponding direct sum of tensor powers of ϕ .

$$\phi_i^* : CHR^i(G, \mathcal{A}) \rightarrow CHR^i(G, \mathcal{B})$$

$$\bigoplus_{j=1}^n (\phi^{\otimes k_{\varepsilon_j}}) : \bigoplus_{j=1}^n ((\mathcal{A}^*)^{\otimes k_{\varepsilon_j}}) \rightarrow \bigoplus_{j=1}^n ((\mathcal{B}^*)^{\otimes k_{\varepsilon_j}})$$

Now, to show that this also induces a map on chromatic cohomology, it is enough to show that it commutes with the chromatic differential on both complexes. However, each chromatic differential ∂ is a signed sum of per-edge maps. Each per-edge map is either given by multiplication or identity. Everything commutes with the identity maps. Since graded R -algebra morphisms respect multiplication by definition, they also commute with the multiplicative per-edge maps.

That is to say that the following square is commutative for each i :

$$\begin{array}{ccc} CHR^{i+1}(G, \mathcal{A}) & \xrightarrow{\phi_{i+1}^*} & CHR^{i+1}(G, \mathcal{B}) \\ \partial \uparrow & & \uparrow \partial \\ CHR^i(G, \mathcal{A}) & \xrightarrow{\phi_i^*} & CHR^i(G, \mathcal{B}) \end{array}$$

□

To lift this to the level of the chromatic bicomplex, it suffices to check if a morphism of DGAs (a co-chain map) $\phi : (\mathcal{A}^*, d) \rightarrow (\mathcal{B}^*, \delta)$ induces a map between the chromatic bicomplexes $(CHR^{**}(G, (\mathcal{A}, d)); d, \partial)$ and $(CHR^{**}(G, (\mathcal{B}, \delta)); d, \partial)$.

Theorem 8.3.2. *Let G be a graph, (\mathcal{A}^*, d) and (\mathcal{B}^*, δ) be DGAs, and $\phi : \mathcal{A}^* \rightarrow \mathcal{B}^*$ be a co-chain map. Then there is an induced morphism between the chromatic bicomplexes*

$$\phi_* : \left(CHR^{**}(G, (\mathcal{A}, d)); d, \partial \right) \longrightarrow \left(CHR^{**}(G, (\mathcal{B}, \delta)); d, \partial \right)$$

which in turn induces a map on their spectral sequences.

Proof. Recall from definition 5.1.8 that a co-chain map is a graded R -algebra morphism. Therefore the induced map on the bicomplexes ϕ_* is defined as in the previous theorem 8.3.1 which demonstrates that it commutes with the chromatic differentials. As a co-chain map, it also commutes with the differentials of the DGAs by definition. Therefore, according to definition 5.4.2, it is a bicomplex morphism and thereby induces morphisms on the resulting spectral sequences. \square

A smooth map $F : M \rightarrow N$ between smooth manifolds induces a co-chain map on their associated deRham complexes, $F^* : \Omega^*(N) \rightarrow \Omega^*(M)$ (Lee 2013). The following theorem then follows directly from theorem 8.3.2.

Theorem 8.3.3. *Let G be a graph, and $F : M \rightarrow N$ be a smooth map between smooth manifolds. Then there is an induced morphism between the chromatic bicomplexes*

$$F^* : \left(CHR^{**}(G, (\Omega_N, d_N)); d, \partial \right) \longrightarrow \left(CHR^{**}(G, (\Omega_M, d_M)); d, \partial \right)$$

which in turn induces a map on their spectral sequences.

Similarly, smooth maps between manifolds induce maps between simplicial bicomplexes as the following theorem shows.

Theorem 8.3.4. *Let G be a graph, and $F : M \rightarrow V$ be a smooth map between smooth manifolds. Then there is an induced morphism between the simplicial bicomplexes*

$$F^* : (SIM^{**}(G, V); d, D^*) \longrightarrow (SIM^{**}(G, M); d, D^*)$$

Proof. For the simplicial bicomplex, recall from lemma 7.2.1 that $SIM^{p,q}(G, M) = \Omega^q(N_p)$ where $N_p \equiv \bigsqcup_{|S|=p+1} \bar{D}_S = \bigsqcup_{|\varepsilon|=p+1} M^{k_\varepsilon}$ where $S \subseteq E(G)$ and k_ε is the number of connected components of the the subgraph $G_\varepsilon = G_S \subseteq G$.

Now, a smooth map $F : M \rightarrow V$ between smooth manifolds extends over Cartesian products and disjoint unions and therefore induces a smooth map

$$F : \bigsqcup_{|\varepsilon|=p+1} M^{k_\varepsilon} \longrightarrow \bigsqcup_{|\varepsilon|=p+1} V^{k_\varepsilon}$$

This in turn induces a co-chain map between their respective deRham complexes

$$F^* : \Omega^* \left(\bigsqcup_{|\varepsilon|=p+1} V^{k_\varepsilon} \right) \longrightarrow \Omega^* \left(\bigsqcup_{|\varepsilon|=p+1} M^{k_\varepsilon} \right)$$

which is equivalent to

$$F^* : SIM^{p,*}(G, V) \longrightarrow SIM^{p,*}(G, M)$$

It remains to show that F^* commutes with the simplicial differential D^* . However, according to lemma 7.2.1, the simplicial differential is a signed sum of pullbacks of inclusion maps which embed subdiagonals into higher order subdiagonals. In this case the smooth map clearly commutes.

For example, let $D_M : M \rightarrow M \times M$ be the diagonal embedding map which takes $m \mapsto (m, m)$ and $D_V : V \rightarrow V \times V$ be the diagonal embedding map which takes $v \mapsto (v, v)$. Lastly, let $m \in M$ and $F(m) \in V$ be its image under F . Then $D_V(F(m)) = (F(m), F(m)) \in V \times V$

and $(F \times F) \circ D_M(m) = (F \times F)(m, m) = (F(m), F(m)) \in V \times V$. □

8.3.2 Functoriality in the Graph

Now, let's consider the functoriality in the graph input. First, note that graph morphisms do not, in general, induce maps between their respective chromatic polynomials (Tutte 1984). However, the benefit of categorification is that the additional structure allows for the possibility of functoriality which is not present in the original construction. Let's see if that's true here.

Since the spectral sequences converge to the homology of configuration space $H_*(M_G)$, let's start there and work backwards. In their paper Eastwood and Hugget (2007) show that the graph configuration spaces are functorial with respect to the graph.

Lemma 8.3.5. *(Eastwood and Hugget 2007) Let M be a smooth manifold and $\phi : G \rightarrow H$ be a graph morphism between graphs. Then ϕ induces a smooth map $\phi^* : M_H \rightarrow M_G$.*

Proof. A point $m \in M_H$ is a map $m : V(H) \rightarrow M$ such that if $e = [v, w] \in E(H)$, then $m(v) \neq m(w)$. Similarly, a point $n \in M_G$ is a map $n : V(G) \rightarrow M$ such that if $e = [v, w] \in E(G)$ then $n(v) \neq n(w)$. Thought of in this way, the graph morphism ϕ induces a map from M_H to M_G via pre-composition. for $v \in V(G)$, the map $\phi^*(m) : V(G) \rightarrow M$ is given by $\phi^*(m)(v) = m(\phi(v))$. Because ϕ is a graph morphism, if $[v, w] \in E(G)$ then $[\phi(v), \phi(w)] \in E(H)$. Therefore $m(\phi(v)) \neq m(\phi(w))$ which by definition of ϕ^{ast} implies that $\phi^*(m)(v) \neq \phi^*(m)(w)$. □

With this in mind, it follows that a graph morphism $\phi : G \rightarrow H$ induces a map on the homologies of the graph configuration spaces $\phi^* : H_*(M_H) \rightarrow H_*(M_G)$. Dualizing (using the isomorphism of lemma 7.2.4) yields the map $\phi^* : H^*(M, D_{E(G)}) \rightarrow H^*(M, D_{E(H)})$. Because these are the limit spaces of the spectral sequences arising the chromatic and simplicial

bicomplexes, if they are functorial in their graph inputs, then the functoriality must be covariant. That's at least a start.

It is known that certain morphisms between graphs produce morphisms between their associated chromatic complexes. Namely, the chromatic complex categorifies the deletion-contraction rule 6.1 (Helme-Guizon and Rong 2005a). Let G be a graph and $e \in E(G)$. Then there is an inclusion map $i_e : G/e \hookrightarrow G$ and a map $p_e : G \rightarrow G \setminus e$. Helme-Guizon and Rong (2005a) Show that these are co-chain maps which give rise to a short exact sequence in their respective chromatic complexes

$$0 \rightarrow CHR^{i-1}(G/e) \xrightarrow{p_e^*} CHR^i(G) \xrightarrow{i_e^*} CHR^i(G \setminus e) \rightarrow 0$$

which in turn gives rise to a long exact sequence on the chromatic cohomology

$$0 \rightarrow H_{chr}^0(G) \xrightarrow{i_e^*} H_{chr}^0(G \setminus e) \xrightarrow{\gamma^*} H_{chr}^0(G/e) \xrightarrow{p_e^*} H_{chr}^1(G) \xrightarrow{i_e^*} \dots$$

where γ^* is the connecting homomorphism.

In fact, in Jasso-Hernandez and Rong (2006) it is shown how any inclusion of subgraphs induces co-chain map on the chromatic complexes. However, note that this construction is contravariant. Therefore, while these graph morphisms induce co-chain maps which lift to the spectral sequences arising from their chromatic bicomplexes, they do not recover the functoriality of the Eastwood and Hugget (2007) construction.

In addition, it has been shown that the chromatic homology is completely determined by the chromatic polynomial when computed with rational coefficients (Chumtov et al. 2008) as well as with integer coefficients (Lowrance and Sazdanović 2017). However, this does not hold for all choices of algebras (see Pabiniak et al. (2008) for an example with coefficients in A_3).

This, in conjunction with the aforementioned fact that graph morphisms do not in general induce maps between their respective chromatic polynomials, implies that the likelihood of the existence of covariant functoriality in the chromatic complex, and thus resulting bicomplex, is small.

Considering all of this, as well as the authors numerous attempts at establishing functoriality, the author is fairly confident in the following conjecture.

Conjecture 8.3.1. *A graph morphism does not induce a covariant morphism on chromatic (bi)complexes.*

Note that if there were such a functoriality in the simplicial bicomplex, then it would get carried over to the chromatic bicomplex via their relationship as described in 8.1. Therefore, the lack in the chromatic complex implies the lack in the simplicial bicomplex.

CHAPTER

9

CHROMATIC HOMOLOGY AND PDES?

9.1 An Example Computation

Here an attempt is made to compute the E_2^{**} page of the spectral sequence arising from the horizontal filtration of the chromatic bicomplex. As the simplest non-trivial computation, consider the graph $G = P_1$ and $M = \mathbb{R}^1$ with the compactly supported deRham complex, $\Omega_c^*(M)$. Because the manifold is known in this example, the notation will be simplified to Ω_c . Compare this computation to that of horizontal filtration worked out in section 8.2.

Notice that on simpler graphs (multiple vertices and no edges) the computation reduces to deRham cohomology with compact supports when there is only one vertex, and

tensor products thereof for multiple vertices which can be computed via the the Kunneth Isomorphism (as in Hatcher (2001) and Lee (2013) for example).

For completeness, the E_0^{**} page is built up from the chromatic complex in the following two examples.

Example 9.1.1. $G = \bullet \text{---} \bullet$

The chromatic diagram and resulting chromatic complex these choices of G and M is given by:

$$\begin{array}{ccccccc}
 & & i = 0 & & i = 1 & & \\
 0 & \longrightarrow & \boxed{\begin{array}{c} \bullet \\ \bullet \end{array}} & \xrightarrow{\partial_*^0} & \boxed{\begin{array}{c} \bullet \text{---} \bullet \\ \bullet \end{array}} & \longrightarrow & 0 \\
 \\
 0 & \longrightarrow & \Omega_c^* \otimes \Omega_c^* & \xrightarrow{\partial^0} & \Omega_c^* & \longrightarrow & 0
 \end{array}$$

Where:

$$\partial^0(\alpha \otimes \beta) = \alpha \wedge \beta$$

For $M = \mathbb{R}^1$, the graded space and its tensor power can be written out explicitly as follows:

$$\begin{aligned}
 \Omega_c^* &= \Omega_c^0 \oplus \Omega_c^1 \\
 \Omega_c^* \otimes \Omega_c^* &= \left(\Omega_c^0 \otimes \Omega_c^0 \right) \oplus \left(\begin{array}{c} \Omega_c^0 \otimes \Omega_c^1 \\ \oplus \\ \Omega_c^1 \otimes \Omega_c^0 \end{array} \right) \oplus \left(\Omega_c^1 \otimes \Omega_c^1 \right)
 \end{aligned}$$

With this expanded form, the chromatic complex can now be written as the following.

Example 9.1.2. $M = \mathbb{R}^1$

$$0 \longrightarrow \Omega_c^0 \xrightarrow{\bar{d}} \Omega_c^1 \longrightarrow 0$$

$\frac{\Omega_c^*}{\Omega_c^*}$

$$0 \longrightarrow \Omega_c^0 \otimes \Omega_c^0 \xrightarrow{\bar{d}} \bigoplus_{\Omega_c^1 \otimes \Omega_c^0}^{\Omega_c^0 \otimes \Omega_c^1} \xrightarrow{\bar{d}} \Omega_c^1 \otimes \Omega_c^1 \longrightarrow 0$$

$\frac{\Omega_c^* \otimes \Omega_c^*}{\Omega_c^* \otimes \Omega_c^*}$

Adding the chromatic differentials to the diagram results is the bicomplex which is the E_0^{**} page of the spectral sequence arising from the vertical filtration of the chromatic bicomplex.

Example 9.1.3. E_0^{**}

$G = \mathbb{I} \quad \& \quad M = \mathbb{R}^1$

$$\begin{array}{ccccccc}
 & & 0 & & 0 & & 0 \\
 & & \uparrow & & \uparrow & & \uparrow \\
 0 & \longrightarrow & \Omega_c^0 & \xrightarrow{\bar{d}} & \Omega_c^1 & \longrightarrow & 0 \longrightarrow 0 \\
 & & \uparrow \partial & & \uparrow \partial & & \uparrow \\
 0 & \longrightarrow & \Omega_c^0 \otimes \Omega_c^0 & \xrightarrow{\bar{d}} & \bigoplus_{\Omega_c^1 \otimes \Omega_c^0}^{\Omega_c^0 \otimes \Omega_c^1} & \xrightarrow{\bar{d}} & \Omega_c^1 \otimes \Omega_c^1 \longrightarrow 0 \\
 & & \uparrow & & \uparrow & & \uparrow \\
 & & 0 & & 0 & & 0
 \end{array}$$

Theorem 9.1.1. *The E_1^{**} page is given by*

$$G = \mathbb{I} \quad \& \quad M = \mathbb{R}^1$$

$$\begin{array}{ccccccc}
 & & 0 & & 0 & & 0 \\
 & & \uparrow & & \uparrow & & \uparrow \\
 0 & \longrightarrow & 0 & \longrightarrow & 0 & \longrightarrow & 0 \longrightarrow 0 \\
 & & \uparrow & & \uparrow & & \uparrow \\
 0 & \longrightarrow & E_1^{00} & \xrightarrow{\bar{d}} & E_1^{10} & \xrightarrow{\bar{d}} & E_1^{20} \longrightarrow 0 \\
 & & \uparrow & & \uparrow & & \uparrow \\
 & & 0 & & 0 & & 0
 \end{array}$$

Where:

$$E_1^{00} = \{f \otimes g \in \Omega_c^0 \otimes \Omega_c^0 \mid f \cdot g = 0\}$$

$$E_1^{10} = \{(\alpha \otimes g, f \otimes \beta) \mid \alpha \cdot g + f \cdot \beta = 0\}$$

$$E_1^{20} = \Omega_c^1 \otimes \Omega_c^1$$

The proof is given as the sequence of following lemmas.

Lemma 9.1.2.

$$\begin{aligned}
 E_1^{00} &= \{f \otimes g \in \Omega_c^0 \otimes \Omega_c^0 \mid f \wedge g = 0\} \\
 &= \{f \otimes g \in \Omega_c^0 \otimes \Omega_c^0 \mid f \cdot g = 0\} \\
 &= \{f \otimes g \in \Omega_c^0 \otimes \Omega_c^0 \mid \text{supp}(f) \cap \text{supp}(g) = \emptyset\}
 \end{aligned}$$

Proof. Note that E_1^{00} is given by the kernel of

$$\partial : \Omega_c^0 \otimes \Omega_c^0 \rightarrow \Omega_c^0$$

That is

$$E_1^{00} = \text{Ker}(\partial) = \{f \otimes g \in \Omega_c^0 \otimes \Omega_c^0 \mid f \wedge g = 0\}$$

Since f and g are smooth compactly supported functions on \mathbb{R}^1 , the wedge product is just the point-wise product, $f \wedge g = f \cdot g$. Therefore, the condition that $f \wedge g = 0$ is equivalent to f and g having disjoint support. \square

Lemma 9.1.3.

$$E_1^{01} = 0$$

Proof. It is enough to show that $\partial : \Omega_c^0 \otimes \Omega_c^1 \rightarrow \Omega_c^1$ is surjective. Therefore, let $h \in \Omega_c^0$ and $U \subset \mathbb{R}^1$ be open and such that $\text{supp}(h) \subset U$. Then there exists a bump function, ρ_U , with compact support in U such that its restriction to $\text{supp}(h)$ is constant 1. Therefore, $h \otimes \rho_U \in \Omega_c^0 \otimes \Omega_c^0$ is such that $\partial(h \otimes \rho_U) = h \cdot \rho_U = h$. \square

Lemma 9.1.4.

$$\begin{aligned} E_1^{10} &= \{(\alpha \otimes g, f \otimes \beta) \mid \alpha \wedge g + f \wedge \beta = 0\} \\ &= \{(\alpha \otimes g, f \otimes \beta) \mid \alpha \cdot g + f \cdot \beta = 0\} \end{aligned}$$

Proof. E_1^{10} is given by the kernel of the map

$$\partial : (\Omega_c^1 \otimes \Omega_c^0) \oplus (\Omega_c^0 \otimes \Omega_c^1) \rightarrow \Omega_c^1$$

where

$$\partial(\alpha \otimes g, g \otimes \beta) = \alpha \wedge g + f \wedge \beta$$

Therefore,

$$E_1^{10} = \text{Ker}(\partial) = \{(\alpha \otimes s, t \otimes \beta) \mid \alpha \wedge s + t \wedge \beta = 0\}$$

Furthermore, since $f, g \in \Omega_c^0$ the wedge products are just point-wise products. \square

Lemma 9.1.5.

$$E_1^{11} = 0$$

Proof. It is enough to show that the map

$$\partial : (\Omega_c^1 \otimes \Omega_c^0) \oplus (\Omega_c^0 \otimes \Omega_c^1) \rightarrow \Omega_c^1$$

is surjective.

Let $w \in \Omega_c^1$ and $U \subset \mathbb{R}^1$ be open and such that $\text{supp}(w) \subset U$. Then there exists a bump function, ρ_U , with compact support in U such that its restriction to $\text{supp}(w)$ is the constant 1. Therefore

$$(w \otimes \rho_U, 0 \otimes 0) \in (\Omega_c^1 \otimes \Omega_c^0) \oplus (\Omega_c^0 \otimes \Omega_c^1)$$

is such that $\partial(w \otimes \rho_U, 0 \otimes 0) = w \cdot \rho_U + 0 \cdot 0 = w$. \square

Lemma 9.1.6.

$$E_1^{20} = \Omega_c^1 \otimes \Omega_c^1$$

Proof. Here the vertical maps coming into and out of $\Omega_c^1 \otimes \Omega_c^1$ are both zero maps. \square

Theorem 9.1.7. *The E_2^{**} page is given by*

$$G = \mathbb{I} \quad \& \quad M = \mathbb{R}^1$$

$$\begin{array}{ccccccc}
 & & 0 & & 0 & & 0 \\
 & & \uparrow & & \uparrow & & \uparrow \\
 0 & \longrightarrow & 0 & \longrightarrow & 0 & \longrightarrow & 0 \longrightarrow 0 \\
 & & \uparrow & & \uparrow & & \uparrow \\
 0 & \longrightarrow & 0 & \longrightarrow & 0 & \longrightarrow & E_2^{20} \longrightarrow 0 \\
 & & \uparrow & & \uparrow & & \uparrow \\
 & & 0 & & 0 & & 0
 \end{array}$$

Where:

$$E_2^{20} = \frac{\Omega_c^1 \otimes \Omega_c^1}{\text{Img}(\bar{d})}$$

The proof is given as the sequence of following lemmas.

Lemma 9.1.8.

$$E_2^{00} = 0$$

Proof. It is enough to show that the kernel of $\bar{d} : E_1^{00} \rightarrow E_1^{10}$ is zero. The kernel is given by the following.

$$\text{Ker}(d) = \{f \otimes g \in \Omega_c^0 \otimes \Omega_c^0 \mid f \cdot g = 0 \text{ \& } (df \otimes g, f \otimes dg) = (0, 0)\}$$

The condition that $(df \otimes g, f \otimes dg) = (0, 0)$ is equivalent to $df = 0$ and $dg = 0$. Since $f, g \in \Omega_c^0$, it follows that $f = 0$ and $g = 0$. □

Lemma 9.1.9.

$$E_2^{10} = 0$$

Proof. It is enough to show that the kernel of $\bar{d} : E_1^{10} \rightarrow E_1^{20}$ is contained in the image of $\bar{d} : E_1^{00} \rightarrow E_1^{10}$.

Explicitly they are given by the following.

$$\text{Ker}(\bar{d}) = \{(\alpha \otimes g, f \otimes \beta) \mid \alpha \cdot g + f \cdot \beta = 0 \text{ \& } -\alpha \otimes dg + df \otimes \beta = 0\}$$

$$\text{Img}(\bar{d}) = \{(ds \otimes t, s \otimes dt) \mid s \cdot t = 0\}$$

Let $(\alpha \otimes g, f \otimes \beta) \in \text{Ker}(\bar{d})$. Then $\alpha \otimes dg = df \otimes \beta$. Since the tensor product is over \mathbb{R} , this implies that $\alpha = \lambda df$ and $dg = \frac{1}{\lambda} \beta$ for some non-zero constant, $\lambda \in \mathbb{R}$. Therefore, we can rewrite $(\alpha \otimes g, f \otimes \beta) = (\lambda df \otimes g, f \otimes \lambda df)$.

The condition that $\alpha \cdot g + f \cdot \beta = 0$ then becomes $\lambda df \cdot g + f \cdot \lambda dg = 0$. By the product rule, this is equivalent to $\lambda d(f \cdot g) = 0$. This implies that $f \cdot g = 0$ since $f, g \in \Omega_c^0$. \square

Lemma 9.1.10.

$$E_2^{20} = \frac{E_1^{20}}{\text{Img}(\bar{d})}$$

where

$$E_1^{20} = \Omega_c^1 \otimes \Omega_c^1$$

$$\text{Img}(\bar{d}) = \{-\alpha \otimes dg + df \otimes \beta \mid \alpha \cdot g + f \cdot \beta = 0\}$$

The details of the calculation of E_2^{20} are to be found in the next section.

9.2 The Problem Child

As seen in lemma 9.1.10, E_2^{20} is given by

$$E_2^{20} = \frac{E_1^{20}}{\text{Img}(\bar{d})}$$

where

$$E_1^{20} = \Omega_c^1 \otimes \Omega_c^1$$

$$\text{Img}(\bar{d}) = \{-\gamma \otimes dg + df \otimes \eta \mid \gamma \cdot g + f \cdot \eta = 0\}$$

Note that the requirement

$$\gamma \cdot g + f \cdot \eta = 0 \tag{9.1}$$

will be essential to the following computations.

Let's start by determining the necessary and sufficient conditions for two elements of $\Omega_c^1 \otimes \Omega_c^1$ to be in the same class. Let $\alpha \otimes \beta, \omega \otimes \nu \in \Omega_c^1 \otimes \Omega_c^1$ such that $[\alpha \otimes \beta] = [\omega \otimes \nu] \in E_2^{20}$. It follows that there exists $-\gamma \otimes df + dg \otimes \eta \in \text{Img}(\bar{d})$ such that $\alpha \otimes \beta - \omega \otimes \nu = -\gamma \otimes df + dg \otimes \eta$.

This analysis will rely on the fact that an element $\alpha \in \Omega_c^1$ is exact if and only if $\int \alpha = 0$ (Bott and Tu 1982). If this is the case, then there exists $p \in \Omega_c^0$ such that $dp = \alpha$. In such cases, p will be called the *primitive* of α . Furthermore, note that in this context it also holds that if $ds = dt$ for $s, t \in \Omega_c^0$, then $s = t$.

The computation proceeds by cases via partial integration. Namely, integrating the equation

$$\alpha \otimes \beta - \omega \otimes \nu = -\gamma \otimes df + dg \otimes \eta \tag{9.2}$$

in the first and second factors respectively results in the equations.

$$\beta \cdot \int \alpha - \nu \cdot \int \omega = -df \cdot \int \gamma \quad (9.3)$$

$$\alpha \cdot \int \beta - \omega \cdot \int \nu = dg \cdot \int \eta \quad (9.4)$$

There are 16 cases to consider. They are summarized in the table below.

$\int \beta = 0, \int \nu = 0$	$\int \beta = 0, \int \nu \neq 0$	$\int \beta \neq 0, \int \nu = 0$	$\int \beta \neq 0, \int \nu \neq 0$
$\int \alpha = 0, \int \omega = 0$	$\int \alpha = 0, \int \omega = 0$	$\int \alpha = 0, \int \omega = 0$	$\int \alpha = 0, \int \omega = 0$
$\int \alpha = 0, \int \omega \neq 0$	$\int \alpha = 0, \int \omega \neq 0$	$\int \alpha = 0, \int \omega \neq 0$	$\int \alpha = 0, \int \omega \neq 0$
$\int \alpha \neq 0, \int \omega = 0$	$\int \alpha \neq 0, \int \omega = 0$	$\int \alpha \neq 0, \int \omega = 0$	$\int \alpha \neq 0, \int \omega = 0$
$\int \alpha \neq 0, \int \omega \neq 0$	$\int \alpha \neq 0, \int \omega \neq 0$	$\int \alpha \neq 0, \int \omega \neq 0$	$\int \alpha \neq 0, \int \omega \neq 0$

Table 9.1: 16 cases to consider for determining if $[\alpha \otimes \beta] = [\omega \otimes \nu] \in E_2^{20}$. For each of the four choices of assumptions about $\int \beta$ and $\int \nu$, there are four choices for $\int \alpha$ and $\int \omega$.

Given non-zero $\alpha, \beta, \omega, \nu \in \Omega_c^1$, the goal is to determine whether or not there exists $f, g \in \Omega_c^0$ and $\gamma, \eta \in \Omega_c^1$ such that equations 9.3, 9.4, and 9.1 are satisfied. To do this, the following computational procedure was used.

A given case in table 9.1 determines which, if any, of the 1-forms $\alpha, \beta, \omega, \nu$ are exact. For a given case, the exact 1-forms, if any, are rewritten using their primitives and substituted into equations 9.3 and 9.4. The resulting equations are then solved for the unknowns f, g, γ, η . The resulting equations are then substituted into equation 9.2. The structure of tensor products is then used to produce a coupled pair of equations which are further solved for f, g, γ, η in terms of $\alpha, \beta, \omega, \nu$ (or their primitives). Finally, the results of that analysis are substituted into equation 9.1 to determine what differential equation $\alpha, \beta, \omega, \nu$ (or their primitives) must satisfy in order for $\alpha \otimes \beta$ and $\omega \otimes \nu$ to be in the same class in E_2^{20} .

Often it is the case that not all of the terms f, g, γ, η (or their primitives) can be eliminated in the course of the computation. In those cases the final result is interpreted as a differential equation, for given $\alpha, \beta, \omega, \nu$ (or their primitives), in the remaining term(s). Then, whether or not $\alpha \otimes \beta$ is in the same class as $\omega \otimes \nu$ in E_2^{20} is determined by the existence (or lack thereof) of a solution to the resulting differential equation.

Starting with the first column, suppose that $\int \beta = 0$ and $\int \nu = 0$. Then β and ν are exact. Let $s, m \in \Omega_c^0$ be the primitives of β and ν respectively and write $\beta = ds$ and $\nu = dm$. Applying this to equation 9.4 yields $0 = dg \int \eta$ which implies that $\int \eta = 0$. Therefore, $\eta \in \Omega_c^1$ is exact. Denote its primitive by $q \in \Omega_c^0$ so that $\eta = dq$. Applying all of this to equation 9.3 yields

$$ds \cdot \int \alpha - dm \cdot \int \omega = -df \int \gamma \quad (9.5)$$

9.2.1 The First Case in the First Column

The first case in first column is that $\int \alpha = 0$ and $\int \omega = 0$. Then α and ω are exact. Let $p, n \in \Omega_c^0$ be the primitives of α and ω respectively and write $\alpha = dp$ and $\omega = dn$. Applying this to equation 9.5 yields $0 = -df \int \gamma$ which implies that $\int \gamma = 0$. Therefore, $\gamma \in \Omega_c^1$ is exact. Let $r \in \Omega_c^0$ be γ 's primitive and write $\gamma = dr$. Applying the results to equation 9.2 yields the following.

$$dp \otimes ds - dn \otimes dm = -dr \otimes df + dg \otimes dq$$

Applying equation 9.1 gives the following result:

$$mdn + pds = 0$$

9.2.2 The Second Case in the First Column

For the second case in the first column, it is assumed that $\int \alpha = 0$ and $\int \omega \neq 0$. Again, this implies that $\alpha \in \Omega_c^1$ is exact and can thus be written $\alpha = dp$ for $p \in \Omega_c^0$. Applying this to equation 9.5 yields the equation $-dm \int \omega = -df \int \gamma$ which simplifies to the following.

$$m \int \omega = f \int \gamma$$

Because $\int \omega \neq 0$ by assumption, it follows that $\int \gamma \neq 0$. Solving for f and substituting into equation 9.2 gives the equation

$$dp \otimes ds + \left(\frac{\int \omega}{\int \gamma} \gamma - \omega \right) \otimes dm = dg \otimes dq \quad (9.6)$$

In order for the equality to hold, two of the three tensor products must combine. This can only happen if one of their factors are equal up to a scalar multiple. Letting $\lambda_0 \neq 0 \in \mathbb{R}$, this requirement leads to the following six cases.

$$\begin{aligned} \lambda_0 g &= p \\ \lambda_0 dg &= \frac{\int \omega}{\int \gamma} \gamma - \omega \\ \lambda_0 dp &= \frac{\int \omega}{\int \gamma} \gamma - \omega \\ \lambda_0 q &= s \\ \lambda_0 s &= m \\ \lambda_0 q &= m \end{aligned}$$

There is a symmetry in the first three cases and another in the last pair. Therefore, only three of the six cases will be worked out in detail here. They are $\lambda_0 g = p$, $\lambda_0 q = s$, and

$$\lambda_0 s = m.$$

First, substituting $\lambda_0 g = p$ into equation 9.6 allows for the following simplification

$$\left(\frac{\int \omega}{\int \gamma} \gamma - \omega \right) \otimes dm = dp \otimes d\left(\frac{1}{\lambda_0} q - s \right)$$

Because the tensor product is over \mathbb{R} , it follows that the respective factors of the tensor product are equal up to a scalar multiple. Therefore, letting $\lambda_1 \neq 0 \in \mathbb{R}$ the following pair of equations are obtained.

$$\begin{aligned} \lambda_1 \left(\left(\frac{\int \omega}{\int \gamma} \right) \gamma - \omega \right) &= dp \\ \left(\frac{1}{\lambda_1} \right) m &= \left(\frac{1}{\lambda_0} \right) q - s \end{aligned}$$

Solving for γ and q yields

$$\begin{aligned} \gamma &= \left(\frac{\int \gamma}{\int \omega} \right) \left(\omega + \frac{1}{\lambda_1} dp \right) \\ q &= \left(\frac{\lambda_0}{\lambda_1} \right) m + \lambda_0 s \end{aligned}$$

Recalling that $\eta = dq$, these equations can be substituted into equation 9.1 to produce the following equation

$$\left(\frac{\int \gamma}{\int \omega} \right) \left(\omega + \frac{1}{\lambda_1} dp \right) \cdot \left(\frac{\int \omega}{\int \gamma} \right) m + \frac{1}{\lambda_0} p \cdot \left(\frac{\lambda_0}{\lambda_1} dm + \lambda_0 ds \right) = 0$$

Simplifying yields the following

$$\boxed{\omega \cdot m + \frac{1}{\lambda_1} d(p \cdot m) + p \cdot ds = 0}$$

As mentioned, cases $\lambda_0 g = p$, $\lambda_0 dg = \frac{\int \omega}{\int \gamma} \gamma - w$ and $\lambda_0 dp = \frac{\int \omega}{\int \gamma} \gamma - w$ are symmetric. Therefore

the computations of the latter two cases are omitted and the results simply stated.

$$\begin{aligned} dg &= \frac{\int \omega}{\int \gamma} \gamma - \omega \Rightarrow \boxed{\omega \cdot m + \lambda_1 d(p \cdot m) + p \cdot ds = 0} \\ dp &= \frac{\int \omega}{\int \gamma} \gamma - \omega \Rightarrow \boxed{\omega \cdot m + d(p \cdot m) + p \cdot ds = 0} \end{aligned}$$

Next, let $\lambda_0 q = s$. Then equation 9.6 simplifies to.

$$\left(\frac{\int \omega}{\int \gamma} \gamma - \omega \right) \otimes dm = d \left(\frac{1}{\lambda_0} g - p \right) \otimes ds$$

Again, since the tensor product is over \mathbb{R} , letting $\lambda_1 \neq 0 \in \mathbb{R}$ allows this to be rewritten as the following pair of equations.

$$\lambda_1 \left(\frac{\int \omega}{\int \gamma} \gamma - \omega \right) = \frac{1}{\lambda_0} dg - dp$$

$$\frac{1}{\lambda_1} dm = ds$$

Note that the second equation implies that $m = \lambda_1 s = \lambda_0 \lambda_1 q$. Solving for γ in the first equation and substituting into equation 9.1 yields the following equation.

$$\left(\frac{\int \gamma}{\int \omega} \right) \left(\frac{1}{\lambda_1} \left(\frac{1}{\lambda_0} dg - dp \right) + \omega \right) \cdot \left(\frac{\int \omega}{\int \gamma} \right) \cdot \lambda_1 s + \frac{1}{\lambda_0} g \cdot ds = 0$$

Simplifying this result leads to

$$\boxed{\frac{1}{\lambda_0} d(g \cdot s) - s \cdot dp + \lambda_1 s \cdot \omega = 0}$$

Note that in this case, a dependence on g remains. Therefore the statement in this case is, under these assumptions, $[\alpha \otimes \beta] = [\omega \otimes \eta] \in E_2^{20}$ if and only if there exists $g \in \Omega_c^0$ such that $\frac{1}{\lambda_0} d(g \cdot s) - s \cdot dp + \lambda_1 s \cdot \omega = 0$ holds where $\beta = ds$, $\nu = dm$, and $\alpha = dp$.

Finally, as previously mentioned, the assumptions that $\lambda_0 s = m$ and $\lambda_0 q = m$ are symmetric. Therefore, only the first will be computed in detail. Letting $\lambda_0 s = m$, equation 9.6 becomes

$$\left(\frac{1}{\lambda_0} dp + \left(\frac{\int \omega}{\int \gamma} \right) \cdot \gamma - \omega \right) \otimes dm = dg \otimes dq$$

Again letting $\lambda_1 \neq 0 \in \mathbb{R}$, this splits into the following two equations.

$$\lambda_1 \left(\frac{1}{\lambda_0} dp + \left(\frac{\int \omega}{\int \gamma} \right) \cdot \gamma - \omega \right) = dg$$

$$\frac{1}{\lambda_1} dm = dq$$

Note that the second equation simplifies to $m = \lambda_1 q = \lambda_0 s$. Solving the first equation for γ and substituting into equation 9.1 yields the following.

$$\left(\frac{\int \gamma}{\int \omega} \right) \cdot \left(-\frac{1}{\lambda_0} dp + \frac{1}{\lambda_1} dg + \omega \right) \cdot \left(\frac{\int \omega}{\int \gamma} \right) \cdot m + g \cdot \left(\frac{1}{\lambda_1} \right) \cdot dm = 0$$

Simplifying gives the following.

$$\boxed{-\frac{1}{\lambda_0} s \cdot dp + m \cdot \omega + \left(\frac{1}{\lambda_1} \right) \cdot d(m \cdot g) = 0}$$

The last of the six cases similarly gives

$$q = m \Rightarrow \boxed{-\frac{1}{\lambda_0} s \cdot dp + m \cdot \omega + d(m \cdot g) = 0}$$

This concludes the computations for the second case in first column of table 9.1. The remaining 14 cases can be computed using the same procedure and are omitted from the current discourse for brevity.

9.2.3 Conclusion

As seen in the previous computation, computing the spectral sequences arising from the horizontal filtration of the chromatic complex is highly non-trivial. The other twelve cases can be computed using the same methods and a complete characterization of the conditions under which $[\alpha \otimes \beta] = [\omega \otimes \eta] \in E_2^{20}$ can be obtained. However, those computations are omitted here for brevity.

The take away from the exercise is that the characterization depends on whether or not one out of a collection of differential equations is satisfied (the boxed equations). In fact, a similar computation can be done to characterize the conditions under which $[\alpha \otimes \beta] = [0] \in E_2^{20}$. In this case, it is determined by the existence of solutions to coupled differential equations on \mathbb{R}^1 .

While the author cannot provide a general proof at this time, there is enough evidence to make the following conjecture.

Conjecture 9.2.1. *Let M be a smooth manifold and G be a finite simple graph. Then the intermediate pages of the spectral sequence arising from the horizontal filtration of the chromatic complex are determined by the existence of solutions to coupled systems of differential equations on M , the form and couplings of the which are determined by the connectivity information of G (as captured by the subgraphs G_S), the page of the spectral sequence, and M itself.*

REFERENCES

- Anderson, D. W. (1972). A generalization of the Eilenberg-Moore spectral sequence. *Bulletin of the American Mathematical Society*, 78(5):784–786.
- Baranovsky, V. and Sazdanovic, R. (2012). Graph homology and graph configuration spaces. *Journal of Homotopy and Related Structures*, 7(2):223–235.
- Bendersky, M. and Gitler, S. (1991). The cohomology of certain function spaces. *Transactions of the American Mathematical Society*, 326(1):423–440.
- Borsuk, K. (1948). On the embedding of systems of compacta in simplicial complexes. *Fundamenta Mathematicae*, 35(1):217–234.
- Bott, R. and Tu, L. (1982). *Differential Forms in Algebraic Topology*. Springer.
- Bubenik, P. (2015). Statistical topological data analysis using persistence landscapes. *Journal of Machine Learning Research*, 16:77–102.
- Bubenik, P. (2018). The persistence landscape and some of its properties. *ArXiv*, pages pre-print.
- Carlsson, G. (2009). Topology and data. *Bulletin of the American Mathematical Society*, 46(2):255–308.
- Carlsson, G., Zomorodian, A., Collins, A., and Guibas, L. (2005). Persistence barcodes for shapes. *International Journal for Shape Modeling*, 11(2):149–187.
- Chumtsov, M., Chumtsov, S., and Rong, Y. (2008). Knight move in chromatic homology. *European Journal of Combinatorics*, 29:311–321.
- Chung, Y.-M. and Lawson, A. (2019). Persistence curves: A canonical framework for summarizing persistence diagrams. *ArXiv*, pages pre-print.
- de Silva, V. and Carlsson, G. (2004). Topological estimation using witness complexes. *Eurographic Symposium on Point-Based Graphics*, 134:157–66.
- Delauney, B. (1934). Sur la sphère vide. a la mémoire de Georges Voronoï. *Bulletin de l'Académie des Sciences de l'USSR*, 6:793–800.
- Delfinado, C. and Edelsbrunner, H. (1995). An incremental algorithm for Betti numbers for simplicial complexes on the 3-sphere. *Computer Aided Geometric Design*, 12(7):771–784.
- Eastwood, M. and Hugget, S. (2007). Euler characteristics and chromatic polynomials. *European Journal of Combinatorics*, 28(6):1553–1560.

- Edelsbrunner, H., Kirkpatrick, D., and Seidel, R. (1983). On the shape of a set of points in the plane. *IEEE Transactions on Information Theory*, 29(4):551–559.
- Edelsbrunner, H., Letscher, D., and Zomorodian, A. (2002). Topological persistence and simplification. *Discrete and Computational Geometry*, 28(4):511–533.
- Edelsbrunner, H. and Mücke, E. (1994). 3-dimensional alpha-shapes. *ACM Transactions on Graphics*, 13(1):43–72.
- Eilenberg, S. (1944). Singular homology theory. *Annals of Mathematics*, 45(3):407–447.
- Goodfellow, I., Bengio, Y., and Courville, A. (2017). *Deep Learning*. MIT Press.
- Hatcher, A. (2001). *Algebraic Topology*. Cambridge University Press.
- Helme-Guizon, L. and Rong, Y. (2005a). A categorification for the chromatic polynomial. *Algebraic and Geometric Topology*, 5:1365–1388.
- Helme-Guizon, L. and Rong, Y. (2005b). Graph cohomologies from arbitrary algebras. *arXiv:math/0506023v1*.
- Jasso-Hernandez, E. and Rong, Y. (2006). A categorification for the Tutte polynomial. *Algebraic and Geometric Topology*, 6:2031–2049.
- Lee, J. M. (2013). *Introduction to Smooth Manifolds*. Springer, 2nd edition.
- Lowrance, A. and Sazdanović, R. (2017). Chromatic homology, Khovanov homology, and torsion. *Topology and its Applications*, 222:77–99.
- Mallikarjuna, P., Targhi, A., Fritz, M., Hayman, E., Caputo, B., and Eklundh, J.-O. (2006). The kth-tips2 database.
- McCleary, J. (1985). *User's Guide to Spectral Sequences*. Publish or Perish Inc.
- Mileyko, Y., Mukherjee, S., and Harer, J. (2011). Probability measures on the space of persistence curves. *Inverse Problems*, 27(12).
- Mischaikow, K. and Nanda, V. (2013). Morse theory for filtrations and efficient computation of persistent homology. *Discrete and Computational Geometry*, 50(2):330–353.
- Pabiniak, M., Przytycki, J., and Sazdanović, R. (2008). On the first group of the chromatic homology of graphs. *Geometriae Dedicata*, 140:19–48.
- Tutte, W. (1984). *Graph Theory*. Addison-Wesley Publishing Company.
- Voronoï, G. (1908a). Nouvelles applications des paramètres continus á la théorie des formes quadratiques. deuxième mémoire. recherches sur les paralléloédres primitifs. *Journal für die Reine und Angewandte Mathematik*, 134:198–287.

- Voronoi, G. (1908b). Nouvelles applications des paramètres continus à la théorie des formes quadratiques. premier mémoire. sur quelques propriétés des formes quadratiques positives parfaites. *Journal für die Reine und Angewandte Mathematik*, 133:97–178.
- Zomorodian, A. and Carlsson, G. (2005). Computing persistence homology. *Discrete and Computational Geometry*, 33(2):249–274.